Available online at www.sciencedirect.com
ScienceDirect
Comput. Methods Appl. Mech. Engrg. 317 (2017) 649–683
Computer methods in applied mechanics and engineering
www.elsevier.com/locate/cma

Review

A framework for polyconvex large strain phase-field methods to fracture

C. Hesch[a,*], A.J. Gil[b,*], R. Ortigosa[b], M. Dittmann[a], C. Bilgen[d], P. Betsch[c], M. Franke[c], A. Janz[c], K. Weinberg[d]

[a] *Chair of Computational Mechanics, University of Siegen, Siegen, Germany*
[b] *Zienkiewicz Centre for Computational Engineering, College of Engineering Swansea University, Swansea, United Kingdom*
[c] *Institute of Mechanics, Karlsruhe Institute of Technology, Karlsruhe, Germany*
[d] *Chair of Solid Mechanics, University of Siegen, Siegen, Germany*

Received 19 August 2016; received in revised form 23 December 2016; accepted 30 December 2016
Available online 9 January 2017

Abstract

Variationally consistent phase-field methods have been shown to be able to predict complex three-dimensional crack patterns. However, current computational methodologies in the context of large deformations lack the necessary numerical stability to ensure robustness in different loading scenarios. In this work, we present a novel formulation for finite strain polyconvex elasticity by introducing a new anisotropic split based on the principal invariants of the right Cauchy–Green tensor, which always ensures polyconvexity of the resulting strain energy function. The presented phase-field approach is embedded in a sophisticated isogeometrical framework with hierarchical refinement for three-dimensional problems using a fourth order Cahn–Hilliard crack density functional with higher-order convergence rates for fracture problems. Additionally, we introduce for the first time a Hu–Washizu mixed variational formulation in the context of phase-field problems, which permits the novel introduction of a variationally consistent stress-driven split. The new polyconvex phase-field fracture formulation guarantees numerical stability for the full range of deformations and for arbitrary hyperelastic materials.

Keywords: Phase-field; Fracture mechanics; Polyconvexity; Finite deformations; Isogeometric analysis

Contents

* Corresponding authors.
E-mail addresses: christian.hesch@kit.edu (C. Hesch), a.j.gil@swansea.ac.uk (A.J. Gil).

http://dx.doi.org/10.1016/j.cma.2016.12.035
0045-7825/

1. Introduction

The numerical prediction of fracture patterns is one of the most challenging problems in computational solid mechanics. In classical fracture mechanics, Griffith and Irwin [1,2] formulated the propagation of brittle fracture by assuming that the material fails locally upon the attainment of a specific fracture energy related to a critical energy-release rate. However, due to the complexity of the evolving fracture surfaces in three-dimensional scenarios, the evaluation of appropriate interface conditions is an extremely challenging task in the context of finite element discretisations.

A straightforward minimisation of the fracture energy is not feasible for finite deformations. Therefore, more generalised numerical formulations have been introduced to avoid the algorithmical tracking of discontinuities within the solid. In particular, phase-field methods provide a framework to formulate variational fracture models based on regularised energy functionals embedded within a global minimiser, cf. Francfort and Marigo [3]. In contrast to classical discontinuous methods, such as interface element formulations [4–6] or local enrichment strategies [7,8], phase-field approaches introduce a non-local diffusive crack zone. Embedded within a continuum mechanical framework, the order parameter $\mathfrak{s}$ of the phase-field allows to easily characterise the current state of fractured material within an arbitrary shaped three-dimensional structure. As a consequence of the evolution of the fracture pattern, the material is degenerated by the phase-field, see Miehe et al. [9].

Regarding the actual formulation employed to describe the anisotropic split in tension and compression (see, e.g. the textbook of Gross & Seelig [10]) various approaches are established. These classical formulations used to characterise the non-linear phase-field fracture are not able to capture the degeneration of the material in a numerically stable manner. Such problems become apparent in the simulation of large deformation problems. Here, the constitutive model must fulfil appropriate convexity criteria which imply material stability. A well-established material stability criterion is polyconvexity in the sense of Ball [11]. This concept has been adapted in a large variety of mechanical problems, see [12–14] and is here extended to the case of phase-field fracture.

To this end, we introduce a novel formulation of phase-field fracture with polyconvex energy functionals based on an anisotropic tension–compression split in terms of the principle invariants. Our formulation satisfies the polyconvexity criteria for the mechanical field regardless of the current state of fracture. We compare this new split with a previously introduced formulation based on an anisotropic split of the eigenvalues, with both formulations in the full

non-linear regime. Alternative splits, e.g. in Ambati et al. [15] and Miehe et al. [16] are specifically designed either for the linear case or based on the eigenvalues of the stresses.

A fourth-order crack energy density functional for the phase-field is chosen in this paper, see Borden et al. [17] and Weinberg and Hesch [18]. In conjunction with the newly proposed anisotropic split, this approach will improve the accuracy and the convergence properties of finite deformation phase-field fracture. An isogeometric finite element framework with hierarchical refinement (see Hesch et al. [19,20]) has been applied for the discretisation of the geometry and the phase-field.

Moreover, a mixed variational formulation of Hu–Washizu type (see, among many others, Zienkiewicz & Taylor [21]) is introduced in this paper for the first time in the context of phase-field problems. Crucially, the classical Rankine condition of brittle fracture (maximum of principal stresses) can now be formulated with primary variables of solution, i.e. in strains and stresses. For the numerical implementation, a local static condensation procedure is carried out, such that we obtain a formulation with computational cost comparable to that of the classical two-field formulation (i.e. displacement and phase-field).

For the ease of derivation and implementation of polyconvex phase-field fracture we follow the concept of Bonet et al. [22–24], which makes use of a tensor cross product operation that helps redefining the area and volume maps, two of the arguments which define polyconvexity. This tensor cross product operation as defined in [24] and its associated algebra simplify dramatically the directional derivatives of these two strain measures, featuring heavily in the formulation.

An outline of the present work is as follows. A brief revision of relevant aspects of nonlinear continuum mechanics in the context of polyconvex elasticity is carried out in Section 2. In Section 3, different phase-field approaches to brittle fracture are introduced. The coupled system of weak forms associated with the two-field formulation (in terms of displacements and the phase-field parameter) is also presented in Section 3. In Section 4 a Hu–Washizu type mixed variational principle is proposed, which is similar to the one presented in Ref. [22] and extended to the context of phase-field fracture. The spatial discretisations of the coupled weak forms both for the two-field and the Hu–Washizu mixed formulations are outlined in Section 5, followed by a variety of representative numerical examples in Section 6. Finally, conclusions are drawn in Section 7.

2. Basics and fundamentals

2.1. Geometry and kinematics

Let us consider the motion of a continuum which, in its initial or material configuration, is defined by a Lipschitz bounded domain $\mathcal{B}_0 \subset \mathbb{R}^3$ of boundary $\partial\mathcal{B}_0$ with outward unit normal $\boldsymbol{N}$. After the motion, the continuum occupies a spatial configuration defined by a domain $\mathcal{B}_t \subset \mathbb{R}^3$ of boundary $\partial\mathcal{B}_t$ with outward unit normal $\boldsymbol{n}$. The motion of the continuum $\mathcal{B}_0 \subset \mathbb{R}^3$ is defined by a pseudo-time t dependent mapping field

$$\boldsymbol{\varphi}(\boldsymbol{X}, t) : \mathcal{B}_0 \times \mathcal{I} \to \mathbb{R}^3, \tag{1}$$

which links a material particle from material configuration $\boldsymbol{X}$ to spatial configuration $\boldsymbol{x}$ at the pseudo-time $t \in \mathcal{I} = [0, T]$, where $T \in \mathbb{R}^+$, according to $\boldsymbol{x} = \boldsymbol{\varphi}(\boldsymbol{X}, t)$. The two-point deformation gradient tensor $\boldsymbol{F} : \mathcal{B}_0 \times \mathcal{I} \to \mathbb{R}^{3\times3}$, which relates a fibre of differential length from the material configuration $\mathrm{d}\boldsymbol{X}$ to the spatial configuration $\mathrm{d}\boldsymbol{x}$, namely $\mathrm{d}\boldsymbol{x} = \boldsymbol{F}\,\mathrm{d}\boldsymbol{X}$, is defined as the material gradient of the mapping $\boldsymbol{\varphi}$ [25], i.e,

$$\boldsymbol{F} := \nabla_{\boldsymbol{X}}\,\boldsymbol{\varphi} = \frac{\partial\boldsymbol{\varphi}}{\partial\boldsymbol{X}}. \tag{2}$$

Infinitesimal area vectors are mapped from initial $\mathrm{d}\boldsymbol{A}$ (colinear with $\boldsymbol{N}$) to final $\mathrm{d}\boldsymbol{a}$ (colinear with $\boldsymbol{n}$) configuration by means of the two-point cofactor or adjoint tensor $\boldsymbol{H} : \mathcal{B}_0 \times \mathcal{I} \to \mathbb{R}^{3\times3}$ as $\mathrm{d}\boldsymbol{a} = \boldsymbol{H}\,\mathrm{d}\boldsymbol{A}$, which is related to the deformation gradient $\boldsymbol{F}$ via the so-called Nanson's rule [25], i.e,

$$\boldsymbol{H} := \operatorname{cof}\boldsymbol{F} = (\det\boldsymbol{F})\,\boldsymbol{F}^{-T}. \tag{3}$$

Finally, $J : \mathcal{B}_0 \times \mathcal{I} \to \mathbb{R}$ represents the Jacobian or volume-map of the deformation, which relates differential volume elements in the material $\mathrm{d}V$ and spatial $\mathrm{d}v$ configurations as $\mathrm{d}v = J\,\mathrm{d}V$ and is defined as

$$J := \det\boldsymbol{F}. \tag{4}$$

With the help of the definition of the tensor cross product operation presented in [22], it is possible to rewrite the area map $\boldsymbol{H}$ (3) and the volume map J (4) as follows

$$\boldsymbol{H} := \frac{1}{2}(\boldsymbol{F}\times\boldsymbol{F}), \qquad J := \frac{1}{6}(\boldsymbol{F}\times\boldsymbol{F}) : \boldsymbol{F}, \tag{5}$$

where the application of the tensor cross product operation $\times$ on any two-point second order tensor $\boldsymbol{A}$ is defined in indicial notation as $(\boldsymbol{A}\times\boldsymbol{A})_{iI} = \mathcal{E}_{ijk}\mathcal{E}_{IJK}A_{jJ}A_{kK}$, with $\mathcal{E}_{ijk}$ (or $\mathcal{E}_{IJK}$) denoting the third order alternating tensor components and where the use of repeated indices implies summation, unless otherwise stated. The alternative definition of the area map in Eq. (5) based on the tensor cross product operation enables a dramatic simplification of the first and second directional derivatives of the cofactor $\boldsymbol{H}$ with respect to virtual and incremental variations of the geometry, namely $\delta\boldsymbol{\varphi}$ and $\Delta\boldsymbol{\varphi}$, as

$$\mathrm{D}\,\boldsymbol{H}[\delta\boldsymbol{\varphi}] = \boldsymbol{F}\times\nabla_{\boldsymbol{X}}\,\delta\boldsymbol{\varphi}, \quad \mathrm{D}^2\,\boldsymbol{H}[\delta\boldsymbol{\varphi},\,\Delta\boldsymbol{\varphi}] = \nabla_{\boldsymbol{X}}\,\delta\boldsymbol{\varphi}\times\nabla_{\boldsymbol{X}}\,\Delta\boldsymbol{\varphi}, \tag{6}$$

where use of

$$\mathrm{D}\,\boldsymbol{F}[\delta\boldsymbol{\varphi}] = \nabla_{\boldsymbol{X}}\,\delta\boldsymbol{\varphi} \tag{7}$$

has been made in Eq. (6). Additionally, the first and second directional derivatives of J based on the definition in Eq. (5) with respect to virtual and incremental variations $\delta\boldsymbol{\varphi}$ and $\Delta\boldsymbol{\varphi}$ are obtained as

$$\mathrm{D}\,J[\delta\boldsymbol{\varphi}] = \boldsymbol{H} : \nabla_{\boldsymbol{X}}\,\delta\boldsymbol{\varphi}, \quad \mathrm{D}^2\,J[\delta\boldsymbol{\varphi},\,\Delta\boldsymbol{\varphi}] = \boldsymbol{F} : (\nabla_{\boldsymbol{X}}\,\delta\boldsymbol{\varphi}\times\nabla_{\boldsymbol{X}}\,\Delta\boldsymbol{\varphi}). \tag{8}$$

2.2. Linear momentum balance equation

Let us consider the continuum $\mathcal{B}_0$ defined in Section 2.1. Dirichlet and Neumann boundary conditions can be prescribed on boundaries $\partial\mathcal{B}_0^u \subset \partial\mathcal{B}_0$ and $\partial\mathcal{B}_0^\sigma \subset \partial\mathcal{B}_0$, respectively, complying with

$$\partial\mathcal{B}_0^u \cup \partial\mathcal{B}_0^\sigma = \partial\mathcal{B}_0; \quad \partial\mathcal{B}_0^u \cap \partial\mathcal{B}_0^\sigma = \emptyset. \tag{9}$$

The space $\mathcal{V}^\varphi$ of virtual or admissible test functions for the mapping $\boldsymbol{\varphi}$ in (1) is defined as

$$\mathcal{V}^\varphi = \{\delta\boldsymbol{\varphi} \in \mathcal{H}^1(\mathcal{B}_0) | \delta\boldsymbol{\varphi} = \boldsymbol{0} \text{ on } \partial\mathcal{B}_0^u\}. \tag{10}$$

The balance of linear momentum for the continuum can be expressed in a total Lagrangian setting as

$$\int_{\mathcal{B}_0} \rho_0\delta\boldsymbol{\varphi}\cdot\ddot{\boldsymbol{\varphi}}\;dV + \int_{\mathcal{B}_0} \boldsymbol{P} : \nabla_{\boldsymbol{X}}\,\delta\boldsymbol{\varphi}\;\mathrm{d}V = \int_{\mathcal{B}_0} \delta\boldsymbol{\varphi}\cdot\bar{\boldsymbol{B}}\;\mathrm{d}V + \int_{\partial\mathcal{B}_0^\sigma} \delta\boldsymbol{\varphi}\cdot\bar{\boldsymbol{T}}\;\mathrm{d}A, \quad \forall\delta\boldsymbol{\varphi} \in \mathcal{V}^\varphi, \tag{11}$$

where ρ_0 represents the material density, $(\ddot{\bullet})$ denotes double differentiation with respect to time of the variable $(\bullet)$ and $\boldsymbol{P}$ denotes the first Piola–Kirchhoff stress tensor. The external contributions, namely the right hand side of above Eq. (11), include the traction force per unit of undeformed area $\bar{\boldsymbol{T}}$ defined as $\boldsymbol{P}\boldsymbol{N} = \bar{\boldsymbol{T}}$ on $\partial\mathcal{B}_0^\sigma$ and the body force per unit of undeformed volume $\bar{\boldsymbol{B}}$ in $\mathcal{B}_0$.

Remark 1. For the remaining of the article we omit inertia terms and thus, we do not specify initial conditions. All results can easily be transferred to transient fracture problems, investigated in detail in Borden et al. [26] and in Hesch & Weinberg [27]. Further investigation in the context of impact mechanics can also be found in Hesch et al. [19].

2.3. Polyconvexity of the strain energy density function

The variational statement in Eq. (11) requires a suitable constitutive law in order to relate the first Piola–Kirchhoff stress tensor $\boldsymbol{P}$ to the deformation gradient tensor $\nabla_{\boldsymbol{X}}\,\boldsymbol{\varphi}$. As it is customary in the case of hyperelasticity, this constitutive law can be given in terms of a strain energy density function Ψ per unit of undeformed volume, defined as

$$\Psi = \Psi\,(\nabla_{\boldsymbol{X}}\,\boldsymbol{\varphi})\,. \tag{12}$$

Computation of the directional derivative of Ψ leads to an expression for the first Piola–Kirchhoff stress tensor $\boldsymbol{P}$ as

$$\mathrm{D}\,\Psi[\delta\boldsymbol{\varphi}] = \boldsymbol{P} : \nabla_{\boldsymbol{X}}\,\delta\boldsymbol{\varphi}; \qquad \boldsymbol{P} = \frac{\partial\,\Psi\,(\nabla_{\boldsymbol{X}}\,\boldsymbol{\varphi})}{\partial\nabla_{\boldsymbol{X}}\,\boldsymbol{\varphi}} \tag{13}$$

where $\delta\boldsymbol{\varphi}$ represents virtual variations of the deformation. Appropriate constitutive restrictions on Ψ are necessary to obtain well-defined, physically admissible solutions. An accepted constitutive restriction is ellipticity (or rank-one convexity) of the strain energy density, with very important physical implications. In particular, satisfaction of this constitutive restriction is intimately related to the existence of material stability and it automatically guarantees the existence and propagation of real wave speeds in the material in the vicinity of an equilibrium configuration (also known as Legendre–Hadamard condition), see Truesdell & Noll [28].

Strict convexity of the strain energy density function with respect to the deformation gradient tensor $\nabla_{\boldsymbol{X}}\,\boldsymbol{\varphi}$ satisfies the Legendre–Hadamard condition. However, this condition is too stringent and it is incompatible with the principle of material frame indifference, see Marsden & Hughes [29] for details. It precludes the onset of buckling and the requirement that $\det(\nabla_{\boldsymbol{X}}\,\boldsymbol{\varphi}) \to \mathbb{R}^+$. In contrast, polyconvexity in the sense of Ball [11] is now well accepted as a fundamental mathematical requirement that should be satisfied by admissible strain energy functions used to describe elastic materials in the large strain regime. Polyconvex energy functionals satisfy the Legendre–Hadamard condition and do not suffer the inherent unphysical behaviour associated with strictly convex energy density functionals. Essentially, the strain energy density must be a function of the deformation gradient via a convex multi-variable functional W as

$$\Psi(\nabla_{\boldsymbol{X}}\,\boldsymbol{\varphi}) \overset{\text{pol}}{=} W(\boldsymbol{F}, \boldsymbol{H}, J), \tag{14}$$

where $W : \mathbb{R}^{3\times3} \times \mathbb{R}^{3\times3} \times \mathbb{R} \to \mathbb{R}$ is convex for all material points $\boldsymbol{X}$ with respect to the 19 variables of $\boldsymbol{F}$, $\boldsymbol{H}$ and J. Moreover, the requirement for objectivity or material frame indifference implies that W must be independent of the rotational components of $\boldsymbol{F}$ and $\boldsymbol{H}$ and hence, must be a function of these tensors via symmetric tensors such as $\boldsymbol{F}^T\boldsymbol{F}$ (also known as the right Cauchy–Green tensor $\boldsymbol{C}$) and $\boldsymbol{H}^T\boldsymbol{H}$. For the case of isotropic hyperelasticity, the strain energy density Ψ is usually defined as

$$\Psi(\nabla_0\boldsymbol{\varphi}) \overset{\text{pol}}{=} W(\boldsymbol{F}, \boldsymbol{H}, J) \overset{\text{iso}}{=} w(II_{\boldsymbol{F}}, II_{\boldsymbol{H}}, J), \tag{15}$$

where $II_\bullet$ denotes $II_\bullet = (\bullet : \bullet)$ [25].[1] As an example, the strain energy density function of a compressible Mooney–Rivlin material can be simply expressed as

$$w_{MR}(II_{\boldsymbol{F}}, II_{\boldsymbol{H}}, J) = \alpha\,(II_{\boldsymbol{F}} - 3) + \beta\,(II_{\boldsymbol{H}} - 3) + f(J), \tag{16}$$

where $f(J)$ must be a convex function of J. Moreover, α and β are two positive material parameters. A possible definition of the convex function $f(J)$ is

$$f(J) = -2\,(\alpha + 2\beta)\ln(J) + \frac{\lambda}{2}\,(J-1)^2\,, \tag{17}$$

which guarantees that the energy and the stresses at the origin (i.e. undeformed configuration) vanish. In above expression (17), λ represents another positive material parameter.

In this paper, an additive decomposition of the strain energy density function into its isochoric and volumetric contributions will be followed. As explained in forthcoming sections, this split proves physically convenient for the proposed formulation of coupled phase-field fracture problems developed in this paper. This additive split, also very typical in the context of truly and nearly incompressible elasticity, requires the strain energy W to be defined as [22,24,30,31]

$$W(\boldsymbol{F}, \boldsymbol{H}, J) = \bar{W}(\boldsymbol{F}, \boldsymbol{H}, J) + U(J), \tag{18}$$

[1] Notice that the invariants $\{II_{\boldsymbol{F}}, II_{\boldsymbol{H}}, J\}$ can be related to the well known principal invariants of the right Cauchy–Green deformation tensor $\boldsymbol{C}$, namely $\{I_1, I_2, I_3\}$ (refer to [13]) as

$$II_{\boldsymbol{F}} = I_1; \qquad II_{\boldsymbol{H}} = I_2; \qquad J^2 = I_3.$$

where U must be a convex function of J accounting for the volumetric component of the deformation and $\bar{W}(\boldsymbol{F}, \boldsymbol{H}, J)$ must be a polyconvex function of $\{\boldsymbol{F}, \boldsymbol{H}, J\}$ which must lead to a pure deviatoric stress tensor. The latter can be guaranteed if the function is defined in terms of the isochoric components of $\{\boldsymbol{F}, \boldsymbol{H}\}$, defined as $\bar{\boldsymbol{F}} = J^{-1/3}\boldsymbol{F}$ and $\bar{\boldsymbol{H}} = J^{-2/3}\boldsymbol{H}$, respectively. More specifically, for the case of isotropic elasticity, $\bar{W}$ can be expressed as

$$\bar{W}(\boldsymbol{F}, \boldsymbol{H}, J) \overset{\text{iso}}{=} \bar{w}\left(II_{\bar{\boldsymbol{F}}}, II_{\bar{\boldsymbol{H}}}\right). \tag{19}$$

As an example, the isochoric strain energy density function of a nearly incompressible Mooney–Rivlin material can be defined as

$$\bar{w}_{MR}\left(II_{\bar{\boldsymbol{F}}}, II_{\bar{\boldsymbol{H}}}\right) = \gamma\left(II_{\bar{\boldsymbol{F}}} - 3\right) + \zeta\left(\left(II_{\bar{\boldsymbol{H}}}\right)^{3/2} - 3^{3/2}\right), \tag{20}$$

where γ and ζ represent positive material parameters. In addition, a possible definition of the convex function $U(J)$ could be

$$U(J) = \frac{\kappa}{2}(J-1)^2, \tag{21}$$

where κ represents another positive material parameter. As above, material parameters $\{\gamma, \zeta, \kappa\}$ can be obtained from a suitable material characterisation [22,32].

Remark 2. In the special case of two-dimensional plane strain,[2] the deformation gradient tensor adopts the following expression

$$\nabla_{\boldsymbol{X}}\boldsymbol{\varphi} = \begin{bmatrix} \boldsymbol{F}_{2D} & \boldsymbol{0} \\ \boldsymbol{0}^T & 1 \end{bmatrix}, \tag{22}$$

where $\boldsymbol{F}_{2D}$ denotes the deformation gradient tensor in the plane of the deformation. In this case, polyconvexity of the strain energy can be postulated as

$$\Psi(\nabla_{\boldsymbol{X}}\boldsymbol{\varphi}) = W(\boldsymbol{F}_{2D}, j), \tag{23}$$

where $W : \mathbb{R}^{2\times 2} \times \mathbb{R} \to \mathbb{R}$ must be convex for all material points $\boldsymbol{X}$ with respect to the 4 independent variables of $\boldsymbol{F}_{2D}$ and the Jacobian in the plane of the deformation, denoted as $j := \det \boldsymbol{F}_{2D}$. In this case, the cofactor is no-longer an independent variable and can be related to both $\boldsymbol{F}_{2D}$ and j as

$$\boldsymbol{H} = \begin{bmatrix} \boldsymbol{H}_{2D} & \boldsymbol{0} \\ \boldsymbol{0}^T & j \end{bmatrix}; \qquad \boldsymbol{H}_{2D} = \text{tr}\boldsymbol{F}_{2D}\boldsymbol{I}_{2D} - \boldsymbol{F}_{2D}^T, \tag{24}$$

where $\boldsymbol{I}_{2D}$ denotes the 2×2 identity matrix. Combination of Eqs. (5) and $(24)_b$ enables the two-dimensional Jacobian j for the case of plane strain to be related to the two-dimensional deformation gradient tensor $\boldsymbol{F}_{2D}$ as

$$j = J = \frac{1}{3}(\boldsymbol{H} : \boldsymbol{F}) = \frac{1}{3}(\boldsymbol{H}_{2D} : \boldsymbol{F}_{2D} + j) \Rightarrow j = \frac{1}{2}\left((\text{tr}\boldsymbol{F}_{2D})^2 - \text{tr}\left(\boldsymbol{F}_{2D}\boldsymbol{F}_{2D}\right)\right). \tag{25}$$

Based on the above identity (24), it is possible to rewrite the invariants $II_{\boldsymbol{F}}$, $II_{\bar{\boldsymbol{F}}}$, $II_{\boldsymbol{H}}$ and $II_{\bar{\boldsymbol{H}}}$ as

$$II_{\boldsymbol{F}} = II_{\boldsymbol{F}_{2D}} + 1; \qquad II_{\boldsymbol{H}} = II_{\boldsymbol{F}_{2D}} + j^2, \tag{26a}$$

$$II_{\bar{\boldsymbol{F}}} = j^{-2/3}\left(II_{\boldsymbol{F}_{2D}} + 1\right); \qquad II_{\bar{\boldsymbol{H}}} = j^{-4/3}II_{\boldsymbol{F}_{2D}} + j^{2/3}. \tag{26b}$$

Therefore, for instance, the compressible polyconvex constitutive model in Eq. (16) can be reduced for plane strain as

$$w^{2D}_{MR}(II_{\boldsymbol{F}_{2D}}, j) = (\alpha+\beta)\left(II_{\boldsymbol{F}_{2D}} - 2\right) + \underbrace{\beta\left(j^2 - 1\right) + f(j)}_{\tilde{f}(j)}. \tag{27}$$

[2] Plane stress problems will not be considered in this paper.

Similarly, the polyconvex constitutive model in Eq. (20) can be reduced for plane strain problems as well

$$w_{MR}^{2D}\left(II_{\boldsymbol{F}_{2D}}, j\right) = \gamma\left(j^{-2/3}\left(II_{\boldsymbol{F}_{2D}}+1\right)-3\right)+\zeta\left(\left(j^{-4/3}II_{\boldsymbol{F}_{2D}}+j^{2/3}\right)^{3/2}-3^{3/2}\right). \tag{28}$$

2.4. Conjugate stresses and elasticity tensors

As shown in Refs. [22,24,32–35], the definition of polyconvexity enables a one-to-one and invertible relationship between the three strain measures $\boldsymbol{F}$, $\boldsymbol{H}$ and J and their respective work conjugates $\boldsymbol{\Sigma}_{\boldsymbol{F}}$, $\boldsymbol{\Sigma}_{\boldsymbol{H}}$ and Σ_J, defined as

$$\boldsymbol{\Sigma}_{\boldsymbol{F}} := \frac{\partial W}{\partial \boldsymbol{F}}; \qquad \boldsymbol{\Sigma}_{\boldsymbol{H}} := \frac{\partial W}{\partial \boldsymbol{H}}; \qquad \Sigma_J := \frac{\partial W}{\partial J}. \tag{29}$$

For instance, for the compressible Mooney–Rivlin constitutive law defined in Eq. (16), the work conjugates are

$$\boldsymbol{\Sigma}_{\boldsymbol{F}} = 2\alpha\boldsymbol{F}; \qquad \boldsymbol{\Sigma}_{\boldsymbol{H}} = 2\beta\boldsymbol{H}; \qquad \Sigma_J = f'(J). \tag{30}$$

Similarly, for the constitutive model defined by Eqs. (20) and (21), the work conjugates are now defined as

$$\boldsymbol{\Sigma}_{\boldsymbol{F}} = 2\gamma J^{-2/3}\boldsymbol{F}; \quad \boldsymbol{\Sigma}_{\boldsymbol{H}} = 3\zeta J^{-2} II_{\boldsymbol{H}}\boldsymbol{H}; \quad \Sigma_J = -\frac{2}{3}\gamma J^{-5/3} II_{\boldsymbol{F}} - 2\zeta J^{-3} II_{\boldsymbol{H}}^{3/2} + U'(J). \tag{31}$$

As already presented in [22–24], a relationship can be established between the above work conjugates and the first Piola–Kirchhoff stress tensor $\boldsymbol{P}$ following the computation of the directional derivative of the strain energy density W with respect to virtual or admissible variations of the geometry $\delta\boldsymbol{\varphi}$, namely

$$\begin{aligned} \mathrm{D}\, W[\delta\boldsymbol{F}, \delta\boldsymbol{H}, \delta J] &= \boldsymbol{\Sigma}_{\boldsymbol{F}} : \delta\boldsymbol{F} + \boldsymbol{\Sigma}_{\boldsymbol{H}} : \delta\boldsymbol{H} + \Sigma_J\, \delta J \\ &= (\boldsymbol{\Sigma}_{\boldsymbol{F}} + \boldsymbol{\Sigma}_{\boldsymbol{H}} \times \boldsymbol{F} + \Sigma_J \boldsymbol{H}) : \nabla_{\boldsymbol{X}}\, \delta\boldsymbol{\varphi}, \end{aligned} \tag{32}$$

where use of Eqs. (6)–(8) has been made in Eq. (32). Comparison of Eq. (32) and $(13)_a$ enables to finally re-define the first Piola–Kirchhoff stress tensor $\boldsymbol{P}$ in terms of the work conjugates in (29) as

$$\boldsymbol{P} = \boldsymbol{\Sigma}_{\boldsymbol{F}} + \boldsymbol{\Sigma}_{\boldsymbol{H}} \times \boldsymbol{F} + \Sigma_J \boldsymbol{H}. \tag{33}$$

With a Newton–Raphson type of solution process in mind, it is useful to derive the tangent elasticity operator. Using Eq. (33) for the first Piola–Kirchhoff stress tensor it is now possible to derive a physically insightful representation of the tangent elasticity operator as

$$\mathrm{D}^2\, W[\delta\boldsymbol{\varphi}; \Delta\boldsymbol{\varphi}] = [\mathbb{S}_\delta]^T\, [\mathbb{H}_W]\, [\mathbb{S}_\Delta] + [\boldsymbol{\Sigma}_H + \Sigma_J \boldsymbol{F}] : (\nabla_{\boldsymbol{X}}\, \delta\boldsymbol{\varphi} \times \nabla_{\boldsymbol{X}}\, \Delta\boldsymbol{\varphi}), \tag{34}$$

with the operators $[\mathbb{S}_\delta]^T$ and $[\mathbb{S}_\Delta]$ defined as

$$[\mathbb{S}_\delta]^T = [\nabla_{\boldsymbol{X}}\, \delta\boldsymbol{\varphi} :\ \nabla_{\boldsymbol{X}}\, \delta\boldsymbol{\varphi} \times \boldsymbol{F} :\ \nabla_{\boldsymbol{X}}\, \delta\boldsymbol{\varphi} : \boldsymbol{H}]; \qquad [\mathbb{S}_\Delta] = \begin{bmatrix} : \nabla_{\boldsymbol{X}}\, \Delta\boldsymbol{\varphi} \\ : \nabla_{\boldsymbol{X}}\, \Delta\boldsymbol{\varphi} \times \boldsymbol{F} \\ \nabla_{\boldsymbol{X}}\, \Delta\boldsymbol{\varphi} : \boldsymbol{H} \end{bmatrix}, \tag{35}$$

and where the Hessian operator $[\mathbb{H}_W]$ in Eq. (34) is defined as

$$[\mathbb{H}_W] = \begin{bmatrix} \dfrac{\partial^2 W}{\partial \boldsymbol{F} \partial \boldsymbol{F}} & \dfrac{\partial^2 W}{\partial \boldsymbol{F} \partial \boldsymbol{H}} & \dfrac{\partial^2 W}{\partial \boldsymbol{F} \partial J} \\ \dfrac{\partial^2 W}{\partial \boldsymbol{H} \partial \boldsymbol{F}} & \dfrac{\partial^2 W}{\partial \boldsymbol{H} \partial \boldsymbol{H}} & \dfrac{\partial^2 W}{\partial \boldsymbol{H} \partial J} \\ \dfrac{\partial^2 W}{\partial J \partial \boldsymbol{F}} & \dfrac{\partial^2 W}{\partial J \partial \boldsymbol{H}} & \dfrac{\partial^2 W}{\partial J \partial J} \end{bmatrix}. \tag{36}$$

As discussed in [22,24], polyconvexity dictates that the first (constitutive) term on the right hand side of Eq. (34) is necessarily positive for a virtual field $\delta\boldsymbol{\varphi} = \Delta\boldsymbol{\varphi}$ and thus, buckling can only be induced by the second (geometrical) term. As also presented in Refs. [22,24], the representation of the tangent operator in (34) enables to appreciate the

relationship between polyconvexity and ellipticity (or rank-one convexity). For instance, the Hessian operator for the constitutive model in Eq. (16) is obtained as

$$[\mathbb{H}_W] = \begin{bmatrix} 2\alpha\boldsymbol{\mathcal{I}} & \mathbf{0} & \mathbf{0} \\ \mathbf{0} & 2\beta\boldsymbol{\mathcal{I}} & \mathbf{0} \\ \mathbf{0} & \mathbf{0} & f''(J) \end{bmatrix}, \tag{37}$$

where $\boldsymbol{\mathcal{I}}$ denotes the fourth order identity tensor with indices $\mathcal{I}_{iIjJ} = \delta_{iI}\delta_{jJ}$. It is easy to observe the positive definite nature of the Hessian operator provided that the constants α and β are positive and that the function $f(J)$ is convex, as that in Eq. (17). Alternatively, for the constitutive model in Eq. (16), a more involved Hessian operator $[\mathbb{H}_W]$ reads

$$[\mathbb{H}_W] = \begin{bmatrix} 2\gamma J^{-2/3}\boldsymbol{\mathcal{I}} & \mathbf{0} & -4/3\gamma J^{-5/3}\boldsymbol{F} \\ \mathbf{0} & 3\zeta J^{-2}(II_{\boldsymbol{C}}^{-1/2}\boldsymbol{H}\otimes\boldsymbol{H} + II_{\boldsymbol{C}}^{1/2}\boldsymbol{\mathcal{I}}) & -6\zeta J^{-3}II_{\boldsymbol{C}}^{1/2}\boldsymbol{H} \\ -4/3\gamma J^{-5/3}\boldsymbol{F}^T & -6\zeta J^{-3}II_{\boldsymbol{C}}^{1/2}\boldsymbol{H}^T & W_{JJ} \end{bmatrix}, \tag{38}$$

where $W_{JJ} = 10/9J^{-8/3}\gamma I_{\boldsymbol{C}} + 6\zeta J^{-4}II_{\boldsymbol{C}}^{3/2} + U''(J)$. A proof of the positive definiteness of the Hessian operator $[\mathbb{H}_W]$ in Eq. (38) is outlined in Schröder & Neff [13], Appendix C.

3. Phase-field fracture models

3.1. Phase-field fracture description

This section describes the formulation of classical brittle fracture problems employing the phase-field method. More sophisticated constitutive models including thermal effects and/or plasticity for the modelling of ductile fracture can be considered, as shown in [16,36]. However, without loss of generality, this paper focuses on the modelling of elastic brittle fracture. With this in mind, the propagation of the fracture pattern, initially localised at an internal boundary $\Gamma_0^{cr} \subset \mathcal{B}_0$, is described by an auxiliary field $\mathfrak{s}$ defined as the crack phase-field. A Lagrangian description of this phase-field variable $\mathfrak{s}$ is followed, where $\mathfrak{s}$ is related to each material particle $\boldsymbol{X}$ as

$$\mathfrak{s}(\boldsymbol{X}, t) : \mathcal{B}_0 \times \mathcal{I} \to \mathbb{R}, \quad \mathfrak{s} \in [0, 1], \tag{39}$$

where the value $\mathfrak{s} = 0$ refers to the undamaged state and $\mathfrak{s} = 1$ to the fully broken state of the material. The unknowns $\{\boldsymbol{\varphi},\ \mathfrak{s}\}$ form a configuration space in $\mathbb{R}^4$, representing the primal degrees of freedom to be found for all pseudo-times of interest. In the phase-field approach, the crack interface is regularised and the evolution of the phase-field is governed by the partial differential equation associated with the regularised profile of the crack. The fracture energy E^{cr} is defined as

$$E^{cr} = \int_{\Gamma_0^{cr}} g_c \ \mathrm{d}\Gamma, \tag{40}$$

where g_c denotes the critical local fracture energy density, which can be approximated using the crack surface density function $\gamma(\mathfrak{s})$ (related to the regularised profile of the crack)

$$\int_{\Gamma_0^{cr}} g_c \ \mathrm{d}\Gamma \approx \int_{\mathcal{B}_0} g_c\gamma(\mathfrak{s}) \ \mathrm{d}V. \tag{41}$$

This approach postulates that the material fails locally upon the attainment of a specific fracture energy, represented by g_c. A commonly used expression for $\gamma(\mathfrak{s})$ is given by the second order Allen–Cahn energy density functional, defined as

$$\gamma(\mathfrak{s}) = \frac{1}{2l}\mathfrak{s}^2 + \frac{l}{2}\nabla_{\boldsymbol{X}}\,\mathfrak{s}\cdot\nabla_{\boldsymbol{X}}\,\mathfrak{s}, \tag{42}$$

where the intrinsic length scale parameter l controls the regularisation zone.[3] Alternatively, a higher order regularisation of the crack topology can be utilised to obtain better accuracy and convergence rates of the numerical solution

[3] The length scale parameter l has a substantial impact on the crack initialisation and can be regarded as a material parameter, see Miehe et al. [16].

(see Weinberg & Hesch [18] and Borden et al. [17] for details), such as the fourth order Cahn–Hilliard type profile regularisation, defined as

$$\gamma(\mathfrak{s}) = \frac{1}{4l}\mathfrak{s}^2 + \frac{l}{2}\nabla_{\boldsymbol{X}}\,\mathfrak{s}\cdot\nabla_{\boldsymbol{X}}\,\mathfrak{s} + \frac{l^3}{4}\,(\Delta_{\boldsymbol{X}}\mathfrak{s})^2\,, \tag{43}$$

where $\Delta_{\boldsymbol{X}}(\bullet)$ represents the material Laplacian operator of the field $\bullet$.

Remark 3. Notice the material character of the gradient $\nabla_{\boldsymbol{X}}\,\bullet$ and Laplacian $\Delta_{\boldsymbol{X}}\bullet$ operators in expressions (42) and (43). This is in contrast to the case of small strains, where, logically, no distinction between spatial or material operators is necessary. Although their spatial counterparts could have also been used (e.g. $\nabla_{\boldsymbol{x}}\bullet$ and $\Delta_{\boldsymbol{x}}\bullet$), this would lead to cumbersome contributions (via pull-back and push-forward operations) to the tangent operator (necessary in case of using a Newton–Raphson solution type approach).

3.2. Variational formulation of coupled phase-field model of fracture

Next, we present the set of governing equations (in a weak or variational sense) emerging in the modelling of fracture via the phase-field method. For that purpose, it is useful to introduce the *coupled* total potential energy $E^{tot}(\boldsymbol{\varphi},\mathfrak{s})$ of the continuum, defined in a total Lagrangian manner in $\mathcal{B}_0$, as

$$E^{tot}(\boldsymbol{\varphi},\mathfrak{s}) = \int_{\mathcal{B}_0} \Psi^{\mathfrak{s}}(\nabla_{\boldsymbol{X}}\,\boldsymbol{\varphi},\mathfrak{s})\;\mathrm{d}V + \int_{\mathcal{B}_0} g_c\gamma(\mathfrak{s})\;\mathrm{d}V + \Pi^{ext}(\boldsymbol{\varphi}), \tag{44}$$

where the first term on the right hand side represents the *possibly* damaged phase-field dependent strain energy, the second term denotes the regularised fracture energy and the third term symbolises the external work acting on the system. A suitable definition of the phase-field dependent strain energy density function $\Psi^{\mathfrak{s}}(\nabla_{\boldsymbol{X}}\,\boldsymbol{\varphi},\mathfrak{s})$ will be provided in forthcoming sections.

The set of weak forms for the coupled phase-field problem in consideration is now obtained by computing the directional derivative of the total potential energy E^{tot} in Eq. (44) with respect to admissible variations $\delta\boldsymbol{\varphi}$ and $\delta\mathfrak{s}$, yielding

$$\begin{aligned}
\mathrm{D}\,E^{tot}[\delta\boldsymbol{\varphi}] &= \int_{\mathcal{B}_0} \boldsymbol{P} : \nabla_{\boldsymbol{X}}\,\delta\boldsymbol{\varphi}\;\mathrm{d}V - \int_{\mathcal{B}_0} \delta\boldsymbol{\varphi}\cdot\bar{\boldsymbol{B}}\;\mathrm{d}V - \int_{\partial\mathcal{B}_0^{\sigma}} \delta\boldsymbol{\varphi}\cdot\bar{\boldsymbol{T}}\;\mathrm{d}A = 0, \qquad \forall\delta\boldsymbol{\varphi}\in\mathcal{V}^{\varphi},\\
\mathrm{D}\,E^{tot}[\delta\mathfrak{s}] &= \int_{\mathcal{B}_0} \mathcal{H}\delta\mathfrak{s}\;\mathrm{d}V + \int_{\mathcal{B}_0} g_c\,\mathrm{D}\,\gamma(\mathfrak{s})[\delta\mathfrak{s}]\;\mathrm{d}V = 0, \qquad \forall\delta\mathfrak{s}\in\mathcal{V}_i^{\mathfrak{s}},
\end{aligned} \tag{45}$$

with

$$\boldsymbol{P} := \frac{\partial\,\Psi^{\mathfrak{s}}(\nabla_{\boldsymbol{X}}\,\boldsymbol{\varphi},\mathfrak{s})}{\partial\nabla_{\boldsymbol{X}}\,\boldsymbol{\varphi}}; \qquad \mathcal{H} := \frac{\partial\,\Psi^{\mathfrak{s}}(\nabla_{\boldsymbol{X}}\,\boldsymbol{\varphi},\mathfrak{s})}{\partial\mathfrak{s}}, \tag{46}$$

where $\boldsymbol{P}$ represents the first Piola–Kirchhoff stress tensor and $\mathcal{H}$ contains the driving force of the phase-field. Moreover, the space of admissible test functions $\mathcal{V}^{\varphi}$ has already been defined in Eq. (10) and $\mathcal{V}_i^{\mathfrak{s}}$ denotes the space of admissible test functions for the phase-field, which depends on the choice of crack energy density $\gamma(\mathfrak{s})$ under consideration (refer to the previous Section). In particular, the set of admissible test functions for the second order Allen–Cahn crack energy functional reads

$$\mathcal{V}_1^{\mathfrak{s}} = \{\delta\mathfrak{s}\in\mathcal{H}^1(\mathcal{B}_0)\,|\,\delta\mathfrak{s}=0\ \text{on}\ \Gamma_0^{cr}\}, \tag{47}$$

i.e. the fully broken state on Γ_0^{cr} is treated as a Dirichlet-type constraint. Alternatively, the set of admissible test functions $\mathcal{V}_2^{\mathfrak{s}}$ for the fourth order Cahn–Hilliard crack energy density functional (43) is defined as

$$\mathcal{V}_2^{\mathfrak{s}} = \{\delta\mathfrak{s}\in\mathcal{H}^2(\mathcal{B}_0)\,|\,\delta\mathfrak{s}=0\ \text{on}\ \Gamma_0^{cr}\}. \tag{48}$$

Provided that a suitable alternative definition of the phase-field dependent strain energy density $\Psi^{\mathfrak{s}}(\nabla_{\boldsymbol{X}}\,\boldsymbol{\varphi},\mathfrak{s})$ is given in terms of the strain measures $\{\boldsymbol{F},\boldsymbol{H},J\}$ (as will be shown in forthcoming sections), it is possible to re-write $\boldsymbol{P}$ as

in Eq. (33), with the conjugate stresses $\boldsymbol{\Sigma}_{\boldsymbol{F}}$, $\boldsymbol{\Sigma}_{\boldsymbol{H}}$ and Σ_J also depending upon the phase-field parameter $\mathfrak{s}$. Particularisation of Eq. $(45)_b$ to the Allen–Cahn density functional (42) yields

$$\mathrm{D}\, E^{tot}[\delta\mathfrak{s}] = \int_{\mathcal{B}_0} \mathcal{H}\delta\mathfrak{s}\, \mathrm{d}V + \int_{\mathcal{B}_0} \left(\delta\mathfrak{s}\frac{g_c}{l}\mathfrak{s} + g_c l\, (\nabla_{\boldsymbol{X}}\, \delta\mathfrak{s}) \cdot (\nabla_{\boldsymbol{X}}\, \mathfrak{s}) \right) \mathrm{d}V = 0, \quad \forall \delta\mathfrak{s} \in \mathcal{V}_1^{\mathfrak{s}}. \tag{49}$$

Analogously, particularisation of Eq. $(45)_b$ to the Cahn–Hilliard crack energy density functional (43) yields

$$\begin{aligned} \mathrm{D}\, E^{tot}[\delta\mathfrak{s}] = \int_{\mathcal{B}_0} \mathcal{H}\delta\mathfrak{s}\, \mathrm{d}V + \int_{\mathcal{B}_0} \Bigg(& \delta\mathfrak{s}\frac{g_c}{2l}\mathfrak{s} + g_c l\, (\nabla_{\boldsymbol{X}}\, \delta\mathfrak{s}) \cdot (\nabla_{\boldsymbol{X}}\, \mathfrak{s}) \\ & + \frac{g_c l^3}{2}\, (\Delta_{\boldsymbol{X}}\delta\mathfrak{s})\, (\Delta_{\boldsymbol{X}}\mathfrak{s}) \Bigg) \mathrm{d}V = 0, \quad \forall \delta\mathfrak{s} \in \mathcal{V}_2^{\mathfrak{s}}. \end{aligned} \tag{50}$$

3.3. Constitutive crack strain energy density functional

The objective of this section is to propose a suitable definition of the *damaged* strain energy density $\Psi^{\mathfrak{s}}(\nabla_{\boldsymbol{X}}\, \boldsymbol{\varphi}, \mathfrak{s})$. The simplest approach consists of multiplying the *undamaged* strain energy density $\Psi(\nabla_{\boldsymbol{X}}\, \boldsymbol{\varphi})$ by a degradation function $g(\mathfrak{s})$ as

$$\Psi^{\mathfrak{s}}(\nabla_{\boldsymbol{X}}\, \boldsymbol{\varphi}, \mathfrak{s}) := g(\mathfrak{s})\, \Psi(\nabla_{\boldsymbol{X}}\, \boldsymbol{\varphi}). \tag{51}$$

This approach is usually referred to as isotropic degeneration, as it is sensitive to both tension and compression components. The degradation function $g(\mathfrak{s})$ is defined as a monotonically decreasing function complying with the following restrictions, i.e. $g(0) = 1$, $g(1) = 0$ and $g'(1) = 0$. The simplest function $g(\mathfrak{s})$ satisfying the aforementioned constraints is $g(\mathfrak{s}) = (1 - \mathfrak{s})^2$. Alternatively, a more sophisticated definition of $g(\mathfrak{s})$ is the following cubic function

$$g(\mathfrak{s}) = \big(a_g - 2\big)\, (1 - \mathfrak{s})^3 + \big(3 - a_g\big)\, (1 - \mathfrak{s})^2; \qquad a_g \geq 0, \tag{52}$$

which complies with the above restrictions and with a_g an arbitrary modelling parameter in the range $(0, 2]$. Note that the above cubic degradation function (52) degenerates to the simpler quadratic degradation function $(1 - \mathfrak{s})^2$ by setting $a_g = 2$. In order to avoid that small strains, even far from a crack, contribute noticeably to the computed fracture energy (cf. Borden [37]), we advocate in this paper the cubic degradation function (52) in conjunction with the use of small values of the modelling parameter a_g.

In contrast to (51), a more reasonable formulation from the physical standpoint would require the fracture propagation to be exclusively sensitive to a *tension* state of deformation. This *tension sensitive* approach is usually referred to as anisotropic split [9,27]. A novel anisotropic split is presented in the following section.

3.3.1. Proposed anisotropic split in terms of the principal invariants

In this section, a novel anisotropic split of the damaged strain energy density $\Psi^{\mathfrak{s}}$ is introduced following a polyconvex representation of the undamaged strain energy density Ψ as that formulated in Eq. (14) and a further additive split of this energy density as that proposed in Eq. (18). Specifically, $\Psi^{\mathfrak{s}}$ is rewritten as

$$\Psi^{\mathfrak{s}}(\nabla_{\boldsymbol{X}}\, \boldsymbol{\varphi}, \mathfrak{s}) = W^{\mathfrak{s}}(\boldsymbol{F}, \boldsymbol{H}, J, \mathfrak{s}) = \bar{W}^{\mathfrak{s}}(\boldsymbol{F}, \boldsymbol{H}, J, \mathfrak{s}) + U^{\mathfrak{s}}(J, \mathfrak{s}), \tag{53}$$

where $W^{\mathfrak{s}}$ is a polyconvex function *with respect to the strain measures* $\{\boldsymbol{F}, \boldsymbol{H}, J\}$ (for any value of the phase-field $\mathfrak{s}$) and $\bar{W}^{\mathfrak{s}}$ and $U^{\mathfrak{s}}$ its isochoric and volumetric contributions, respectively. For the definition of a suitable anisotropic split, we further introduce the tensile and compressive parts of the invariant arguments of such decomposition, namely $I\!I_{\bar{\boldsymbol{F}}}$, $I\!I_{\bar{\boldsymbol{H}}}$ and J, as

$$\begin{aligned} I\!I^{\pm}_{\bar{\boldsymbol{F}}} &:= J^{-2/3} \left(\frac{(I\!I_{\boldsymbol{F}} - 3) \pm |I\!I_{\boldsymbol{F}} - 3|}{2} + 3 \right), \\ I\!I^{\pm}_{\bar{\boldsymbol{H}}} &:= J^{-4/3} \left(\frac{(I\!I_{\boldsymbol{H}} - 3) \pm |I\!I_{\boldsymbol{H}} - 3|}{2} + 3 \right), \\ J^{\pm} &:= \frac{(J - 1) \pm |J - 1|}{2} + 1, \end{aligned} \tag{54}$$

where the superscripts + and − refer to the tensile and compressive components, respectively. In this case, the strain energy density contributions $W^{\mathfrak{s}}$ and $U^{\mathfrak{s}}$ in (53) can then be formulated as

$$\bar{W}^{\mathfrak{s}}(\boldsymbol{F},\boldsymbol{H},J,\mathfrak{s}) = \bar{w}^{\mathfrak{s}}\left(II^{\pm}_{\bar{\boldsymbol{F}}}, II^{\pm}_{\bar{\boldsymbol{H}}}, \mathfrak{s}\right); \qquad U^{\mathfrak{s}}(J,\mathfrak{s}) = u^{\mathfrak{s}}(J^{\pm},\mathfrak{s}), \tag{55}$$

with $\bar{w}^{\mathfrak{s}}$ and $u^{\mathfrak{s}}$ suitable functions. Please note that this additive decomposition of the strain energy into volumetric and isochoric components is essential as the volumetric components of the first and second invariants, i.e. $II_{\boldsymbol{F}}$ and $II_{\boldsymbol{H}}$, might contradict the anisotropic split of the Jacobian J, resulting in a non-physical behaviour of the formulation. This justifies the use of the isochoric invariants $II_{\bar{\boldsymbol{F}}}$ and $II_{\bar{\boldsymbol{H}}}$ instead. Regarding the form of the functions $\bar{w}^{\mathfrak{s}}$ and $\bar{u}^{\mathfrak{s}}$, these could be defined as

$$\begin{aligned}\bar{w}^{\mathfrak{s}}\left(II^{\pm}_{\bar{\boldsymbol{F}}}, II^{\pm}_{\bar{\boldsymbol{H}}}, \mathfrak{s}\right) &= g(\mathfrak{s})\bar{w}\left(II^{+}_{\bar{\boldsymbol{F}}}, II^{+}_{\bar{\boldsymbol{H}}}\right) + \bar{w}\left(II^{-}_{\bar{\boldsymbol{F}}}, II^{-}_{\bar{\boldsymbol{H}}}\right),\\ \bar{u}^{\mathfrak{s}}\left(J^{\pm},\mathfrak{s}\right) &= g(\mathfrak{s})U\left(J^{+}\right) + U\left(J^{-}\right).\end{aligned} \tag{56}$$

Application of the proposed anisotropic split in (54) in conjunction with the definition of the functions $\bar{w}^{\mathfrak{s}}$ and $\bar{u}^{\mathfrak{s}}$ in Eq. (56) for the specific constitutive model defined in Eqs. (20)–(21) leads to

$$w^{\mathfrak{s}}_{MR}(II_{\bar{\boldsymbol{F}}}, II_{\bar{\boldsymbol{H}}}, J, \mathfrak{s}) = \underbrace{\Lambda_{\bar{\boldsymbol{F}}}(\bar{\boldsymbol{F}},\mathfrak{s})\bar{w}_{\bar{\boldsymbol{F}}}(II_{\bar{\boldsymbol{F}}}) + \Lambda_{\bar{\boldsymbol{H}}}(\bar{\boldsymbol{H}},\mathfrak{s})\bar{w}_{\bar{\boldsymbol{H}}}(II_{\bar{\boldsymbol{H}}})}_{\bar{w}^{\mathfrak{s}}_{MR}(II_{\bar{\boldsymbol{F}}}, II_{\bar{\boldsymbol{H}}},\mathfrak{s})} + \underbrace{\Lambda_J(J,\mathfrak{s})U(J)}_{u^{\mathfrak{s}}(J,\mathfrak{s})}, \tag{57}$$

where

$$\bar{w}_{\bar{\boldsymbol{F}}} = \gamma\left(II_{\bar{\boldsymbol{F}}} - 3\right); \qquad \bar{w}_{\bar{\boldsymbol{H}}} = \zeta\left(\left(II_{\bar{\boldsymbol{H}}}\right)^{3/2} - 3^{3/2}\right); \qquad U = \frac{\kappa}{2}(J-1)^2, \tag{58}$$

and with $\Lambda_{\bar{\boldsymbol{F}}}$, $\Lambda_{\bar{\boldsymbol{H}}}$ and Λ_J defined as[4]

$$\Lambda_{\bar{\boldsymbol{F}}} = \begin{cases} g(\mathfrak{s}) & \text{if } II_{\bar{\boldsymbol{F}}} > 3,\\ 1 & \text{otherwise.}\end{cases} \qquad \Lambda_{\bar{\boldsymbol{H}}} = \begin{cases} g(\mathfrak{s}) & \text{if } II_{\bar{\boldsymbol{H}}} > 3,\\ 1 & \text{otherwise.}\end{cases} \qquad \Lambda_J = \begin{cases} g(\mathfrak{s}) & \text{if } J > 1,\\ 1 & \text{otherwise.}\end{cases} \tag{59}$$

Note that an anisotropic split of the volumetric term in $(58)_3$ using $U(\Lambda_J J)$ can be applied as well. However, in the case of a logarithmic definition of volumetric term, polyconvexity cannot be ensured. For this energy functional, it is now possible to derive the expression for the work conjugates $\boldsymbol{\Sigma}_{\boldsymbol{F}}$, $\boldsymbol{\Sigma}_{\boldsymbol{H}}$ and Σ_J which now depend upon the phase-field parameter $\mathfrak{s}$ as[5]

$$\boldsymbol{\Sigma}_{\boldsymbol{F}}(\boldsymbol{F},J,\mathfrak{s}) = 2\gamma\Lambda_{\bar{\boldsymbol{F}}}J^{-2/3}\boldsymbol{F}, \tag{60a}$$

$$\boldsymbol{\Sigma}_{\boldsymbol{H}}(\boldsymbol{H},J,\mathfrak{s}) = 3\zeta\Lambda_{\bar{\boldsymbol{H}}}J^{-2}(II_{\boldsymbol{H}})^{1/2}\boldsymbol{H}, \tag{60b}$$

$$\Sigma_J(\boldsymbol{F},\boldsymbol{H},J,\mathfrak{s}) = -\frac{2\gamma\Lambda_{\bar{\boldsymbol{F}}}J^{-5/3}II_{\boldsymbol{F}}}{3} - 2\zeta\Lambda_{\bar{\boldsymbol{H}}}J^{-3}\left(II_{\boldsymbol{H}}\right)^{3/2} + \Lambda_J\kappa\left(J-1\right). \tag{60c}$$

With a Newton–Raphson type solver in mind, the tangent operator of the total energy potential E^{tot} in (44)[6] is obtained as

[4] An alternative expression for the function $\Lambda_{\bar{\boldsymbol{F}}}$ is $\Lambda_{\bar{\boldsymbol{F}}}(\bar{\boldsymbol{F}},\mathfrak{s}) = 1 - (1-g(\mathfrak{s}))\,H(II_{\bar{\boldsymbol{F}}} - 3)$, where $H(\bullet)$ is the Heaviside step function. Similar expressions can be derived for $\Lambda_{\bar{\boldsymbol{H}}}$ and Λ_J.

[5] In (60), use of the following identities has been made

$$\frac{\partial\Lambda_{\bar{\boldsymbol{F}}}}{\partial\bar{\boldsymbol{F}}}\left(II_{\bar{\boldsymbol{F}}} - 3\right) = 0; \qquad \frac{\partial\Lambda_{\bar{\boldsymbol{H}}}}{\partial\bar{\boldsymbol{H}}}\left(II_{\bar{\boldsymbol{H}}} - 3\right) = 0; \qquad \frac{\partial\Lambda_J}{\partial J}\left(J-1\right) = 0.$$

[6] Note that for the case of pure elasticity, the tangent operator exclusively concerns the internal energy (if no follower loads are considered), namely $\mathrm{D}^2\,W[\delta\boldsymbol{\varphi};\Delta\boldsymbol{\varphi}]$, refer to Eq. (34). In the more general context of coupled phase-field approaches for the modelling of fracture, as that considered in this section, it is the tangent operator of the total energy potential E^{tot} that must be considered, namely $\mathrm{D}^2\,E^{tot}[\delta\boldsymbol{\varphi},\delta\mathfrak{s};\Delta\boldsymbol{\varphi},\Delta\mathfrak{s}]$, refer to Eq. (61).

$$\mathrm{D}^2 E^{tot}[\delta\boldsymbol{\varphi}, \delta\mathfrak{s}; \Delta\boldsymbol{\varphi}, \Delta\mathfrak{s}] = [[\mathbb{S}_\delta]^T \quad \delta\mathfrak{s}][\mathbb{H}_{W^\mathfrak{s}}] \begin{bmatrix} [\mathbb{S}_\Delta] \\ \Delta\mathfrak{s} \end{bmatrix} + [\boldsymbol{\Sigma}_H + \Sigma_J \boldsymbol{F}] : (\nabla_X \, \delta\boldsymbol{\varphi} \times \nabla_X \, \Delta\boldsymbol{\varphi}) + g_c D^2\gamma(\mathfrak{s})[\delta\mathfrak{s}; \Delta\mathfrak{s}], \tag{61}$$

with $[\mathbb{S}_\delta]^T$ and $[\mathbb{S}_\Delta]$ defined in Eq. (35) and with the Hessian operator $[\mathbb{H}_{W^\mathfrak{s}}]$ defined as

$$[\mathbb{H}_{W^\mathfrak{s}}] = \begin{bmatrix} \frac{\partial^2 W^\mathfrak{s}}{\partial \boldsymbol{F} \partial \boldsymbol{F}} & \frac{\partial^2 W^\mathfrak{s}}{\partial \boldsymbol{F} \partial \boldsymbol{H}} & \frac{\partial^2 W^\mathfrak{s}}{\partial \boldsymbol{F} \partial J} & \frac{\partial^2 W^\mathfrak{s}}{\partial \boldsymbol{F} \partial \mathfrak{s}} \\ \frac{\partial^2 W^\mathfrak{s}}{\partial \boldsymbol{H} \partial \boldsymbol{F}} & \frac{\partial^2 W^\mathfrak{s}}{\partial \boldsymbol{H} \partial \boldsymbol{H}} & \frac{\partial^2 W^\mathfrak{s}}{\partial \boldsymbol{H} \partial J} & \frac{\partial^2 W^\mathfrak{s}}{\partial \boldsymbol{H} \partial \mathfrak{s}} \\ \frac{\partial^2 W^\mathfrak{s}}{\partial J \partial \boldsymbol{F}} & \frac{\partial^2 W^\mathfrak{s}}{\partial J \partial \boldsymbol{H}} & \frac{\partial^2 W^\mathfrak{s}}{\partial J \partial J} & \frac{\partial^2 W^\mathfrak{s}}{\partial J \partial \mathfrak{s}} \\ \frac{\partial^2 W^\mathfrak{s}}{\partial \mathfrak{s} \partial \boldsymbol{F}} & \frac{\partial^2 W^\mathfrak{s}}{\partial \mathfrak{s} \partial \boldsymbol{H}} & \frac{\partial^2 W^\mathfrak{s}}{\partial \mathfrak{s} \partial J} & \frac{\partial^2 W^\mathfrak{s}}{\partial \mathfrak{s} \partial \mathfrak{s}} \end{bmatrix}. \tag{62}$$

For the particular energy functional in Eqs. (57)–(59), the above Hessian operator adopts the following expression

$$[\mathbb{H}_{W^\mathfrak{s}_{MR}}] = \begin{bmatrix} 2\frac{\partial \bar{w}^\mathfrak{s}_{MR}}{\partial I I_{\boldsymbol{F}}} \boldsymbol{\mathcal{I}} & \boldsymbol{0} & 2\frac{\partial^2 \bar{w}^\mathfrak{s}_{MR}}{\partial I I_{\boldsymbol{F}} \partial J} \boldsymbol{F} & 2\frac{\partial^2 \bar{w}^\mathfrak{s}_{MR}}{\partial I I_{\boldsymbol{F}} \partial \mathfrak{s}} \boldsymbol{F} \\ \boldsymbol{0} & 2\frac{\partial \bar{w}^\mathfrak{s}_{MR}}{\partial I I_{\boldsymbol{H}}} \boldsymbol{\mathcal{I}} + 4\frac{\partial^2 \bar{w}^\mathfrak{s}_{MR}}{\partial I I_{\boldsymbol{H}} \partial I I_{\boldsymbol{H}}} \boldsymbol{H} \otimes \boldsymbol{H} & 2\frac{\partial^2 \bar{w}^\mathfrak{s}_{MR}}{\partial I I_{\boldsymbol{H}} \partial J} \boldsymbol{H} & 2\frac{\partial^2 \bar{w}^\mathfrak{s}_{MR}}{\partial I I_{\boldsymbol{H}} \partial \mathfrak{s}} \boldsymbol{H} \\ 2\frac{\partial^2 \bar{w}^\mathfrak{s}_{MR}}{\partial J \partial I I_{\boldsymbol{F}}} \boldsymbol{F}^{\mathrm{T}} & 2\frac{\partial^2 \bar{w}^\mathfrak{s}_{MR}}{\partial J \partial I I_{\boldsymbol{H}}} \boldsymbol{H}^{\mathrm{T}} & \frac{\partial^2 \left(\bar{w}^\mathfrak{s}_{MR} + u^\mathfrak{s}\right)}{\partial J \partial J} & \frac{\partial^2 \left(\bar{w}^\mathfrak{s}_{MR} + u^\mathfrak{s}\right)}{\partial J \partial \mathfrak{s}} \\ 2\frac{\partial^2 \bar{w}^\mathfrak{s}_{MR}}{\partial \mathfrak{s} \partial I I_{\boldsymbol{F}}} \boldsymbol{F}^{\mathrm{T}} & 2\frac{\partial^2 \bar{w}^\mathfrak{s}_{MR}}{\partial \mathfrak{s} \partial I I_{\boldsymbol{H}}} \boldsymbol{H}^{\mathrm{T}} & \frac{\partial^2 \left(\bar{w}^\mathfrak{s}_{MR} + u^\mathfrak{s}\right)}{\partial \mathfrak{s} \partial J} & \frac{\partial^2 \left(\bar{w}^\mathfrak{s}_{MR} + u^\mathfrak{s}\right)}{\partial \mathfrak{s} \partial \mathfrak{s}} \end{bmatrix}. \tag{63}$$

It is important to emphasise that the Hessian operator $[\mathbb{H}^\mathfrak{s}_W]$ in (62) and (63) is, in general, positive definite, because it is not necessarily possible to guarantee the convexity of the total energy E^{tot} in (44) or of its purely elastic contribution W (refer to (44)). In order to identify those contributions in the above tangent operator (61) strictly related to material stability and those responsible for geometrical and material instabilities, the above tangent operator $D^2 E^{tot}[\delta\boldsymbol{\varphi}, \Delta\boldsymbol{\varphi}; \delta\mathfrak{s}, \Delta\mathfrak{s}]$ can be conveniently re-arranged as

$$\mathrm{D}^2 E^{tot}[\delta\boldsymbol{\varphi}, \delta\mathfrak{s}; \Delta\boldsymbol{\varphi}, \Delta\mathfrak{s}] = \underbrace{[\mathbb{S}_\delta]^T [\mathbb{H}_{W^\mathfrak{s}_m}][\mathbb{S}_\Delta]}_{\text{Material stability}} + \underbrace{[[\mathbb{S}_\delta]^T \quad \delta\mathfrak{s}]^T [\mathbb{H}_{W^\mathfrak{s}_\mathfrak{s}}] \begin{bmatrix} [\mathbb{S}_\Delta] \\ \Delta\mathfrak{s} \end{bmatrix}}_{\text{Material instability}} + \underbrace{g_c D^2\gamma(\mathfrak{s})[\delta\mathfrak{s}; \Delta\mathfrak{s}]}_{\text{Regularising/Stabilising term}} + \underbrace{[\boldsymbol{\Sigma}_H + \Sigma_J \boldsymbol{F}] : (\nabla_X \, \delta\boldsymbol{\varphi} \times \nabla_X \, \Delta\boldsymbol{\varphi})}_{\text{Geometrical buckling}}, \tag{64}$$

where the Hessian operator $[\mathbb{H}_{W^\mathfrak{s}_m}]$ accounts exclusively for the derivatives of the strain energy (3×3 upper-left block in Eq. (63)) with respect to $\boldsymbol{F}$, $\boldsymbol{H}$ and J and is defined as in Eq. (36) and with the Hessian contribution $[\mathbb{H}_{W^\mathfrak{s}_\mathfrak{s}}]$ accounting for the coupled second derivatives of the model, defined as

$$[\mathbb{H}_{W^\mathfrak{s}_\mathfrak{s}}] = \begin{bmatrix} \boldsymbol{0} & \boldsymbol{0} & \boldsymbol{0} & \frac{\partial^2 W^\mathfrak{s}}{\partial \boldsymbol{F} \partial \mathfrak{s}} \\ \boldsymbol{0} & \boldsymbol{0} & \boldsymbol{0} & \frac{\partial^2 W^\mathfrak{s}}{\partial \boldsymbol{H} \partial \mathfrak{s}} \\ \boldsymbol{0} & \boldsymbol{0} & \boldsymbol{0} & \frac{\partial^2 W^\mathfrak{s}}{\partial J \partial \mathfrak{s}} \\ \frac{\partial^2 W^\mathfrak{s}}{\partial \mathfrak{s} \partial \boldsymbol{F}} & \frac{\partial^2 W^\mathfrak{s}}{\partial \mathfrak{s} \partial \boldsymbol{H}} & \frac{\partial^2 W^\mathfrak{s}}{\partial \mathfrak{s} \partial J} & \frac{\partial^2 W^\mathfrak{s}}{\partial \mathfrak{s} \partial \mathfrak{s}} \end{bmatrix}. \tag{65}$$

It is possible to verify that the Hessian operator $[\mathbb{H}_{W^\mathfrak{s}_m}]$ (first term on the left hand side of (64)) is positive definite for the proposed anisotropic split based on (54) and (56), as each term is pre-multiplied by either 1 (undamaged state)

or $g(\mathfrak{s})$ (damaged state). This can be ensured by introducing a small positive parameter $\epsilon \approx 0$ such that $g(1) = \epsilon$ and a full degradation of strain energy at a fully broken state $\mathfrak{s} = 1$ is prevented. The fourth term on the right hand side of above Eq. (64) plays the same role as the second term on the right hand side of (34) for the purely mechanical case, and is responsible for geometrical instabilities as buckling. The second term on the right hand side of (64) brings additional instabilities into the problem as this term is responsible for material instabilities. Finally, the third term on the right hand side of (64) can be understood as a stabilising term which regularises the effect of the second term.

Remark 4. A different anisotropic split to that proposed in this paper, has been previously presented in Hesch & Weinberg [27] in the context of large strains, based upon a multiplicative split in terms of the principal eigenvalues. In this approach, the elastic, fracture insensitive part of the deformation gradient tensor is expressed as

$$\boldsymbol{F}^{\mathrm{e}} = \sum_{a=1}^{3} (\lambda_a^+)^{g(\mathfrak{s})} \lambda_a^- \boldsymbol{n}_a \otimes \boldsymbol{N}_a, \tag{66}$$

where $\lambda^{\pm} = [(\lambda - 1) \pm |\lambda - 1|]/2 + 1$. Introducing the abbreviation $\lambda_a^{\mathrm{e}} = (\lambda_a^+)^{g(\mathfrak{s})} \lambda_a^-$, it is possible to redefine any strain energy functional as follows

$$\Psi^{\mathfrak{s}}(\boldsymbol{\varphi}, \mathfrak{s}) = \omega_\lambda^{\mathfrak{s}}(\lambda_1^{\mathrm{e}}, \lambda_2^{\mathrm{e}}, \lambda_3^{\mathrm{e}}, \mathfrak{s}). \tag{67}$$

Following Hartmann & Neff [12], Appendix C, and also Dacorogna [38], it is possible to check the rank-one convexity of any energy functional expressed in its eigenvalue representation if the following inequality is verified, i.e,

$$\frac{\partial^2 \omega_\lambda^{\mathfrak{s}}(\lambda_1, \lambda_2, \lambda_3)}{\partial \lambda_i^2} \geq 0, \qquad 1 \leq i \leq 3. \tag{68}$$

In order to check above inequality (68), the principal stresses are initially obtained as

$$\frac{\partial \omega_\lambda{}^{\mathfrak{s}}}{\partial \lambda_a} = \frac{\partial \omega_\lambda{}^{\mathfrak{s}}}{\partial ((\lambda_a^{\mathrm{e}})^2)} \frac{\partial ((\lambda_a^{\mathrm{e}})^2)}{\partial \lambda_a}. \tag{69}$$

The second derivative with respect to the principal eigenvalues of the principal stresses follows immediately by applying the chain rule as

$$\frac{\partial^2 \omega_\lambda^{\mathfrak{s}}}{\partial \lambda_a \partial \lambda_a} = \frac{\partial^2 \omega_\lambda^{\mathfrak{s}}}{\partial ((\lambda_a^{\mathrm{e}})^2) \partial ((\lambda_a^{\mathrm{e}})^2)} \left(\frac{\partial ((\lambda_a^{\mathrm{e}})^2)}{\partial \lambda_a} \right)^2 + \frac{\partial \omega_\lambda^{\mathfrak{s}}}{\partial ((\lambda_a^{\mathrm{e}})^2)} \frac{\partial^2 ((\lambda_a^{\mathrm{e}})^2)}{\partial \lambda_a \partial \lambda_a}. \tag{70}$$

For instance, for the first invariant of the compressible Mooney–Rivlin model in Eq. (16), re-written in terms of the eigenvalues λ_a^e as

$$\alpha(I I_{\boldsymbol{F}^e} - 3) = \alpha\left(\left(\lambda_1^e\right)^2 + \left(\lambda_2^e\right)^2 + \left(\lambda_3^e\right)^2\right), \tag{71}$$

where the first term on the right hand side of (70) is clearly zero. The term $\frac{\partial^2 ((\lambda_a^{\mathrm{e}})^2)}{\partial \lambda_a \partial \lambda_a}$ on the right hand side of Eq. (70) is written as

$$\frac{\partial^2 ((\lambda_a^{\mathrm{e}})^2)}{\partial \lambda_a \partial \lambda_a} = 2g(\mathfrak{s})(2g(\mathfrak{s}) - 1)(\lambda_a)^{(2g(\mathfrak{s})-2)}. \tag{72}$$

Hence, $\frac{\partial^2 \omega_\lambda^{\mathfrak{s}}}{\partial \lambda_a \partial \lambda_a}$ in (70) becomes negative (as $\frac{\partial \omega_\lambda^{\mathfrak{s}}}{\partial ((\lambda_a^{\mathrm{e}})^2)}$ is always positive for $\alpha(I I_{\boldsymbol{F}^e} - 3)$ provided $\alpha > 0$) for $g(\mathfrak{s}) < 0.5$ and the invariant $\alpha(I I_{\boldsymbol{F}^e} - 3)$ is then not rank-one convex. Therefore, unlike the proposed anisotropic split in Eqs. (54) and (56), this eigenvalue-based split does not reflect the material stability of the mechanical part of the energy. In particular, the Hessian operator in the first term on the left hand side of Eq. (64) is not always positive definite irrespectively of the value of the parameter $\mathfrak{s}$, and hence material instabilities could be induced by this term, too. This indicates that this approach (eigenvalue-based split) should be numerically more unstable than the one proposed in this paper (invariant-based split).

4. Mixed variational principles in phase-field problems

Most important for fracture mechanics is the definition of the failure criteria. As already stated in the 19th century by St. Venant and C. Bach, a crack propagates if a critical value of the principal stretches is reached. Alternatively, Rankine, Lamé and Navier assumed that a crack propagates if a critical value of the principal stresses is reached, see the textbook of Gross & Seelig [10] for a comprehensive review on this topic. Independent of the chosen definition in terms of stresses or strains, it is favourable for a variationally consistent construction of the phase-field approach to obtain the strain as well as the stress field as primary variables in the energy function, as provided in a mixed Hu–Washizu type formulation.

4.1. Hu–Washizu mixed variational principle

Following the work of Bonet et al. [22,24] in the context of polyconvex large strain deformations, it is possible to derive an eight field mixed variational principle where not only displacements $\boldsymbol{\varphi}$ and the phase-field $\mathfrak{s}$ are part of the unknowns of the problems, but also the kinematic entities $\{\boldsymbol{F}, \boldsymbol{H}, J\}$ and their respective work conjugates $\{\boldsymbol{\Sigma}_{\boldsymbol{F}}, \boldsymbol{\Sigma}_{\boldsymbol{H}}, \Sigma_J\}$,

$$\begin{aligned}\Pi_{HW}(\boldsymbol{\varphi}, \mathfrak{s}, \boldsymbol{F}, \boldsymbol{H}, J, \boldsymbol{\Sigma}_{\boldsymbol{F}}, \boldsymbol{\Sigma}_{\boldsymbol{H}}, \Sigma_J) = &\int_{\mathcal{B}_0} W^s(\boldsymbol{F}, \boldsymbol{H}, J, \mathfrak{s})\,\mathrm{d}V + \int_{\mathcal{B}_0} g_c\gamma(\mathfrak{s})\,\mathrm{d}V \\ &+ \int_{\mathcal{B}_0} \boldsymbol{\Sigma}_{\boldsymbol{F}} : (\boldsymbol{F}_{\boldsymbol{x}} - \boldsymbol{F})\,\mathrm{d}V + \int_{\mathcal{B}_0} \boldsymbol{\Sigma}_{\boldsymbol{H}} : (\boldsymbol{H}_{\boldsymbol{x}} - \boldsymbol{H})\,\mathrm{d}V \\ &+ \int_{\mathcal{B}_0} \Sigma_J\,(J_{\boldsymbol{x}} - J)\,\mathrm{d}V + \Pi^{\mathrm{ext}}(\boldsymbol{\varphi}).\end{aligned} \tag{73}$$

Here, the external contribution $\Pi^{\mathrm{ext}}(\boldsymbol{\varphi})$ is defined as

$$\Pi^{\mathrm{ext}}(\boldsymbol{\varphi}) = -\int_{\mathcal{B}_0} \boldsymbol{\varphi}\cdot\bar{\boldsymbol{B}}\,\mathrm{d}V - \int_{\partial\mathcal{B}_0^{\sigma}} \boldsymbol{\varphi}\cdot\bar{\boldsymbol{T}}\,\mathrm{d}A, \tag{74}$$

and $\{\boldsymbol{F}_{\boldsymbol{x}}, \boldsymbol{H}_{\boldsymbol{x}}, J_{\boldsymbol{x}}\}$ denote the compatible strain measures, namely

$$\boldsymbol{F}_x := \nabla_{\boldsymbol{X}}\boldsymbol{\varphi}; \qquad \boldsymbol{H}_{\boldsymbol{x}} := \frac{1}{2}\nabla_{\boldsymbol{X}}\boldsymbol{\varphi}\times\nabla_{\boldsymbol{X}}\boldsymbol{\varphi}; \qquad J_{\boldsymbol{x}} := \frac{1}{6}\,(\nabla_{\boldsymbol{X}}\boldsymbol{\varphi}\times\nabla_{\boldsymbol{X}}\boldsymbol{\varphi}) : \nabla_{\boldsymbol{X}}\boldsymbol{\varphi}. \tag{75}$$

An alternative but similar mixed variational principle in terms of $\{\bar{\boldsymbol{F}}, \bar{\boldsymbol{H}}, J\}$ and their work conjugates $\{\boldsymbol{\Sigma}_{\bar{\boldsymbol{F}}}, \boldsymbol{\Sigma}_{\bar{\boldsymbol{H}}}, \Sigma_J\}$, tailor-made for the anisotropic split proposed in this paper, can be defined as

$$\begin{aligned}\bar{\Pi}_{HW}(\boldsymbol{\varphi}, \mathfrak{s}, \bar{\boldsymbol{F}}, \bar{\boldsymbol{H}}, J, \boldsymbol{\Sigma}_{\bar{\boldsymbol{F}}}, \boldsymbol{\Sigma}_{\bar{\boldsymbol{H}}}, \Sigma_J) = &\int_{\mathcal{B}_0} \left(\bar{W}^s(\bar{\boldsymbol{F}}, \bar{\boldsymbol{H}}, J, \mathfrak{s}) + U^{\mathfrak{s}}(J, \mathfrak{s})\right)\mathrm{d}V + \int_{\mathcal{B}_0} g_c\gamma(\mathfrak{s})\,\mathrm{d}V \\ &+ \int_{\mathcal{B}_0} \boldsymbol{\Sigma}_{\bar{\boldsymbol{F}}} : \left(\bar{\boldsymbol{F}}_{\boldsymbol{x}} - \bar{\boldsymbol{F}}\right)\mathrm{d}V + \int_{\mathcal{B}_0} \boldsymbol{\Sigma}_{\bar{\boldsymbol{H}}} : \left(\bar{\boldsymbol{H}}_{\boldsymbol{x}} - \bar{\boldsymbol{H}}\right)\mathrm{d}V \\ &+ \int_{\mathcal{B}_0} \Sigma_J\,(J_{\boldsymbol{x}} - J)\,\mathrm{d}V + \Pi^{\mathrm{ext}}(\boldsymbol{\varphi}).\end{aligned} \tag{76}$$

Remark 5. For two-dimensional plane strain, the above mixed variational principle is degenerated into the following eight-field mixed variational principle as

$$\begin{aligned}\bar{\Pi}^{2D}_{HW}(\boldsymbol{\varphi}, \mathfrak{s}, \bar{\boldsymbol{F}}_{2D}, \bar{F}_{33}, j, \boldsymbol{\Sigma}^{2D}_{\bar{\boldsymbol{F}}}, \Sigma_{\bar{F}_{33}}, \Sigma_j) = &\int_{\mathcal{B}_0} \left(\bar{W}^s(\bar{\boldsymbol{F}}^{2D}, \bar{F}_{33}, \mathfrak{s}) + U^{\mathfrak{s}}(j, \mathfrak{s})\right)\mathrm{d}V + \int_{\mathcal{B}_0} g_c\gamma(\mathfrak{s})\,\mathrm{d}V \\ &+ \int_{\mathcal{B}_0} \boldsymbol{\Sigma}^{2D}_{\bar{\boldsymbol{F}}} : \left(\bar{\boldsymbol{F}}_{\boldsymbol{x}2D} - \bar{\boldsymbol{F}}_{2D}\right)\mathrm{d}V + \int_{\mathcal{B}_0} \Sigma_{\bar{F}_{33}}\left(j_{\boldsymbol{x}}^{-1/3} - \bar{F}_{33}\right)\mathrm{d}V \\ &+ \int_{\mathcal{B}_0} \Sigma_j\,(j_{\boldsymbol{x}} - j)\,\mathrm{d}V + \Pi^{\mathrm{ext}}(\boldsymbol{\varphi}),\end{aligned} \tag{77}$$

where the compatible strain measures $\{\bar{\boldsymbol{F}}_{\boldsymbol{x}2D},\, j\}$ are defined as

$$\bar{\boldsymbol{F}}_{\boldsymbol{x}2D} := j_{\boldsymbol{x}}^{-1/3}\boldsymbol{F}_{\boldsymbol{x}2D}; \qquad j_{\boldsymbol{x}} = \frac{1}{2}\left((\mathrm{tr}\boldsymbol{F}_{\boldsymbol{x}2D})^2 - \mathrm{tr}\left(\boldsymbol{F}_{\boldsymbol{x}2D}^T\boldsymbol{F}_{\boldsymbol{x}2D}\right)\right), \tag{78}$$

with $\boldsymbol{F}_{\boldsymbol{x}2D} = \nabla_{\boldsymbol{X}}\boldsymbol{\varphi}$.

For the constitutive model defined in Eqs. (57)–(59) the Hu–Washizu mixed variational principle presented in Eq. (76) can be alternatively written as

$$\begin{aligned}\bar{\Pi}_{HW}(\boldsymbol{\varphi}, \mathfrak{s}, \bar{\boldsymbol{F}}, \bar{\boldsymbol{H}}, J, \boldsymbol{\Sigma}_{\bar{\boldsymbol{F}}}, \boldsymbol{\Sigma}_{\bar{\boldsymbol{H}}}, \Sigma_J) = &\int_{\mathcal{B}_0}\left(\Lambda_{\bar{\boldsymbol{F}}}\bar{w}_{\bar{\boldsymbol{F}}} + \Lambda_{\bar{\boldsymbol{H}}}\bar{w}_{\bar{\boldsymbol{H}}} + \Lambda_J U\right)\mathrm{d}V + \int_{\mathcal{B}_0} g_c\gamma(\mathfrak{s})\,\mathrm{d}V \\ &+ \int_{\mathcal{B}_0}\boldsymbol{\Sigma}_{\bar{\boldsymbol{F}}} : \left(\bar{\boldsymbol{F}}_{\boldsymbol{x}} - \bar{\boldsymbol{F}}\right)\mathrm{d}V \int_{\mathcal{B}_0}\boldsymbol{\Sigma}_{\bar{\boldsymbol{H}}} : \left(\bar{\boldsymbol{H}}_{\boldsymbol{x}} - \bar{\boldsymbol{H}}\right)\mathrm{d}V \\ &+ \int_{\mathcal{B}_0}\Sigma_J\,(J_{\boldsymbol{x}} - J)\,\mathrm{d}V + \Pi^{\mathrm{ext}}(\boldsymbol{\varphi}).\end{aligned} \tag{79}$$

Note that we have applied the anisotropic split analogues to the two-field $\boldsymbol{\varphi}$–$\mathfrak{s}$ formulation, i.e. we follow the geometric definition of $\Lambda_\bullet$ as outlined in Eq. (59).

4.1.1. Directional derivatives

The directional derivatives of the above mixed variational principle (79) with respect to virtual variations of the deformation $\boldsymbol{\varphi}$ and virtual variations of the phase-field parameter $\mathfrak{s}$ yield

$$\begin{aligned}\mathrm{D}\,\bar{\Pi}_{HW}[\delta\boldsymbol{\varphi}] &= \int_{\mathcal{B}_0}\boldsymbol{P}_{HW} : \nabla_{\boldsymbol{X}}\,\delta\boldsymbol{\varphi}\;\mathrm{d}V - \int_{\mathcal{B}_0}\delta\boldsymbol{\varphi}\cdot\bar{\boldsymbol{B}}\;\mathrm{d}V - \int_{\partial\mathcal{B}_0^\sigma}\delta\boldsymbol{\varphi}\cdot\bar{\boldsymbol{T}}\;\mathrm{d}A = 0, \\ \mathrm{D}\,\bar{\Pi}_{HW}[\delta\mathfrak{s}] &= \int_{\mathcal{B}_0}\mathcal{H}_{HW}\delta\mathfrak{s}\;\mathrm{d}V + \int_{\mathcal{B}_0} g_c\,\mathrm{D}\,\gamma(\mathfrak{s})[\delta\mathfrak{s}]\;\mathrm{d}V = 0,\end{aligned} \tag{80}$$

where the first Piola–Kirchhoff stress tensor $\boldsymbol{P}_{HW}$ and the driving force term $\mathcal{H}_{HW}$ are evaluated as

$$\begin{aligned}\boldsymbol{P}_{HW} &= J_{\boldsymbol{x}}^{-1/3}\boldsymbol{\Sigma}_{\bar{\boldsymbol{F}}} + J_{\boldsymbol{x}}^{-2/3}\boldsymbol{\Sigma}_{\bar{\boldsymbol{H}}}\times\boldsymbol{F}_{\boldsymbol{x}} + \left(\Sigma_J - \frac{1}{3}J_{\boldsymbol{x}}^{-4/3}\left(\boldsymbol{\Sigma}_{\bar{\boldsymbol{F}}} : \boldsymbol{F}_{\boldsymbol{x}}\right) - \frac{2}{3}J_{\boldsymbol{x}}^{-5/3}\left(\boldsymbol{\Sigma}_{\bar{\boldsymbol{H}}} : \boldsymbol{H}_{\boldsymbol{x}}\right)\right)\boldsymbol{H}_{\boldsymbol{x}}, \\ \mathcal{H}_{HW} &= \frac{\partial\Lambda_{\bar{\boldsymbol{F}}}}{\partial\mathfrak{s}}\bar{w}_{\bar{\boldsymbol{F}}} + \frac{\partial\Lambda_{\bar{\boldsymbol{H}}}}{\partial\mathfrak{s}}\bar{w}_{\bar{\boldsymbol{H}}} + \frac{\partial\Lambda_J}{\partial\mathfrak{s}}U.\end{aligned} \tag{81}$$

The directional derivatives of the mixed variational principle in (79) with respect to virtual variations of the fields $\{\bar{\boldsymbol{F}}, \bar{\boldsymbol{H}}, J\}$ yield the weak form of the constitutive equations, namely

$$\begin{aligned}\mathrm{D}\,\bar{\Pi}_{HW}[\delta\bar{\boldsymbol{F}}] &= \int_{\mathcal{B}_0}\left(\Lambda_{\bar{\boldsymbol{F}}}\frac{\partial\bar{w}_{\bar{\boldsymbol{F}}}}{\partial\bar{\boldsymbol{F}}} - \boldsymbol{\Sigma}_{\bar{\boldsymbol{F}}}\right) : \delta\bar{\boldsymbol{F}}\,\mathrm{d}V, \\ \mathrm{D}\,\bar{\Pi}_{HW}[\delta\bar{\boldsymbol{H}}] &= \int_{\mathcal{B}_0}\left(\Lambda_{\bar{\boldsymbol{H}}}\frac{\partial\bar{w}_{\bar{\boldsymbol{H}}}}{\partial\bar{\boldsymbol{H}}} - \boldsymbol{\Sigma}_{\bar{\boldsymbol{H}}}\right) : \delta\bar{\boldsymbol{H}}\,\mathrm{d}V, \\ \mathrm{D}\,\bar{\Pi}_{HW}[\delta J] &= \int_{\mathcal{B}_0}\left(\Lambda_J\frac{\partial U}{\partial J} - \Sigma_J\right)\delta J\,\mathrm{d}V.\end{aligned} \tag{82}$$

Finally, the directional derivatives of the mixed variational principle in (79) with respect to virtual variations of the fields $\{\boldsymbol{\Sigma}_{\bar{\boldsymbol{F}}}, \boldsymbol{\Sigma}_{\bar{\boldsymbol{H}}}, \Sigma_J\}$ lead to the weak form of the compatibility equations, namely

$$\begin{aligned}\mathrm{D}\,\bar{\Pi}_{HW}[\delta\boldsymbol{\Sigma}_{\bar{\boldsymbol{F}}}] &= \int_{\mathcal{B}_0}\left(\bar{\boldsymbol{F}}_{\boldsymbol{x}} - \bar{\boldsymbol{F}}\right) : \delta\boldsymbol{\Sigma}_{\bar{\boldsymbol{F}}}\,\mathrm{d}V, \\ \mathrm{D}\,\bar{\Pi}_{HW}[\delta\boldsymbol{\Sigma}_{\bar{\boldsymbol{H}}}] &= \int_{\mathcal{B}_0}\left(\bar{\boldsymbol{H}}_{\boldsymbol{x}} - \bar{\boldsymbol{H}}\right) : \delta\boldsymbol{\Sigma}_{\bar{\boldsymbol{H}}}\,\mathrm{d}V, \\ \mathrm{D}\,\bar{\Pi}_{HW}[\delta\Sigma_J] &= \int_{\mathcal{B}_0}\left(J_{\boldsymbol{x}} - J\right)\delta\Sigma_J\,\mathrm{d}V.\end{aligned} \tag{83}$$

For the extended set of variables, the corresponding set of admissible test functions is defined as

$$\mathcal{V}^{[F,H,J]} = \{[\delta\bar{\boldsymbol{F}}, \delta\bar{\boldsymbol{H}}, \delta J] \in \mathcal{L}^2(\mathcal{B}_0)\}, \tag{84}$$

and

$$\mathcal{V}^{[\Sigma_F,\Sigma_H,\Sigma_J]} = \{[\delta\boldsymbol{\Sigma}_{\bar{\boldsymbol{F}}}, \delta\boldsymbol{\Sigma}_{\bar{\boldsymbol{H}}}, \delta\Sigma_J] \in \mathcal{L}^2(\mathcal{B}_0)\}. \tag{85}$$

4.1.2. Linearisation

In this Section, the consistent linearisation of the set of weak forms in Eqs. (80), (82) and (83) is described.

Directional derivatives of $\mathrm{D}\,\bar{\Pi}_{HW}[\delta\boldsymbol{\varphi}]$. The directional derivative of the weak form in Eq. $(80)_a$ with respect to incremental variations $\Delta\boldsymbol{\varphi}$ is obtained as

$$\begin{aligned}
&\mathrm{D}^2\,\bar{\Pi}_{HW}[\delta\boldsymbol{\varphi};\,\Delta\boldsymbol{\varphi}] \\
&= -\int_{\mathcal{B}_0} \frac{J_{\boldsymbol{x}}^{-4/3}}{3}\left[\left(\boldsymbol{\Sigma}_{\bar{\boldsymbol{F}}} : \nabla_0\delta\boldsymbol{\varphi}\right)\left(\boldsymbol{H}_{\boldsymbol{x}} : \nabla_0\Delta\boldsymbol{\varphi}\right) - \left(\boldsymbol{\Sigma}_{\bar{\boldsymbol{F}}} : \nabla_0\Delta\boldsymbol{\varphi}\right)\left(\boldsymbol{H}_{\boldsymbol{x}} : \nabla_0\delta\boldsymbol{\varphi}\right)\right]\mathrm{d}V \\
&\quad - \int_{\mathcal{B}_0} \frac{2J_{\boldsymbol{x}}^{-5/3}}{3}\left[\left(\left(\boldsymbol{\Sigma}_{\bar{\boldsymbol{H}}}\times\boldsymbol{F}_{\boldsymbol{x}}\right) : \nabla_0\delta\boldsymbol{\varphi}\right)\left(\boldsymbol{H}_{\boldsymbol{x}} : \nabla_0\Delta\boldsymbol{\varphi}\right) + \left(\boldsymbol{H}_{\boldsymbol{x}} : \nabla_0\delta\boldsymbol{\varphi}\right)\left(\left(\boldsymbol{\Sigma}_{\bar{\boldsymbol{H}}}\times\boldsymbol{F}_{\boldsymbol{x}}\right) : \nabla_0\Delta\boldsymbol{\varphi}\right)\right]\mathrm{d}V \\
&\quad + \int_{\mathcal{B}_0} J_{\boldsymbol{x}}^{-2/3}\left(\boldsymbol{\Sigma}_{\bar{\boldsymbol{H}}} : \left(\nabla_0\delta\boldsymbol{\varphi}\times\nabla_0\Delta\boldsymbol{\varphi}\right)\right)\mathrm{d}V \\
&\quad + \int_{\mathcal{B}_0}\left(\Sigma_J - \frac{J_{\boldsymbol{x}}^{-4/3}}{3}\left(\boldsymbol{\Sigma}_{\bar{\boldsymbol{F}}} : \boldsymbol{F}_{\boldsymbol{x}}\right) - \frac{2J_{\boldsymbol{x}}^{-5/3}}{3}\left(\boldsymbol{\Sigma}_{\bar{\boldsymbol{H}}} : \boldsymbol{H}_{\boldsymbol{x}}\right)\right)\left(\boldsymbol{F}_{\boldsymbol{x}} : \left(\nabla_0\delta\boldsymbol{\varphi}\times\nabla_0\Delta\boldsymbol{\varphi}\right)\right)\mathrm{d}V \\
&\quad + \int_{\mathcal{B}_0} \frac{4J_{\boldsymbol{x}}^{-7/3}}{9}\left(\boldsymbol{\Sigma}_{\bar{\boldsymbol{F}}} : \boldsymbol{F}_{\boldsymbol{x}}\right)\left(\boldsymbol{H}_{\boldsymbol{x}} : \nabla_0\delta\boldsymbol{\varphi}\right)\left(\boldsymbol{H}_{\boldsymbol{x}} : \nabla_0\Delta\boldsymbol{\varphi}\right)\mathrm{d}V \\
&\quad - \int_{\mathcal{B}_0} \frac{10J_{\boldsymbol{x}}^{-8/3}}{9}\left(\boldsymbol{\Sigma}_{\bar{\boldsymbol{H}}} : \boldsymbol{H}_{\boldsymbol{x}}\right)\left(\boldsymbol{H}_{\boldsymbol{x}} : \nabla_0\delta\boldsymbol{\varphi}\right)\left(\boldsymbol{H}_{\boldsymbol{x}} : \nabla_0\Delta\boldsymbol{\varphi}\right)\mathrm{d}V.
\end{aligned} \tag{86}$$

The incremental variation of the weak form in Eq. $(80)_a$ with respect to incremental variations $\{\Delta\boldsymbol{\Sigma}_{\bar{\boldsymbol{F}}}, \Delta\boldsymbol{\Sigma}_{\bar{\boldsymbol{H}}}, \Delta\Sigma_J\}$ is obtained as

$$\begin{aligned}
\mathrm{D}^2\,\bar{\Pi}_{HW}[\delta\boldsymbol{\varphi};\,\Delta\boldsymbol{\Sigma}_{\bar{\boldsymbol{F}}}] &= \int_{\mathcal{B}_0}\left[J_{\boldsymbol{x}}^{-1/3}\left(\Delta\boldsymbol{\Sigma}_{\bar{\boldsymbol{F}}} : \nabla_0\delta\boldsymbol{\varphi}\right) - \frac{1}{3}J_{\boldsymbol{x}}^{-4/3}\left(\Delta\boldsymbol{\Sigma}_{\bar{\boldsymbol{F}}} : \boldsymbol{F}_{\boldsymbol{x}}\right)\left(\boldsymbol{H}_{\boldsymbol{x}} : \nabla_0\delta\boldsymbol{\varphi}\right)\right]\mathrm{d}V, \\
\mathrm{D}^2\,\bar{\Pi}_{HW}[\delta\boldsymbol{\varphi};\,\Delta\boldsymbol{\Sigma}_{\bar{\boldsymbol{H}}}] &= \int_{\mathcal{B}_0}\left[J_{\boldsymbol{x}}^{-2/3}\Delta\boldsymbol{\Sigma}_{\bar{\boldsymbol{H}}}\times\boldsymbol{F}_{\boldsymbol{x}} : \nabla_0\delta\boldsymbol{\varphi} - \frac{2}{3}J_{\boldsymbol{x}}^{-5/3}\left(\Delta\boldsymbol{\Sigma}_{\bar{\boldsymbol{H}}} : \boldsymbol{H}_{\boldsymbol{x}}\right)\left(\boldsymbol{H}_{\boldsymbol{x}} : \nabla_0\delta\boldsymbol{\varphi}\right)\right]\mathrm{d}V, \\
\mathrm{D}^2\,\bar{\Pi}_{HW}[\delta\boldsymbol{\varphi};\,\Delta\Sigma_J] &= \int_{\mathcal{B}_0}\Delta\Sigma_J\left(\boldsymbol{H}_{\boldsymbol{x}} : \nabla_0\delta\boldsymbol{\varphi}\right)\mathrm{d}V.
\end{aligned} \tag{87}$$

Directional derivatives of $\mathrm{D}\,\bar{\Pi}_{HW}[\delta\mathfrak{s}]$. The incremental variation of the weak form in Eq. $(80)_b$ with respect to incremental variations $\{\Delta\mathfrak{s}\}$ is obtained as

$$\begin{aligned}
\mathrm{D}^2\,\bar{\Pi}_{HW}[\delta\mathfrak{s};\,\Delta\mathfrak{s}] &= \int_{\mathcal{B}_0}\delta\mathfrak{s}\left(\frac{\partial^2\Lambda_{\bar{\boldsymbol{F}}}}{\partial\mathfrak{s}^2}\bar{w}_{\bar{\boldsymbol{F}}} + \frac{\partial^2\Lambda_{\bar{\boldsymbol{H}}}}{\partial\mathfrak{s}^2}\bar{w}_{\bar{\boldsymbol{H}}} + \frac{\partial^2\Lambda_J}{\partial\mathfrak{s}^2}U\right)\Delta\mathfrak{s}\,\mathrm{d}V \\
&\quad + \int_{\mathcal{B}_0} g_c\,\mathrm{D}^2\,\gamma(\mathfrak{s})[\delta\mathfrak{s};\,\Delta\mathfrak{s}]\,\mathrm{d}V = 0.
\end{aligned} \tag{88}$$

The incremental variation of the weak form in Eq. $(80)_b$ with respect to incremental variations $\{\Delta\boldsymbol{\Sigma}_{\bar{\boldsymbol{F}}}, \Delta\boldsymbol{\Sigma}_{\bar{\boldsymbol{H}}}, \Delta\Sigma_J\}$ is obtained as

$$
\begin{aligned}
\mathrm{D}^2\,\bar{\Pi}_{HW}[\delta\mathfrak{s};\,\Delta\boldsymbol{\Sigma}_{\bar{\boldsymbol{F}}}] &= \int_{\mathcal{B}_0} \delta\mathfrak{s}\frac{\partial\Lambda_{\bar{\boldsymbol{F}}}}{\partial\mathfrak{s}}\left(\frac{\partial\bar{w}_{\bar{\boldsymbol{F}}}}{\partial\bar{\boldsymbol{F}}} : \Delta\boldsymbol{\Sigma}_{\bar{\boldsymbol{F}}}\right)\,\mathrm{d}V,\\
\mathrm{D}^2\,\bar{\Pi}_{HW}[\delta\mathfrak{s};\,\Delta\boldsymbol{\Sigma}_{\bar{\boldsymbol{H}}}] &= \int_{\mathcal{B}_0} \delta\mathfrak{s}\frac{\partial\Lambda_{\bar{\boldsymbol{H}}}}{\partial\mathfrak{s}}\left(\frac{\partial\bar{w}_{\bar{\boldsymbol{H}}}}{\partial\bar{\boldsymbol{H}}} : \Delta\boldsymbol{\Sigma}_{\bar{\boldsymbol{H}}}\right)\,\mathrm{d}V,\\
\mathrm{D}^2\,\bar{\Pi}_{HW}[\delta\mathfrak{s};\,\Delta\Sigma_J] &= \int_{\mathcal{B}_0} \delta\mathfrak{s}\frac{\partial\Lambda_J}{\partial\mathfrak{s}}\left(\frac{\partial U}{\partial J}\Delta\Sigma_J\right)\,\mathrm{d}V.
\end{aligned}
\tag{89}
$$

Directional derivatives of $\mathrm{D}\,\bar{\Pi}_{HW}[\delta\bar{\boldsymbol{F}}]$, $\mathrm{D}\,\bar{\Pi}_{HW}[\delta\bar{\boldsymbol{H}}]$ **and** $\mathrm{D}\,\bar{\Pi}_{HW}[\delta J]$. The incremental variation of the weak form in Eq. (82) with respect to incremental variations $\{\Delta\bar{\boldsymbol{F}},\,\Delta\bar{\boldsymbol{H}},\,\Delta J\}$ is obtained as

$$
\begin{aligned}
\mathrm{D}^2\,\bar{\Pi}_{HW}[\delta\bar{\boldsymbol{F}};\,\Delta\bar{\boldsymbol{F}}] &= \int_{\mathcal{B}_0} \delta\bar{\boldsymbol{F}} : \Lambda_{\bar{\boldsymbol{F}}}\frac{\partial^2\bar{w}_{\bar{\boldsymbol{F}}}}{\partial\bar{\boldsymbol{F}}\partial\bar{\boldsymbol{F}}} : \Delta\bar{\boldsymbol{F}}\,\mathrm{d}V,\\
\mathrm{D}^2\,\bar{\Pi}_{HW}[\delta\bar{\boldsymbol{H}};\,\Delta\bar{\boldsymbol{H}}] &= \int_{\mathcal{B}_0} \delta\bar{\boldsymbol{H}} : \Lambda_{\bar{\boldsymbol{H}}}\frac{\partial^2\bar{w}_{\bar{\boldsymbol{H}}}}{\partial\bar{\boldsymbol{H}}\partial\bar{\boldsymbol{H}}} : \Delta\bar{\boldsymbol{H}}\,\mathrm{d}V,\\
\mathrm{D}^2\,\bar{\Pi}_{HW}[\delta J;\,\Delta J] &= \int_{\mathcal{B}_0} \delta J\,\Lambda_J\frac{\partial^2 U}{\partial J^2}\Delta J\,\mathrm{d}V.
\end{aligned}
\tag{90}
$$

Finally, the incremental variation of the weak form in Eq. (82) with respect to incremental variations $\{\Delta\boldsymbol{\Sigma}_{\bar{\boldsymbol{F}}},\,\Delta\boldsymbol{\Sigma}_{\bar{\boldsymbol{H}}},\,\Delta\Sigma_J\}$ is obtained as

$$
\begin{aligned}
\mathrm{D}^2\,\bar{\Pi}_{HW}[\delta\bar{\boldsymbol{F}};\,\Delta\boldsymbol{\Sigma}_{\bar{\boldsymbol{F}}}] &= -\int_{\mathcal{B}_0} \delta\bar{\boldsymbol{F}} : \Delta\boldsymbol{\Sigma}_{\bar{\boldsymbol{F}}}\,\mathrm{d}V,\\
\mathrm{D}^2\,\bar{\Pi}_{HW}[\delta\bar{\boldsymbol{H}};\,\Delta\boldsymbol{\Sigma}_{\bar{\boldsymbol{H}}}] &= -\int_{\mathcal{B}_0} \delta\bar{\boldsymbol{H}} : \Delta\boldsymbol{\Sigma}_{\bar{\boldsymbol{H}}}\,\mathrm{d}V,\\
\mathrm{D}^2\,\bar{\Pi}_{HW}[\delta J;\,\Delta\Sigma_J] &= -\int_{\mathcal{B}_0} \delta J\,\Delta\Sigma_J\,\mathrm{d}V.
\end{aligned}
\tag{91}
$$

Notice that although a larger number of directional derivatives and associated linearisations are obtained with respect to the classical two-field formulation presented in Section 3.2, the level of non-linearity of the different terms is dramatically reduced. For example, if a staggered scheme is applied between the displacement/stress/strain fields and the phase/stress/strain fields, the non-linearity of the latter term solely depends on the degeneration function $g(\mathfrak{s})$ and the second derivative of the strain energy with respect to the strain and stresses in (89) and (90).

5. Spatial discretisation

The finite element implementation of the two weak forms introduced in the previous sections will be presented next. For that purpose, as customary in finite elements, the domain $\mathcal{B}_0$ featuring in the integrands of the weak forms in (45) must be subdivided into a finite set of non-overlapping elements $e \in \mathbb{E}$, such that

$$
\mathcal{B}_0 \approx \mathcal{B}_0^{\mathrm{h}} = \bigcup_{e\in\mathbb{E}} \mathcal{B}_{0e}.
\tag{92}
$$

Note that the unknowns associated to the weak forms in (45) are the displacement field $\boldsymbol{\varphi}$ and the phase-field parameter $\mathfrak{s}$. In this paper, the same approximation will be used for both the displacement field $\boldsymbol{\varphi}$ and phase-field parameter $\mathfrak{s}$. Polynomial approximations employ either Lagrangian shape functions, when the second-order Allen–Cahn crack energy functional in (42) is considered, or non-uniform rational B-splines (NURBS) for the Cahn–Hilliard like crack energy function to achieve the necessary C^1 continuity.

5.1. Finite element implementation of the two-field ($\boldsymbol{\varphi}$–$\mathfrak{s}$) formulation

The approximations of the displacement field $\boldsymbol{\varphi}$ and its virtual variation $\delta\boldsymbol{\varphi}$ are obtained as

$$
\boldsymbol{\varphi}^{\mathrm{h}} = \sum_{A\in\omega} N^A(\boldsymbol{X})\boldsymbol{q}_A \quad \text{and} \quad \delta\boldsymbol{\varphi}^{\mathrm{h}} = \sum_{A\in\omega} N^A(\boldsymbol{X})\delta\boldsymbol{q}_A,
\tag{93}
$$

where, $A \in \omega = \{1, \ldots, n\}$, with n the number of nodes used to discretise the displacement field and with $\boldsymbol{q}_A \in \mathbb{R}^3$ denoting the nodal values of the displacement field and $N^A(\boldsymbol{X}) : \mathcal{B}_0 \to \mathbb{R}$, the global shape functions. Similarly, the phase-field is discretised using the same polynomial basis as in Eq. (93) in order to avoid the application of transfer matrices, i.e.

$$\mathfrak{s}^{\mathrm{h}} = \sum_{A\in\omega} N^A(\boldsymbol{X})\mathfrak{s}_A \quad \text{and} \quad \delta\mathfrak{s}^{\mathrm{h}} = \sum_{A\in\omega} N^A(\boldsymbol{X})\delta\mathfrak{s}_A, \tag{94}$$

where $\mathfrak{s}_A \in \mathbb{R}$ denotes the phase-field parameter at node $A \in \omega = \{1, \ldots, n\}$. Introduction of the discretised expressions for both the displacement field $\boldsymbol{\varphi}$ in (93) and the phase-field parameter $\mathfrak{s}$ in (94) into the weak forms in Eq. (45) yields

$$\begin{aligned} \mathrm{D}\, E^{tot\,\mathrm{h}}[\delta\boldsymbol{q}_A] &= \delta\boldsymbol{q}_A \cdot \left[\int_{\mathcal{B}_0} \boldsymbol{P}^{\mathrm{h}} \nabla_{\boldsymbol{X}} \left(N^A(\boldsymbol{X})\right)\, \mathrm{d}V - \int_{\mathcal{B}_0} N^A \bar{\boldsymbol{B}}(\boldsymbol{X})\, \mathrm{d}V - \int_{\partial\mathcal{B}_0^\sigma} N^A \bar{\boldsymbol{T}}\, \mathrm{d}A\right] = \boldsymbol{0}, \\ \mathrm{D}\, E^{tot\,\mathrm{h}}[\delta\mathfrak{s}_A] &= \delta\mathfrak{s}_A \int_{\mathcal{B}_0} N^A \mathcal{H}^{\mathrm{h}}\, \mathrm{d}V + \int_{\mathcal{B}_0} g_c\, \mathrm{D}\,\gamma\left(\mathfrak{s}_B N^B\right)[\delta\mathfrak{s}_A]\, \mathrm{d}V = 0, \end{aligned} \tag{95}$$

where $E^{tot\,\mathrm{h}}$, $\boldsymbol{P}^{\mathrm{h}}$ and $\mathcal{H}^{\mathrm{h}}$ denote the discrete total energy (44), the discrete first Piola–Kirchhoff stress tensor and the discrete driving force of the phase-field. Particularisation of Eq. $(95)_b$ to the Allen–Cahn energy crack density in (42) yields

$$\mathrm{D}\, E^{tot\,\mathrm{h}}[\delta\mathfrak{s}_A] = \delta\mathfrak{s}_A \left[\int_{\mathcal{B}_0} N^A \mathcal{H}^{\mathrm{h}}\, \mathrm{d}V + \int_{\mathcal{B}_0} \left(\frac{g_c}{l} N^A N^B \mathfrak{s}_B + g_c l \left(\nabla_{\boldsymbol{X}} N^A\right) \cdot \left(\nabla_{\boldsymbol{X}} N^B\right) \mathfrak{s}_B\right)\, \mathrm{d}V\right] = 0. \tag{96}$$

Finally, particularisation of Eq. $(95)_2$ to the Cahn–Hilliard energy crack density in (43) yields

$$\begin{aligned} \mathrm{D}\, E^{tot\,\mathrm{h}}[\delta\mathfrak{s}_A] = \delta\mathfrak{s}_A \Bigg[\int_{\mathcal{B}_0} N^A \mathcal{H}^{\mathrm{h}}\, \mathrm{d}V + \int_{\mathcal{B}_0} \Bigg(&\frac{g_c}{l} N^A N^B \mathfrak{s}_B \\ &+ g_c l \left(\nabla_{\boldsymbol{X}} N^A\right) \cdot \left(\nabla_{\boldsymbol{X}} N^B\right) \mathfrak{s}_B + \frac{g_c l^3}{2} \left(\Delta_{\boldsymbol{X}} N^A\right) \left(\Delta_{\boldsymbol{X}} N^B\right) \mathfrak{s}_B\Bigg)\, \mathrm{d}V\Bigg] = 0. \end{aligned} \tag{97}$$

5.2. Finite element discretisation of directional derivatives of the Hu–Washizu mixed variational principle

The directional derivatives of the above mixed variational principle (79) with respect to virtual variations of the deformation $\boldsymbol{\varphi}$ and virtual variations of the phase-field parameter $\mathfrak{s}$ give

$$\begin{aligned} \mathrm{D}\,\bar{\Pi}_{HW}[\delta\boldsymbol{\varphi}] &= \sum_{A=1}^{n_x} \boldsymbol{R}^A_{\boldsymbol{x}} \cdot \delta\boldsymbol{q}_A;\ \boldsymbol{R}^A_{\boldsymbol{x}} = \int_{\mathcal{B}_0} \boldsymbol{P}^h_{HW} N^A_{\boldsymbol{x}}\, \mathrm{d}V - \int_{\mathcal{B}_0} N^A_{\boldsymbol{x}} \bar{\boldsymbol{B}}\, \mathrm{d}V - \int_{\partial\mathcal{B}_0^\sigma} N^A_{\boldsymbol{x}} \bar{\boldsymbol{T}}\, \mathrm{d}A = 0, \\ \mathrm{D}\,\bar{\Pi}_{HW}[\delta\mathfrak{s}] &= \sum_{A=1}^{n_x} \boldsymbol{R}^A_{\mathfrak{s}} \cdot \delta\mathfrak{s}_A;\ \boldsymbol{R}^A_{\mathfrak{s}} = \int_{\mathcal{B}_0} \mathcal{H}^h_{HW} N^A_{\mathfrak{s}} \delta\mathfrak{s}\, \mathrm{d}V + \int_{\mathcal{B}_0} g_c\, \mathrm{D}\,\gamma(\mathfrak{s})[\delta\mathfrak{s}_A]\, \mathrm{d}V = 0, \end{aligned} \tag{98}$$

where $\boldsymbol{P}^h_{HW}$ and $\mathcal{H}^h_{HW}$ are the discrete counterparts of $\boldsymbol{P}_{HW}$ and $\mathcal{H}_{HW}$ (refer to Eq. (81)). Next, we have to define suitable interpolation spaces for the strains and stresses. Inside each element (i.e. element piecewise interpolation) we define shape functions $N^A_{\bar{\boldsymbol{F}}}$, $N^A_{\bar{\boldsymbol{H}}}$ and N^A_J (bilinear for the 2D and trilinear for the 3D case), and obtain

$$\begin{aligned} \bar{\boldsymbol{F}}^{\mathrm{h}} &= \sum_{A\in\omega_{\bar{\boldsymbol{F}}}} N^A_{\bar{\boldsymbol{F}}} \bar{\boldsymbol{F}}_A; \qquad \bar{\boldsymbol{H}}^{\mathrm{h}} = \sum_{A\in\omega_{\bar{\boldsymbol{H}}}} N^A_{\bar{\boldsymbol{H}}} \bar{\boldsymbol{H}}_A; \qquad J^{\mathrm{h}} = \sum_{A\in\omega_J} N^A_J J_A, \\ \delta\bar{\boldsymbol{F}}^{\mathrm{h}} &= \sum_{A\in\omega_{\bar{\boldsymbol{F}}}} N^A_{\bar{\boldsymbol{F}}} \delta\bar{\boldsymbol{F}}_A; \qquad \delta\bar{\boldsymbol{H}}^{\mathrm{h}} = \sum_{A\in\omega_{\bar{\boldsymbol{H}}}} N^A_{\bar{\boldsymbol{H}}} \delta\bar{\boldsymbol{H}}_A; \qquad \delta J^{\mathrm{h}} = \sum_{A\in\omega_J} N^A_J \delta J_A, \end{aligned} \tag{99}$$

and

$$\begin{aligned}
\boldsymbol{\Sigma}^{\mathrm{h}}_{\bar{\boldsymbol{F}}} &= \sum_{A\in\omega_{\bar{\boldsymbol{F}}}} N^A_{\bar{\boldsymbol{F}}}\,\boldsymbol{\Sigma}_{\bar{\boldsymbol{F}}A}; \qquad \boldsymbol{\Sigma}^{\mathrm{h}}_{\bar{\boldsymbol{H}}} = \sum_{A\in\omega_{\bar{\boldsymbol{H}}}} N^A_{\bar{\boldsymbol{H}}}\,\boldsymbol{\Sigma}_{\bar{\boldsymbol{H}}A}; \qquad \Sigma^{\mathrm{h}}_J = \sum_{A\in\omega_J} N^A_J\,\Sigma_{JA},\\
\delta\boldsymbol{\Sigma}^{\mathrm{h}}_{\bar{\boldsymbol{F}}} &= \sum_{A\in\omega_{\bar{\boldsymbol{F}}}} N^A_{\bar{\boldsymbol{F}}}\,\delta\boldsymbol{\Sigma}_{\bar{\boldsymbol{F}}A}; \qquad \delta\boldsymbol{\Sigma}^{\mathrm{h}}_{\bar{\boldsymbol{H}}} = \sum_{A\in\omega_{\bar{\boldsymbol{H}}}} N^A_{\bar{\boldsymbol{H}}}\,\delta\boldsymbol{\Sigma}_{\bar{\boldsymbol{H}}A}; \qquad \delta\Sigma^{\mathrm{h}}_J = \sum_{A\in\omega_J} N^A_J\,\delta\Sigma_{JA},
\end{aligned} \tag{100}$$

i.e. identical interpolation spaces are used for strain and stress fields and with $A \in \omega_\bullet = \{1, \ldots, n_\bullet\}$ and $n_\bullet$ the number of nodes per element associated with the discretisation of the field $\bullet$. For both, displacement and phase-field interpolations $N^A_{\boldsymbol{x}}$ and $N^A_{\mathfrak{s}}$, quadratic shape functions (either Lagrange or NURBS) are used. Then, the discretisation of Eq. (82) yields

$$D\bar{\Pi}_{HW}[\delta\bar{\boldsymbol{F}}, \delta\bar{\boldsymbol{H}}, \delta J] = \sum_{A=1}^{n_{\bar{\boldsymbol{F}}}} \boldsymbol{R}^A_{\bar{\boldsymbol{F}}} : \delta\bar{\boldsymbol{F}}_A + \sum_{A=1}^{n_{\bar{\boldsymbol{H}}}} \boldsymbol{R}^A_{\bar{\boldsymbol{H}}} : \delta\bar{\boldsymbol{H}}_A + \sum_{A=1}^{n_J} R^A_J\,\delta J_A, \tag{101}$$

where the different residuals associated with the weakly enforced constitutive equations are

$$\begin{aligned}
\boldsymbol{R}^A_{\bar{\boldsymbol{F}}} &= \int_{\mathcal{B}_0} \left(\Lambda_{\bar{\boldsymbol{F}}}\frac{\partial\bar{w}_{\bar{\boldsymbol{F}}}}{\partial\bar{\boldsymbol{F}}^{\mathrm{h}}} - \boldsymbol{\Sigma}^{\mathrm{h}}_{\bar{\boldsymbol{F}}}\right) N^A_{\bar{\boldsymbol{F}}}\,\mathrm{d}V,\\
\boldsymbol{R}^A_{\bar{\boldsymbol{H}}} &= \int_{\mathcal{B}_0} \left(\Lambda_{\bar{\boldsymbol{H}}}\frac{\partial\bar{w}_{\bar{\boldsymbol{H}}}}{\partial\bar{\boldsymbol{H}}^{\mathrm{h}}} - \boldsymbol{\Sigma}^{\mathrm{h}}_{\bar{\boldsymbol{H}}}\right) N^A_{\bar{\boldsymbol{H}}}\,\mathrm{d}V,\\
R^A_J &= \int_{\mathcal{B}_0} \left(\Lambda_J\frac{\partial U}{\partial J^{\mathrm{h}}} - \Sigma^{\mathrm{h}}_J\right) N^A_J\,\mathrm{d}V.
\end{aligned} \tag{102}$$

Finally, discretisation of Eq. (83) leads to

$$D\bar{\Pi}_{HW}[\delta\boldsymbol{\Sigma}_{\bar{\boldsymbol{F}}}, \delta\boldsymbol{\Sigma}_{\bar{\boldsymbol{H}}}, \delta\Sigma_J] = \sum_{A=1}^{n_{\bar{\boldsymbol{F}}}} \boldsymbol{R}^A_{\boldsymbol{\Sigma}_{\bar{\boldsymbol{F}}}} : \delta\boldsymbol{\Sigma}_{\bar{\boldsymbol{F}}A} + \sum_{A=1}^{n_{\bar{\boldsymbol{H}}}} \boldsymbol{R}^A_{\boldsymbol{\Sigma}_{\bar{\boldsymbol{H}}}} : \delta\boldsymbol{\Sigma}_{\bar{\boldsymbol{H}}A} + \sum_{A=1}^{n_J} R^A_{\Sigma_J}\,\delta\Sigma_{JA}, \tag{103}$$

where the different residuals associated with the weakly enforced compatibility equations are

$$\begin{aligned}
\boldsymbol{R}^A_{\boldsymbol{\Sigma}_{\bar{\boldsymbol{F}}}} &= \int_{\mathcal{B}_0} \left(\bar{\boldsymbol{F}}^{\mathrm{h}}_{\boldsymbol{x}} - \bar{\boldsymbol{F}}^{\mathrm{h}}\right) N^A_{\bar{\boldsymbol{F}}}\,\mathrm{d}V,\\
\boldsymbol{R}^A_{\boldsymbol{\Sigma}_{\bar{\boldsymbol{H}}}} &= \int_{\mathcal{B}_0} \left(\bar{\boldsymbol{H}}^{\mathrm{h}}_{\boldsymbol{x}} - \bar{\boldsymbol{H}}^{\mathrm{h}}\right) N^A_{\bar{\boldsymbol{H}}}\,\mathrm{d}V,\\
R^A_{\Sigma_J} &= \int_{\mathcal{B}_0} \left(J^{\mathrm{h}}_{\boldsymbol{x}} - J^{\mathrm{h}}\right) N^A_J\,\mathrm{d}V,
\end{aligned} \tag{104}$$

where the subscript $\boldsymbol{x}$ indicates the dependency of the corresponding variable with respect to the actual displacement.

5.2.1. Static condensation procedure for the Hu–Washizu mixed variational principle

The use of discontinuous interpolation spaces across elements for the fields $\{\bar{\boldsymbol{F}}, \bar{\boldsymbol{H}}, J\}$ and $\{\boldsymbol{\Sigma}_{\bar{\boldsymbol{F}}}, \boldsymbol{\Sigma}_{\bar{\boldsymbol{H}}}, \Sigma_J\}$ enables to carry out a static condensation procedure similar to that presented in Ref. [22], where the local degrees of freedom associated with these variables are condensed locally, leading to a formulation with a computational cost comparable to that of the two-field $\boldsymbol{\varphi}$–$\mathfrak{s}$ presented in Section 5.1. For notational convenience, let us introduce the vector $\boldsymbol{\mathcal{D}}$ representing the Voigt notation of the set of strains $\{\bar{\boldsymbol{F}}, \bar{\boldsymbol{H}}, J\}$ and $\boldsymbol{\Sigma}_{\boldsymbol{\mathcal{D}}}$ the Voigt notation of the conjugate set of stresses $\{\boldsymbol{\Sigma}_{\bar{\boldsymbol{F}}}, \boldsymbol{\Sigma}_{\bar{\boldsymbol{H}}}, \Sigma_J\}$. Discretisation of the weak forms and linearisations in Section 4 leads to the following system of equations at each element:

$$\begin{bmatrix}
\boldsymbol{K}^e_{\boldsymbol{x}\boldsymbol{x}} & \boldsymbol{0} & \boldsymbol{0} & \boldsymbol{K}^e_{\boldsymbol{x}\boldsymbol{\Sigma}_{\boldsymbol{\mathcal{D}}}}\\
\boldsymbol{0} & \boldsymbol{K}^e_{\mathfrak{s}\mathfrak{s}} & \boldsymbol{K}^e_{\mathfrak{s}\boldsymbol{\mathcal{D}}} & \boldsymbol{0}\\
\boldsymbol{0} & \boldsymbol{K}^e_{\boldsymbol{\mathcal{D}}\mathfrak{s}} & \boldsymbol{K}^e_{\boldsymbol{\mathcal{D}}\bar{\mathcal{D}}} & \boldsymbol{K}^e_{\boldsymbol{\mathcal{D}}\boldsymbol{\Sigma}_{\boldsymbol{\mathcal{D}}}}\\
\boldsymbol{K}^e_{\boldsymbol{\Sigma}_{\boldsymbol{\mathcal{D}}}\boldsymbol{x}} & \boldsymbol{0} & \boldsymbol{K}^e_{\boldsymbol{\Sigma}_{\boldsymbol{\mathcal{D}}}\boldsymbol{\mathcal{D}}} & \boldsymbol{0}
\end{bmatrix}
\begin{bmatrix}
\Delta\boldsymbol{x}_e\\ \Delta\mathfrak{s}_e\\ \Delta\boldsymbol{\mathcal{D}}_e\\ \Delta\boldsymbol{\Sigma}_{\boldsymbol{\mathcal{D}},e}
\end{bmatrix}
= -
\begin{bmatrix}
\boldsymbol{R}^e_{\boldsymbol{x}}\\ \boldsymbol{R}^e_{\mathfrak{s}}\\ \boldsymbol{R}^e_{\boldsymbol{\mathcal{D}}}\\ \boldsymbol{R}^e_{\boldsymbol{\Sigma}_{\boldsymbol{\mathcal{D}}}}
\end{bmatrix}, \tag{105}$$

where the subscript e is used to indicate the local character of a residual or stiffness at a particular element. The exact definitions of the discrete tangent operators $\boldsymbol{K}^e_{\bullet\bullet}$ corresponding to the continuous functions in (86)–(91) are presented in detail in Appendix A. It is possible to prove that in this formulation, the static condensation procedure will not introduce numerical difficulties, depending on how the static condensation procedure is carried out.

Let us focus on the fourth row in above linear system of equations, from which it is possible to obtain $\Delta\boldsymbol{\mathcal{D}}^e$ as

$$\Delta\boldsymbol{\mathcal{D}}_e = -\left(\boldsymbol{K}^e_{\boldsymbol{\Sigma}_{\boldsymbol{\mathcal{D}}}\boldsymbol{\mathcal{D}}}\right)^{-1}\left(\boldsymbol{R}^e_{\boldsymbol{\Sigma}_{\boldsymbol{\mathcal{D}}}} + \boldsymbol{K}^e_{\boldsymbol{\Sigma}_{\boldsymbol{\mathcal{D}}}\boldsymbol{x}}\Delta\boldsymbol{x}_e\right). \tag{106}$$

Finally, from the third row in above linear system of Eqs. (105), it is possible to obtain $\Delta\boldsymbol{\Sigma}^e_{\boldsymbol{\mathcal{D}}}$ as

$$\Delta\boldsymbol{\Sigma}_{\boldsymbol{\mathcal{D}},e} = -\left(\boldsymbol{K}^e_{\boldsymbol{\mathcal{D}}\boldsymbol{\Sigma}_{\boldsymbol{\mathcal{D}}}}\right)^{-1}\left(\boldsymbol{R}^e_{\boldsymbol{\mathcal{D}}} + \boldsymbol{K}^e_{\boldsymbol{\mathcal{D}}_{\mathfrak{s}}}\Delta\mathfrak{s}_e + \boldsymbol{K}^e_{\boldsymbol{\mathcal{D}}\boldsymbol{\mathcal{D}}}\Delta\boldsymbol{\mathcal{D}}_e\right), \tag{107}$$

with $\Delta\boldsymbol{\mathcal{D}}_e$ defined in (106). Therefore, in order to be able to carry out the static condensation procedure, it is crucial that both stiffness matrices $\boldsymbol{K}^e_{\boldsymbol{\mathcal{D}}\boldsymbol{\Sigma}_{\boldsymbol{\mathcal{D}}}}$ and $\boldsymbol{K}^e_{\boldsymbol{\Sigma}_{\boldsymbol{\mathcal{D}}}\boldsymbol{\mathcal{D}}}$ are invertible. In this particular formulation, it is clear that these matrices are always invertible. Introduction of the expressions for $\Delta\boldsymbol{\mathcal{D}}_e$ (106) and $\Delta\boldsymbol{\Sigma}^e_{\boldsymbol{\mathcal{D}}}$ (107) into the first and second rows of the linear system of equations in (105) enables the local algebraic system of equations to be formulated exclusively in terms of the unknowns $\Delta\boldsymbol{\varphi}_e$ and $\Delta\mathfrak{s}_e$ as

$$\begin{bmatrix} \tilde{\boldsymbol{K}}^e_{\boldsymbol{x}\boldsymbol{x}} & \tilde{\boldsymbol{K}}^e_{\boldsymbol{x}\mathfrak{s}} \\ \left(\tilde{\boldsymbol{K}}^e_{\boldsymbol{x}\mathfrak{s}}\right)^T & \tilde{\boldsymbol{K}}^e_{\mathfrak{s}\mathfrak{s}} \end{bmatrix}\begin{bmatrix} \Delta\boldsymbol{x}_e \\ \Delta\mathfrak{s}_e \end{bmatrix} = -\begin{bmatrix} \tilde{\boldsymbol{R}}^e_{\boldsymbol{x}} \\ \tilde{\boldsymbol{R}}^e_{\mathfrak{s}} \end{bmatrix}, \tag{108}$$

where the modified stiffness matrices $\tilde{\boldsymbol{K}}^e_{\boldsymbol{x}\boldsymbol{x}}$, $\tilde{\boldsymbol{K}}^e_{\boldsymbol{x}\mathfrak{s}}$ and $\tilde{\boldsymbol{K}}^e_{\mathfrak{s}\mathfrak{s}}$ are obtained as

$$\begin{aligned} \tilde{\boldsymbol{K}}^e_{\boldsymbol{x}\boldsymbol{x}} &= \boldsymbol{K}^e_{\boldsymbol{x}\boldsymbol{x}} + \boldsymbol{K}^e_{\boldsymbol{x}\boldsymbol{\Sigma}_{\boldsymbol{\mathcal{D}}}}\left(\boldsymbol{K}^e_{\boldsymbol{\mathcal{D}}\boldsymbol{\Sigma}_{\boldsymbol{\mathcal{D}}}}\right)^{-1}\boldsymbol{K}^e_{\boldsymbol{\mathcal{D}}\boldsymbol{\mathcal{D}}}\left(\boldsymbol{K}^e_{\boldsymbol{\Sigma}_{\boldsymbol{\mathcal{D}}}\boldsymbol{\mathcal{D}}}\right)^{-1}\boldsymbol{K}^e_{\boldsymbol{\Sigma}_{\boldsymbol{\mathcal{D}}}\boldsymbol{x}}, \\ \tilde{\boldsymbol{K}}^e_{\boldsymbol{x}\mathfrak{s}} &= -\boldsymbol{K}^e_{\boldsymbol{x}\boldsymbol{\Sigma}_{\boldsymbol{\mathcal{D}}}}\left(\boldsymbol{K}^e_{\boldsymbol{\mathcal{D}}\boldsymbol{\Sigma}_{\boldsymbol{\mathcal{D}}}}\right)^{-1}\boldsymbol{K}^e_{\boldsymbol{\mathcal{D}}_{\mathfrak{s}}}, \\ \tilde{\boldsymbol{K}}^e_{\mathfrak{s}\mathfrak{s}} &= \boldsymbol{K}^e_{\mathfrak{s}\mathfrak{s}}. \end{aligned} \tag{109}$$

Finally, the modified residuals $\tilde{\boldsymbol{R}}^e_{\boldsymbol{x}}$ and $\tilde{\boldsymbol{R}}^e_{\mathfrak{s}}$ are obtained as

$$\begin{aligned} \tilde{\boldsymbol{R}}^e_{\boldsymbol{x}} &= \boldsymbol{R}^e_{\boldsymbol{x}} - \boldsymbol{K}^e_{\boldsymbol{x}\boldsymbol{\Sigma}_{\boldsymbol{\mathcal{D}}}}\left(\boldsymbol{K}^e_{\boldsymbol{\mathcal{D}}\boldsymbol{\Sigma}_{\boldsymbol{\mathcal{D}}}}\right)^{-1}\boldsymbol{R}^e_{\boldsymbol{\mathcal{D}}} + \boldsymbol{K}^e_{\boldsymbol{x}\boldsymbol{\Sigma}_{\boldsymbol{\mathcal{D}}}}\left(\boldsymbol{K}^e_{\boldsymbol{\mathcal{D}}\boldsymbol{\Sigma}_{\boldsymbol{\mathcal{D}}}}\right)^{-1}\boldsymbol{K}^e_{\boldsymbol{\mathcal{D}}\boldsymbol{\mathcal{D}}}\left(\boldsymbol{K}^e_{\boldsymbol{\Sigma}_{\boldsymbol{\mathcal{D}}}\boldsymbol{\mathcal{D}}}\right)^{-1}\boldsymbol{R}^e_{\boldsymbol{\Sigma}_{\boldsymbol{\mathcal{D}}}}, \\ \tilde{\boldsymbol{R}}^e_{\boldsymbol{x}} &= \boldsymbol{R}^e_{\mathfrak{s}} - \boldsymbol{K}^e_{\mathfrak{s}\boldsymbol{\mathcal{D}}}\left(\boldsymbol{K}^e_{\boldsymbol{\Sigma}_{\boldsymbol{\mathcal{D}}}\boldsymbol{\mathcal{D}}}\right)^{-1}\boldsymbol{R}^e_{\boldsymbol{\Sigma}_{\boldsymbol{\mathcal{D}}}}. \end{aligned} \tag{110}$$

An alternative static condensation procedure is given in Appendix B.

Remark 6. It is worth emphasising that in this procedure, the invertibility of matrices $\boldsymbol{K}^e_{\boldsymbol{\mathcal{D}}\boldsymbol{\Sigma}_{\boldsymbol{\mathcal{D}}}}$ and $\boldsymbol{K}^e_{\boldsymbol{\Sigma}_{\boldsymbol{\mathcal{D}}}\boldsymbol{\mathcal{D}}}$ has enabled to obtain the modified matrices and residuals $\tilde{\boldsymbol{K}}^e_{\boldsymbol{x}\boldsymbol{x}}$, $\tilde{\boldsymbol{K}}^e_{\boldsymbol{x}\mathfrak{s}}$ and $\tilde{\boldsymbol{K}}^e_{\mathfrak{s}\mathfrak{s}}$, $\tilde{\boldsymbol{R}}^e_{\boldsymbol{x}}$ and $\tilde{\boldsymbol{R}}^e_{\mathfrak{s}}$ without introducing any additional numerical difficulty. However, the different scales of the mechanical and phase-field problems, related to the first and second rows of the final elemental system of equations in (108) might introduce an overall ill-conditioning which must be efficiently tackled via a suitable pre-conditioner or via a staggered solution approach.

6. Examples

In this section we evaluate the accuracy and performance of the newly proposed methods in the context of large strains. Moreover, a comparison of the new anisotropic split is carried out against the split in terms of principal eigenvalues as given in Ref. [27]. In particular, we focus on static two-dimensional (2D) and three-dimensional (3D) benchmark problems.

6.1. 2D tests

The following two-dimensional benchmark examples have been presented in Ref. [27] (see also [39] for further details). The objective of these examples is to address the following points:

I Comparison of the solution obtained by using linear Lagrange shape functions to that obtained by using quadratic NURBS for the interpolation of the displacement and the phase-field.

II Comparison of the second order Allen–Cahn crack density functional (42) and the fourth order Cahn–Hilliard crack density functional (43) using quadratic NURBS basis functions in both cases. Note that the second order Allen–Cahn type approach will in general produce different results as the fourth order Cahn–Hilliard type approach, since the predefined length scale parameter controls the regularisation zone differently in both approaches. However, we expect at least results which do not differ significantly.

III Study of the performance of the cubic degradation function $g(\mathfrak{s})$ defined in Eq. (52) examining the solution of the problem.

IV Comparison of the solution obtained with the proposed anisotropic split based on principal invariants with that obtained based on the principal eigenvalues of the deformation proposed in Ref. [27].

V Study of the effect of mesh refinement upon the solution.

VI Comparison of the solution obtained with the two-field $\boldsymbol{\varphi}$–$\mathfrak{s}$ formulation presented in Section 5.1 and the Hu–Washizu mixed formulation in Section 5.2.

In order to investigate each of the aforementioned points, a fixed value of the length parameter $l = 7.5 \times 10^{-6}$ m (interpreted as a material parameter) and a critical energy release rate $g_c = 2.7 \times 10^3$ J/m^2 will be chosen. Moreover, a Neo-Hookean material model (in two-dimensional problems, both invariants $I\!I_{\boldsymbol{F}}$ and $I\!I_{\bar{\boldsymbol{F}}}$ are computed as in Eq. (26)) defined as

$$W(\boldsymbol{F}, J) = \frac{\mu}{2}(I\!I_{\boldsymbol{F}} - 3) - \mu \ln(J) + \frac{\lambda}{2}(J-1)^2, \tag{111}$$

has been considered for all the simulations in which the anisotropic split based on the principal eigenvalues is employed. Alternatively, for those simulations in which the newly proposed invariant split is used, this model is conveniently modified in terms of the isochoric–volumetric split defined in Eq. (19), yielding

$$W(\boldsymbol{F}, J) = \frac{\mu}{2}(I\!I_{\bar{\boldsymbol{F}}} - 3) + \frac{\kappa}{2}(J-1)^2. \tag{112}$$

The material parameters have been chosen to be compatible with a Young's modulus of $E = 2.1 \times 10^{11}$ N/m and a Poisson's ratio of $\nu = 0.3$. For that purpose, the following choice of material parameters is required

$$\mu = 80.769 \times 10^9 \text{ N/m}^2; \qquad \lambda = 121.154 \times 10^9 \text{ N/m}^2. \tag{113}$$

The bulk modulus κ in (112) can then be calculated in a straightforward manner.

Tension test.

A well-established benchmark problem is that of a symmetric tension test consisting of a squared plate with a horizontal notch (area with initialised fracture) with the geometry depicted in Fig. 1 (left). The lower boundary is completely constrained as shown in Fig. 1 (left), whereas the upper boundary is incrementally stretched in the (vertical) y-direction reaching a total accumulated displacement of $u = 5.6 \times 10^{-6}$ m. An initial incremental displacement $\Delta u = 10^{-8}$ m is applied on the upper boundary until a total accumulated displacement of $u = 4 \times 10^{-6}$ m is reached. Subsequently, the incremental displacement is reduced by a factor of 10. Notice that this variably applied incremental displacement is necessary from the numerical standpoint. A more effective computational implementation would involve the use of an arc-length methodology, which can cope more efficiently with this type of problems near the verge of snap-through instabilities.

Two structured meshes of 256×256 and 512×512 quadrilateral elements are employed, yielding a uniform ratio between the element size and the length scale parameter l of $h \approx l/2$ and $h \approx l/4$, respectively. Snapshots depicting the contour plot of the phase-field variable $\mathfrak{s}$ at different values of the total accumulated displacement are shown in Fig. 2, where the proposed anisotropic split based on the principal invariants has been used. As already noted in Section 3.3.1, different anisotropic splits for the volumetric term $U^{\mathfrak{s}}(J, \mathfrak{s})$ are possible. Here, we use $U^{\mathfrak{s}}(\Lambda_J J, \mathfrak{s})$ instead of $\Lambda_J U^{\mathfrak{s}}(J, \mathfrak{s})$, since the latter formulation does not compare accordingly with the original anisotropic split in terms of eigenvalues.

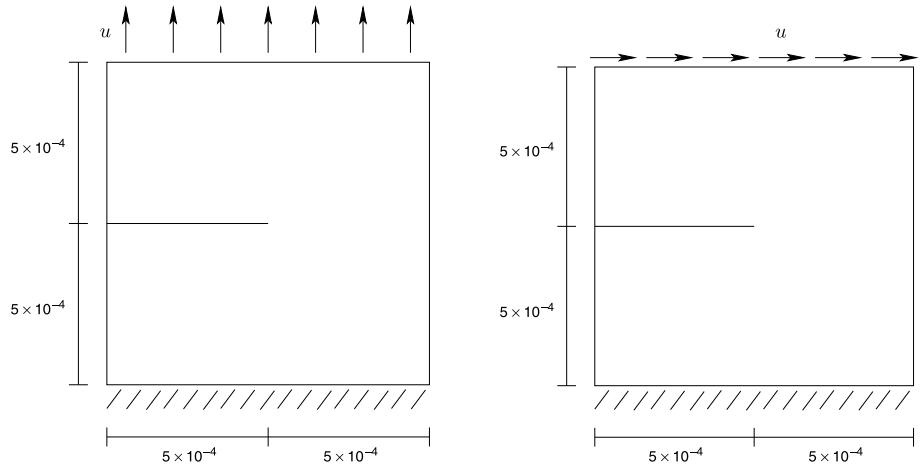

Fig. 1. Geometry and boundary conditions for the tension problem (left) and the shear problem (right).

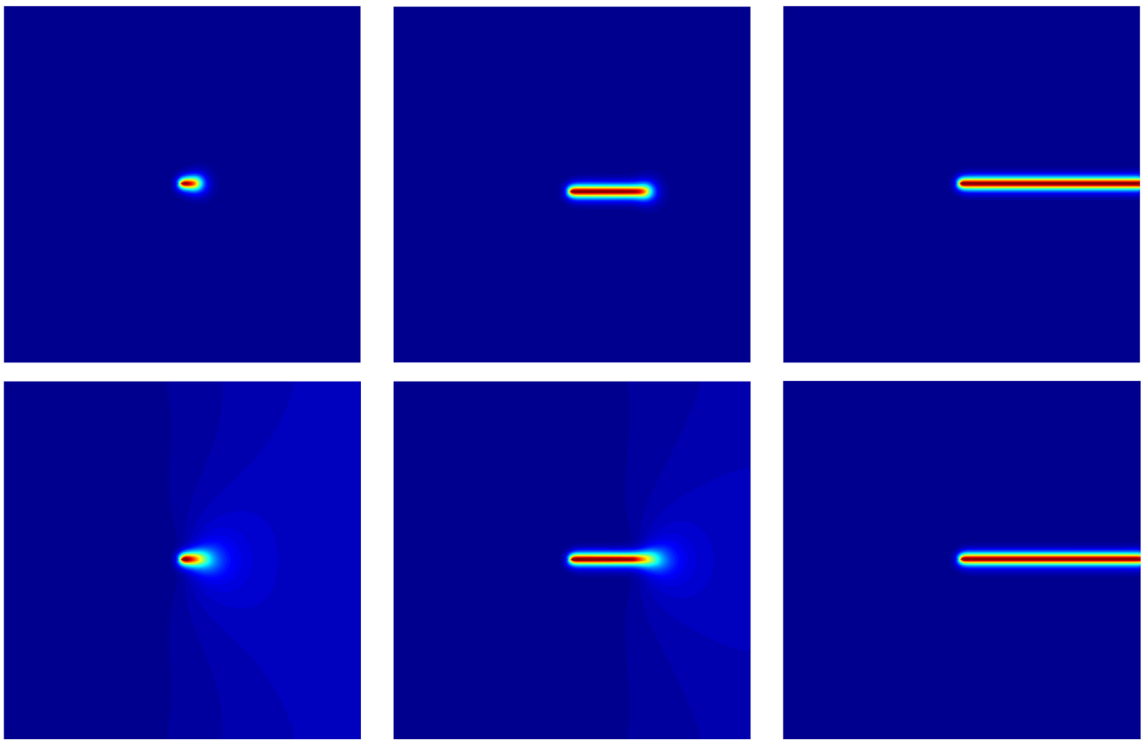

Fig. 2. Tension problem: Phase-field results for displacements of $u_y = [4.73,\ 4.83,\ 4.98] \times 10^{-6}$ m using the cubic degradation function with $a_g = 0.1$ (upper row) and for displacements of $u_y = [4.47,\ 4.69,\ 4.83] \times 10^{-6}$ m using the quadratic degradation function (lower row). Results for the Neo-Hookean model with anisotropic split of the invariants are presented. Results obtained with the two-field ($\boldsymbol{\varphi}$–$\mathfrak{s}$) formulation.

Fig. 3 shows a comparison of the results provided by the anisotropic split based on principal eigenvalues (left) and that based on principal invariants (right). In both approaches, the two-field ($\boldsymbol{\varphi}$–$\mathfrak{s}$) formulation in Section 5.2 has been used. For each approach displayed in Fig. 3, it is possible to observe that the solution obtained for both meshes, namely 256 × 256 quadrilateral elements and 512 × 512 quadrilateral elements are nearly identical, which indicates that for the coarser mesh the solution is already converged. Note that this addresses **point V** above. Regarding **point I**, these two Figures show that for both anisotropic splits, the results obtained using linear Lagrange shape functions

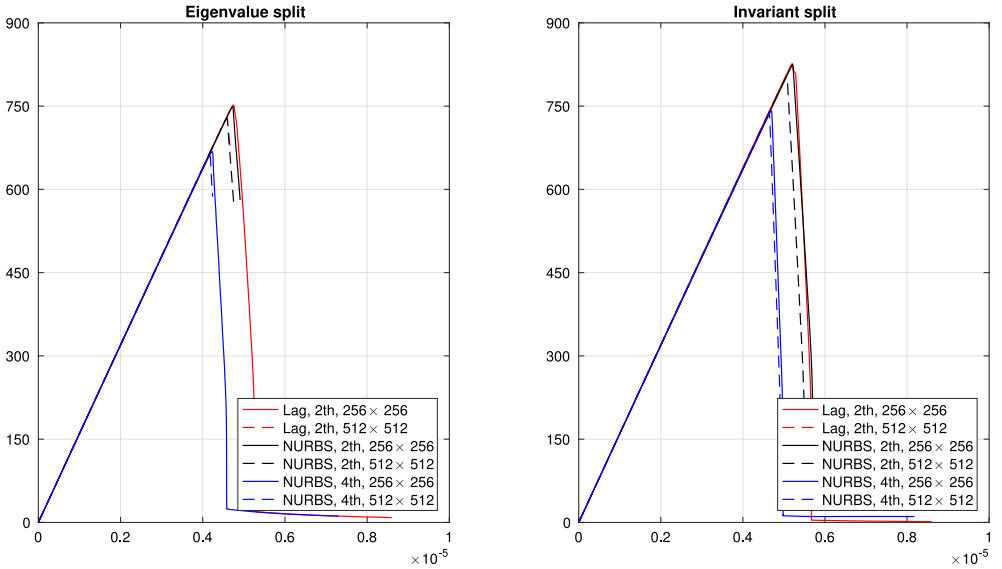

Fig. 3. Load–deflection curves for the tension problem using an eigenvalue split (left) and an invariant split (right). Results obtained with the two-field ($\boldsymbol{\varphi}$–$\mathfrak{s}$) formulation.

match exactly those obtained using quadratic NURBS when the second order Allen–Cahn crack density functional (42) is employed. Notice that this is expected for a sufficiently fine mesh with a converged solution.

Concerning **point IV**, we observe that the solution provided by both anisotropic splits (for the same choice of interpolation spaces, degradation function and crack density functional) differs noticeably regarding the initialisation of the crack. This is due to the fact, that different formulations of the elastic strain energy density functions are applied. Regarding **point III**, it is possible to observe the different influence of the cubic degradation function for a choice of the parameter $a_{\mathrm{g}} = 0.1$. Regarding **point II**, the results obtained when the fourth order Cahn–Hilliard crack density functional in (43) is used (in conjunction with quadratic NURBS) are slightly different from those obtained with the second order Allen–Cahn functional. Note that this was expected, as the fourth order functional regularises the transition zone differently, i.e. the same length scale parameter l yields a different constitutive behaviour in the material.

In Fig. 4, a more extensive comparison of the results of the second order Allen–Cahn crack functional and those obtained with the fourth order Cahn–Hilliard functional is presented. For each choice of crack density functional (second order (Fig. 4_a) and fourth order (Fig. 4_b)), both anisotropic splits have been employed using the cubic degradation function $g(\mathfrak{s})$ (52) with a choice of $a_g = 0.1$. For completeness, a linear degradation function $g(\mathfrak{s}) = 1-s$ has also been considered for the anisotropic split based on eigenvalues.[7] Notice that this linear degradation function was used in Ref. [27]. It can be observed that the cubic degradation function seems to be numerically more stable.

This numerical stability is dramatically affected for the particular choice of $a_g = 2$, degenerating in a quadratic degradation function (refer to Eq. (52)), as observed in Fig. 5, where a mesh of 256×256 quadrilateral elements and linear Lagrange shape functions were employed for all the simulations. In contrast to the cubic degeneration function, the choice of the quadratic degeneration function leads to a softening before crack initialisation for both anisotropic splits. Note that several curves for the eigenvalue split stop before a full breakthrough is even reached. Since we do not use a trust-region or any other similar numerical optimisation strategy, the additional material instability of this approach (refer to Remark 4) becomes apparent in this case. In contrast, the new approach based on principal invariants is numerically more stable.

Furthermore, the performance of the Hu–Washizu mixed variational formulation is investigated. A second order Allen–Cahn functional is used, for two spatial discretisations of 128×128 and 256×256 elements. A value of $a_g = 0.1$ is used for the (cubic) degeneration function. The Lamé and the length parameter are the same as in (113)

[7] The linear degeneration function is only considered within the exponent of the principal stretches.

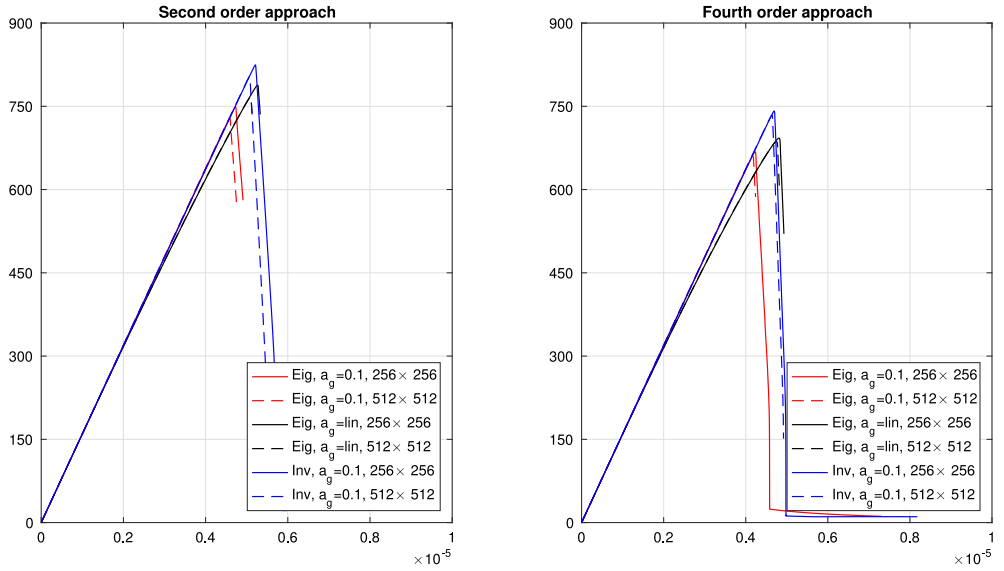

Fig. 4. Load–deflection curves for the tension problem for the second and the fourth order regularisation profile. Results obtained with the two-field ($\boldsymbol{\varphi}$–$\mathfrak{s}$) formulation.

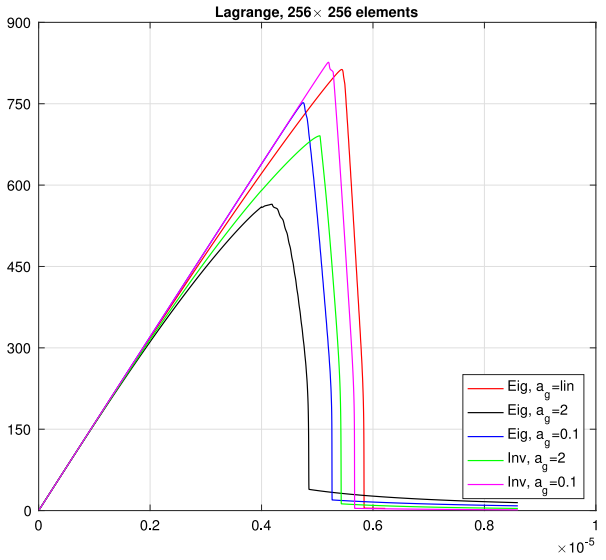

Fig. 5. Load–deflection curves for the tension problem. Study of different a_g parameters for the cubic degeneration function. Results obtained with the two-field ($\boldsymbol{\varphi}$–$\mathfrak{s}$) formulation.

to ensure a realistic comparison with previous results. The incremental displacements on the upper boundary are also prescribed in accordance to the previous examples.

Fig. 6 demonstrates the general applicability of the proposed Hu–Washizu formulation to phase-field problems. In particular, the phase-field as well as the von Mises stress field calculated from the independently approximated stress fields is displayed along with the load–deflection curve. Moreover, the von Mises stress distributions of the two-field ($\boldsymbol{\varphi}$–$\mathfrak{s}$) formulation as well as the Hu–Washizu mixed variational formulation are displayed for the evolving crack tip. The stress distributions are extremely similar, although the Hu–Washizu approach initiates the crack on a slightly higher value, which corresponds to the higher von Mises stress values in the colorbar on the right hand side.

As it is well-known for phase-field methods in statics, a large broken area can lead to numerical instabilities if a node is completely stress free. This has been avoided in the previous examples by applying a sufficient small

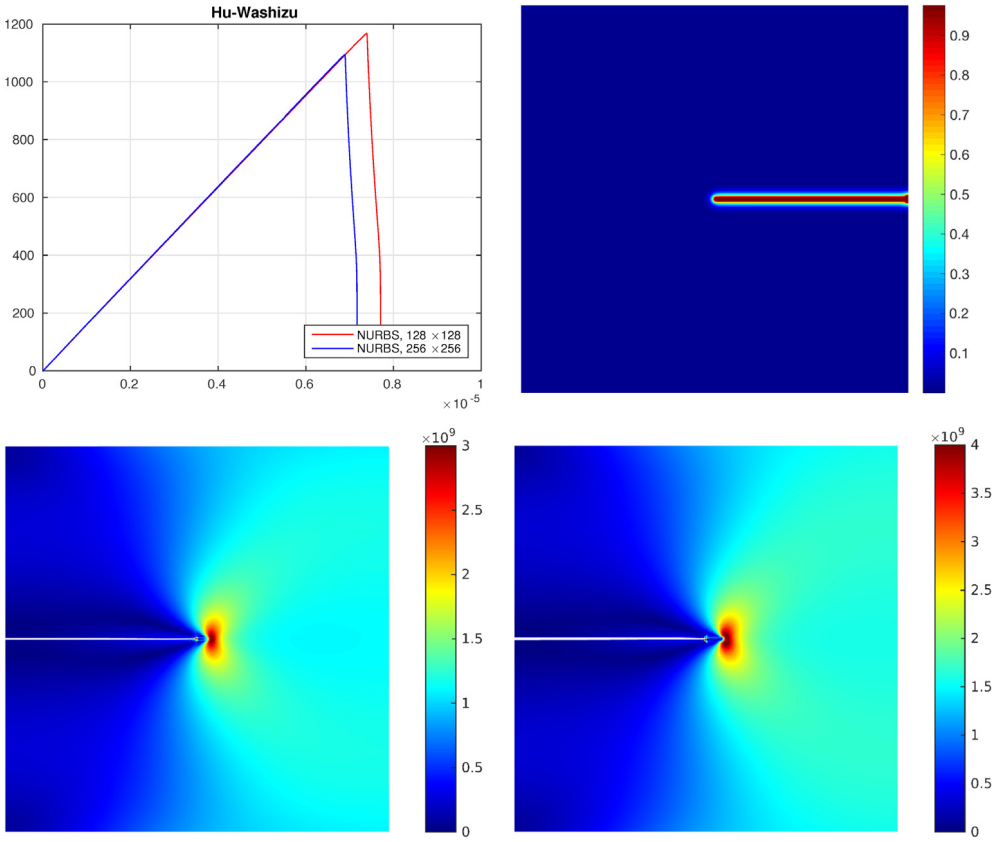

Fig. 6. Tension problem, upper row: Load–deflection curve for the tension problem and phase-field results for the fully broken state. Results obtained with the Hu–Washizu mixed variational formulation. Lower Row: von Mises stress distribution at the crack tip. Left: Two-field ($\boldsymbol{\varphi}$–$\mathfrak{s}$) formulation, right: Hu–Washizu mixed variational formulation. Note the different colorbar ranges. (For interpretation of the references to colour in this figure legend, the reader is referred to the web version of this article.)

length-scale parameter. Here, we observe in the von Mises stress distribution that the crack introduced by the phase-field within the Hu–Washizu formulation using the same length-scale parameter leads to a broader area with reduced stresses compared to the two-field ($\boldsymbol{\varphi}$–$\mathfrak{s}$) formulation. Hence, a smaller length-scale parameter is required for the mixed variational formulation to obtain the same results as for the irreducible approach. As it is well-known, a smaller length-scale parameter reduces the necessary energy to initiate the crack, which would lead to coinciding results for both formulations, see Miehe et al. [16] for a detailed discussion on the influence of the length-scale parameter.

Shear test.

The geometry and boundary conditions of the shear test example are depicted in Fig. 1 (right). The difference with respect to the previous example (tension problem) resides on the application of a (horizontal) x-direction displacement on the upper boundary of the body, yielding a shear type deformation. In contrast to the previous example, a uniform incremental displacement of $\Delta u = 10^{-8}$ m is now applied on this boundary. The material parameters are exactly the same as those for the tension problem.

Fig. 7 shows a series of snapshots for the contour plot of the phase-field variable $\mathfrak{s}$, where the two-field ($\boldsymbol{\varphi}$–$\mathfrak{s}$) formulation has been used. The load–deflection curves for the two anisotropic splits are presented in Fig. 8, yielding analogous conclusions to the tension test. As can be observed, the results for the mesh using 256×256 quadrilateral elements are nearly identical compared with the results of the mesh using 512×512 quadrilateral elements. Additionally, the newly proposed anisotropic split based on the principal invariants initialises slightly differently with respect to the anisotropic split based on the principal eigenvalues. Eventually, Fig. 9 shows the load–deflection

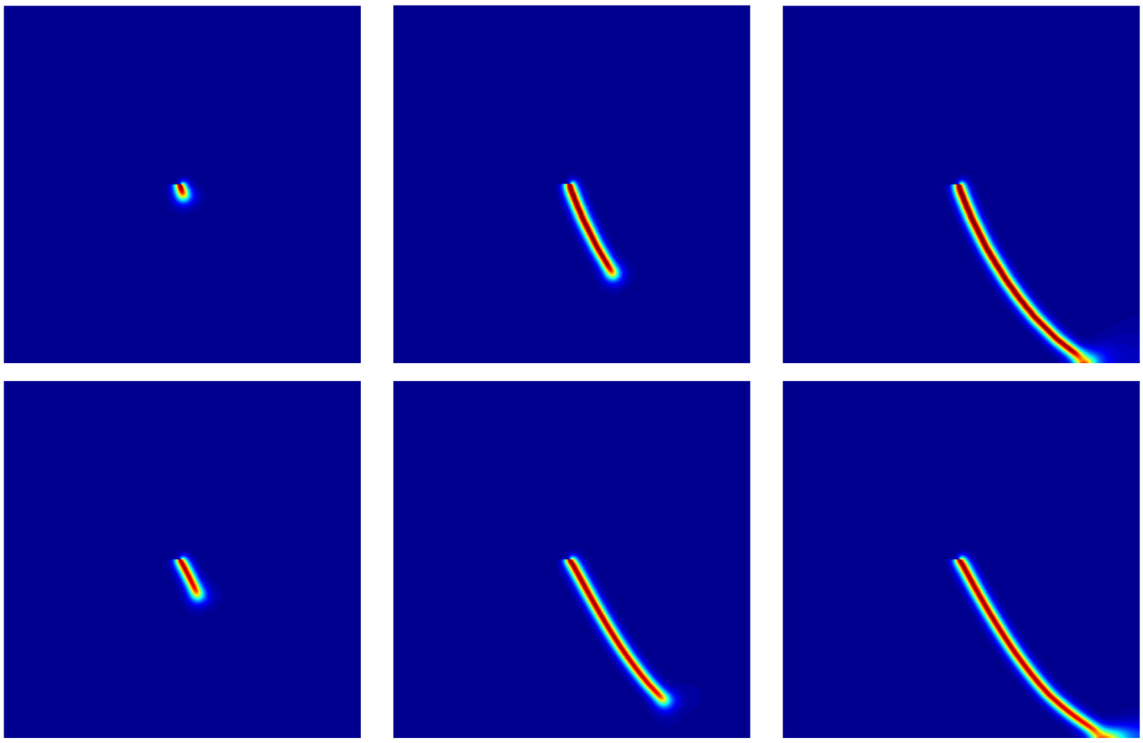

Fig. 7. Shear problem: Phase-field results for displacements of $u_x = [8.5,\ 10.5,\ 1.22] \times 10^{-6}$ m using the Neo-Hookean model with an anisotropic split of the principal invariants (upper row) and for displacements of $u_x = [8.5,\ 10.5,\ 11.05] \times 10^{-6}$ m using the Neo-Hookean model with an anisotropic split of the principal eigenvalues (lower row). In both a parameter of $a_{\mathrm{g}} = 0.1$ is used for the cubic degradation function. Results obtained with the two-field ($\boldsymbol{\varphi}$–$\mathfrak{s}$) formulation.

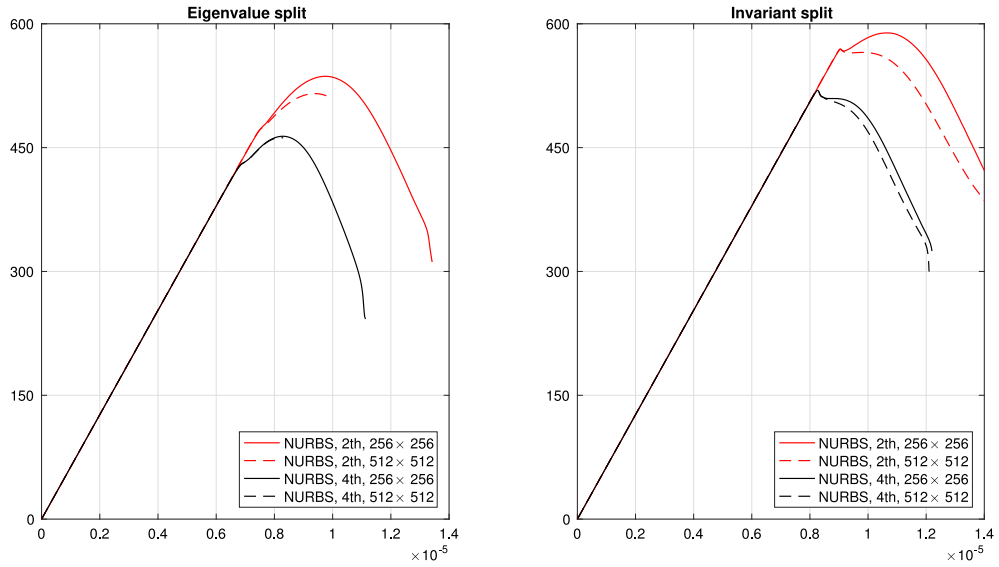

Fig. 8. Load–deflection curves for the shear problem for the different splits using an eigenvalue and a decomposition of the invariants. Results obtained with the two-field ($\boldsymbol{\varphi}$–$\mathfrak{s}$) formulation.

curves for the second and fourth order crack density functionals yielding similar conclusions to those obtained for the tension test in Fig. 4.

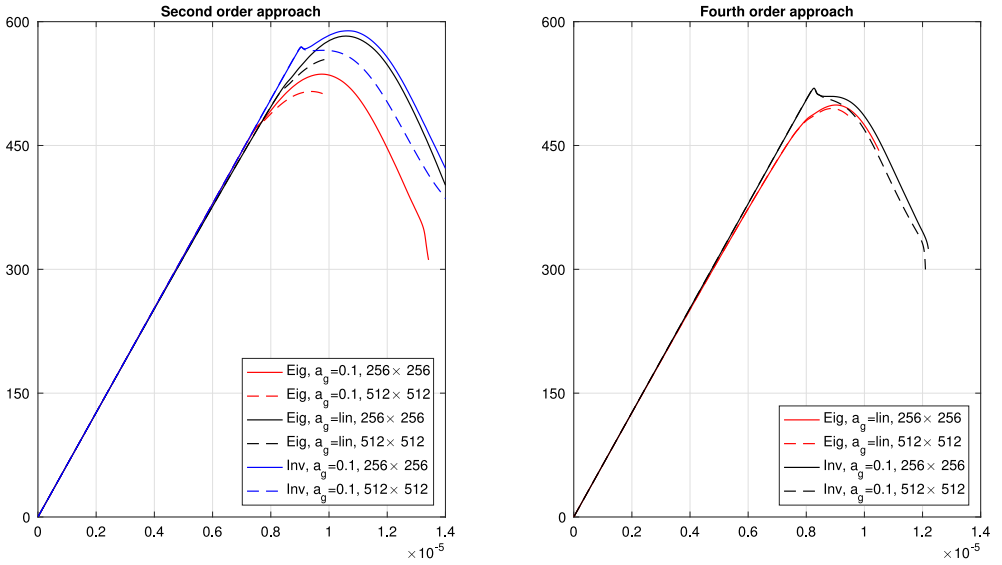

Fig. 9. Load–deflection curves for the shear problem for the second and the fourth order regularisation profile. Results obtained with the two-field ($\boldsymbol{\varphi}$–$\bar{\mathfrak{s}}$) formulation.

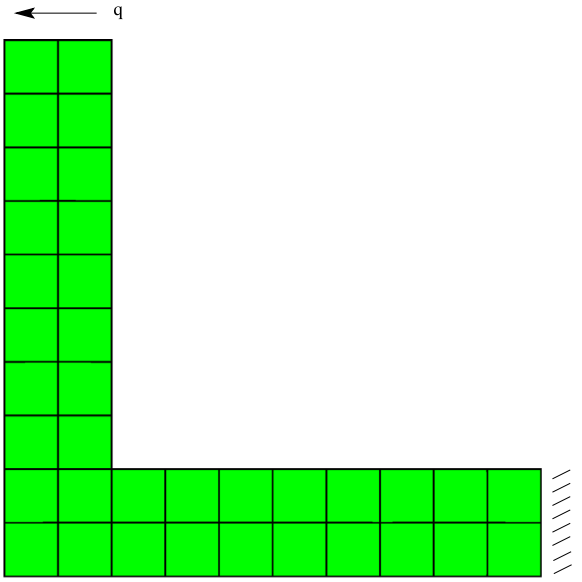

Fig. 10. Reference configuration of the large deformation test. A coarse mesh is displayed for visualisation purposes.

6.2. Large deformation test

The objective of this example is to illustrate the applicability of the formulation to scenarios where large deformations are obtained in the entire computational domain. With that in mind a Neo-Hookean constitutive model is considered with material parameters defined as follows

$$\mu = 8000\ \mathrm{N/m^2}; \qquad \lambda = 4000\ \mathrm{N/m^2}, \tag{114}$$

which correspond to a Young's modulus of $E = 1.0667 \times 10^4$ and a Poisson ratio of $\nu = 0.333$. The reference configuration is given in Fig. 10; the outer length of the beams comprising the L-shape is 10 m and the thickness 2 m. A structured mesh of 99 435 elements with a total number of 301 464 degrees of freedom is considered. A value of

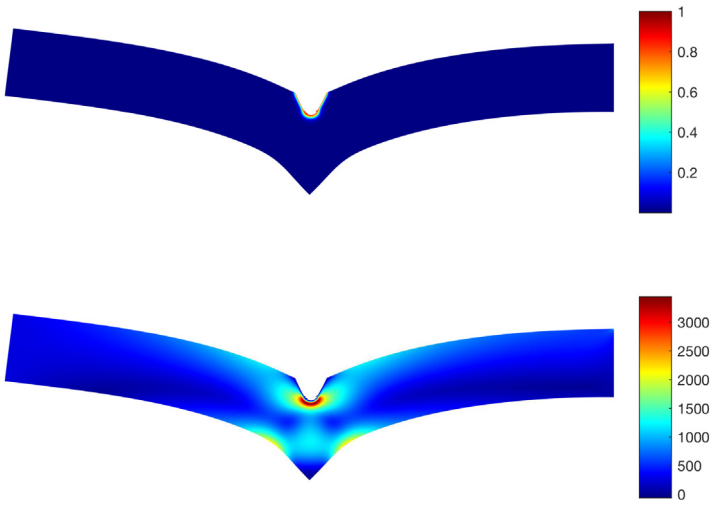

Fig. 11. Results of the large deformation test. Upper picture: Phase-field, lower: von Mises stress distribution. Broken elements are removed.

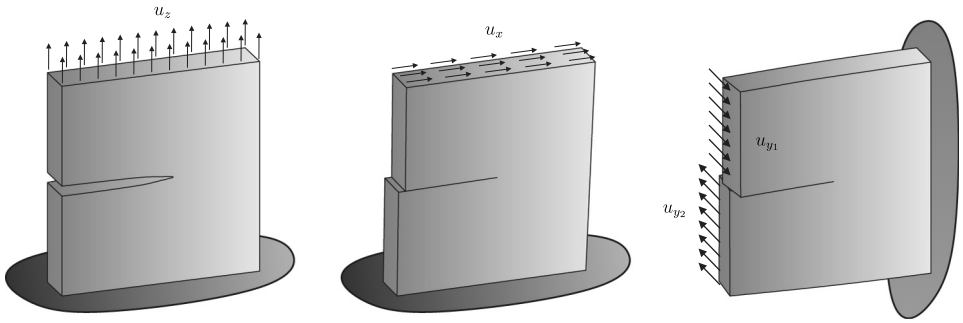

Fig. 12. Boundary conditions for mode I (left), mode II (middle) and mode III (right) crack propagation.

$a_g = 0.1$ is used for the degradation function $g(\mathfrak{s})$ and a critical energy release rate of $g_c = 2.7 \times 10^3$ J/m^2. The length scale parameter has been adapted to the mesh using $l = 0.0381$ m, such that $l = h/2$. A force per unit undeformed area of $\bar{\boldsymbol{T}} = [0,\ -200 \times t]$ N/m^2 has been applied to the upper surface, controlled by a quasi time-step size of $\Delta t = 0.001$ for each load increment. The L-shaped domain is completely constrained on the right hand side boundary.

Fig. 11 displays the phase-field as well as the stress field after crack initialisation at $t = 1.302$ s. As can be seen, the crack evolves as expected. Note that all the broken elements have been removed for post-processing purposes.

6.3. 3D tests

The objective of this Section is to demonstrate the applicability of the newly proposed anisotropic split, in conjunction with the use of the fourth order Cahn–Hilliard crack functional (43), the cubic degradation function (52) and the use of hierarchical refined NURBS for the numerical simulation of fracture using phase-field models in three-dimensional applications. In particular, we consider a horizontal notched plate of size 1 m $\times$ 0.2 m $\times$ 1 m. The classical fracture modes I, II and III (depicted in Fig. 12) are considered in this example, representing the crack propagation due to a unidirectional stretch (mode I), in-plane shear (mode II), and out-of-plane shear (mode III) loadings (see also Hesch et al. [20]).

For the three models, a mesh of $20 \times 4 \times 20$ quadratic B-spline elements on level zero has been used. Additionally, the finite element mesh is locally refined to capture the different crack path for each specific fracture mode as:

Mode I: Three local refinement levels are used for the pure tension test, see Fig. 13, left. In total 46 288 elements with overall 275 354 degrees of freedom are employed. The displacement increment is set to $\Delta u = 0.5 \times 10^{-4}$ m.

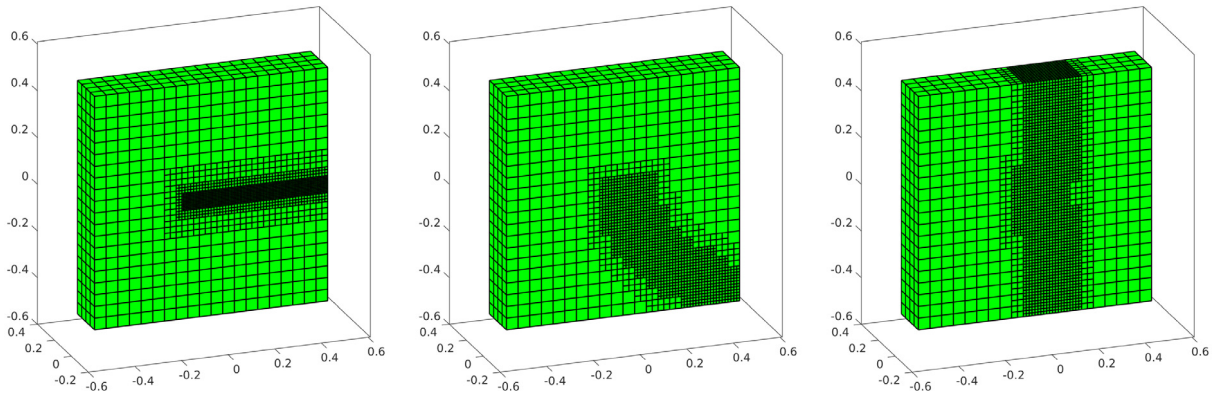

Fig. 13. Initial meshes of mode I (left), mode II (middle) and mode III (right).

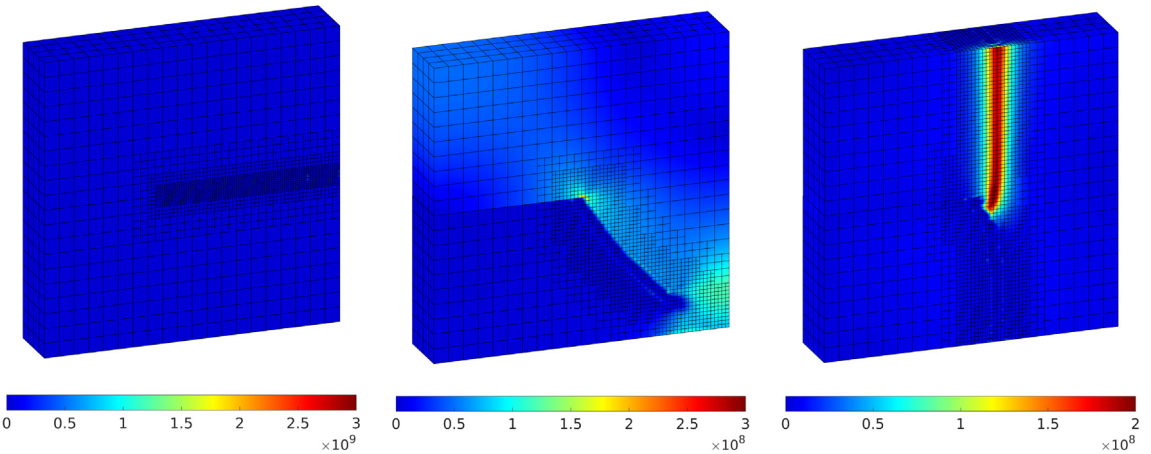

Fig. 14. Von Mises stress results of mode I (left, for displacement $u_z = 0.26 \times 10^{-3}$ m), mode II (middle, for displacement $u_x = 0.37 \times 10^{-3}$ m) and mode III (right, for displacement $u_{y_1} = -u_{y_2} = -1.74 \times 10^{-3}$ m). Results obtained using the two-field ($\boldsymbol{\varphi}$–$\mathfrak{s}$) formulation.

Mode II: Two local refinement levels are used for the in-plane shear test, see Fig. 13, middle. In total 21 900 elements with overall 102 807 degrees of freedom are employed. The displacement increment is set to $\Delta u = 0.5 \times 10^{-4}$ m.

Mode III: Two local refinement levels are used for the out-of-plane shear test, see Fig. 13, right. In total 29 040 elements with overall 135 732 degrees of freedom are employed. The displacement increment is set to $\Delta u = 1 \times 10^{-4}$ m.

The constitutive behaviour is assumed to be governed by the Mooney–Rivlin model in (57) with the volumetric functional U defined as in (21), where the parameters correspond to a steel-like material with $\gamma = 26.923$ GPa, $\zeta = 13.462$ GPa and $\kappa = 175$ GPa. In addition, the phase-field parameters are set to $g_c = 2.7 \times 10^3$ J/m^2, $l = 0.0081$ m and $a_g = 0.085$ for mode I, whereas $l = 0.0138$ m and $a_g = 0.05$ are used for modes II and III. The two-field ($\boldsymbol{\varphi}$–$\mathfrak{s}$) formulation has been used in this example.

Fig. 14 shows the von Mises stress distribution for the three modes at a specific displacement increment. The contour plot of the phase-field variable $\mathfrak{s}$ is depicted using isosurfaces for $\mathfrak{s} = 0.8$ in Fig. 15, displaying detailed snapshots of the crack progression for the different modes. Note that the NURBS meshes have been created using condensed higher order domain decomposition constraints between two rectangular blocks starting at the centre up to the right hand boundary, such that we obtain an initial crack from the left hand boundary to the centre. The meshes in Fig. 15 indicate this construction by displaying the internal interface.

Summarised, the fourth order Cahn–Hilliard crack functional (43) in conjunction with cubic degradation function (52) and the proposed polyconvex anisotropic split based upon the principal invariants has been used in this example.

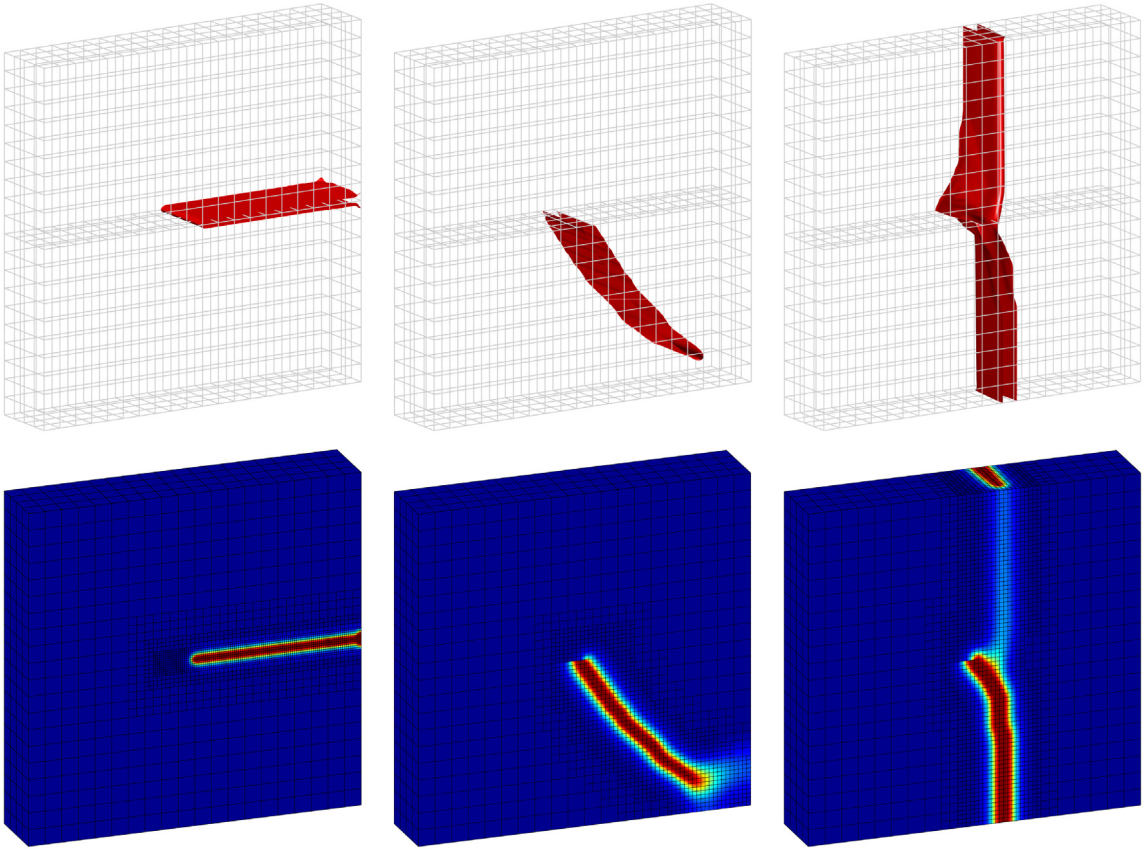

Fig. 15. Final phase-field results of mode I (left, for displacement $u_z = 0.26 \times 10^{-3}$ m), mode II (middle, for displacement $u_x = 0.37 \times 10^{-3}$ m) and mode III (right, for displacement $u_{y_1} = -u_{y_2} = -1.74 \times 10^{-3}$ m). Results obtained using the two-field ($\boldsymbol{\varphi}$–$\mathfrak{s}$) formulation.

The effective prediction of arbitrary three-dimensional crack propagation patterns, with special mention to the mode III shear test, is extremely complex in the sense that three-dimensional patterns have been obtained as shown in Fig. 15$_c$. Note that the mode III example does not produce a perfect crack path as expected for the linear theory. We conducted additional tests with different boundary conditions (e.g. by constraining all degrees of freedom of the front surfaces) and obtain results analogous to the presented ones, i.e. the complex fracture patterns emanate from the non-linear theory used in this example.

7. Conclusions

In this paper, a framework for polyconvex non-linear elasticity in the context of phase-field fracture is presented. The phase-field methodology is based upon a novel anisotropic split in terms of the principal invariants of the right Cauchy–Green deformation tensor.

The novel formulation based on principle invariants improves the numerical stability of the non-linear fracture problem tremendously. Numerical stability, related to the material stability of the Hessian operator $[\mathbb{H}_{W_m^{\mathfrak{s}}}]$, is one of the major issues for a stable simulation of crack propagation. An insightful decomposition of the Hessian operator is presented in this paper, which allows to identify the possible sources of instability as fracture propagates.

Furthermore, for the first time in the context of phase-field fracture mechanics, a Hu–Washizu type of mixed variational principle is presented. This principle allows for a direct access of the strains and stresses as primary variables of the system and opens the door for novel variationally consistent formulations of the phase-field methodology. The mixed formulation considers an extended set of variables including the kinematic entities $\{\bar{\boldsymbol{F}},\ \bar{\boldsymbol{H}},\ J\}$ and their work conjugates $\{\boldsymbol{\Sigma}_{\bar{\boldsymbol{F}}},\ \boldsymbol{\Sigma}_{\bar{\boldsymbol{H}}},\ \Sigma_J\}$. This formulation, in conjunction with the use of the tensor cross product in [22] simplifies the algebra drastically in comparison with the two-field ($\boldsymbol{\varphi}$–$\mathfrak{s}$) formulation. Additionally, a static condensation

procedure has been carried in order to condense out the discontinuous strain–stress fields, leading to a formulation with a computational cost comparable to that of the two-field formulation.

Finally, a Hu–Washizu type mixed variational principle is applied for the first time to higher order Cahn–Hilliard crack energy density functionals in conjunction with the use of NURBS based shape functions with hierarchical refinement in two and three-dimensional applications. This demonstrates the applicability as well as the generality of the chosen approach. Future work will extend this formulation to transient large-scale multi-physical simulations.

Acknowledgements

Support for this research was provided by the Deutsche Forschungsgemeinschaft (DFG) under grants HE5943/6-1 and BE2285/9-1. The authors C. Hesch and K. Weinberg gratefully acknowledge support by the DFG in the framework of the Priority Programme "Reliable Simulation Techniques in Solid Mechanics. Development of Non-standard Discretisation Methods, Mechanical and Mathematical Analysis" (SPP 1748) under projects HE5943/5-1 and WE2525/5-1. The authors A.J. Gil and R. Ortigosa acknowledge the financial support provided by the Sêr Cymru National Research Network for Advanced Engineering and Materials.

Appendix A. Finite element discretisation of linearisations

Directional derivatives of $\mathrm{D}\,\bar{\Pi}_{HW}[\delta\boldsymbol{\varphi}]$. The discretisation of Eq. (86) enables to define the stiffness matrix contribution $\boldsymbol{K}_{\boldsymbol{x}\boldsymbol{x}}$ as

$$\begin{aligned}
\boldsymbol{K}_{\boldsymbol{x}\boldsymbol{x}}^{AB} =& -\int_{\mathcal{B}_0} \frac{J_{\boldsymbol{x}}^{-4/3}}{3}\left[\left(\boldsymbol{\Sigma}_{\bar{\boldsymbol{F}}}\boldsymbol{\nabla}_0 N_{\boldsymbol{x}}^A\right)\otimes\left(\boldsymbol{H}_{\boldsymbol{x}}\boldsymbol{\nabla}_0 N_{\boldsymbol{x}}^B\right)+\left(\boldsymbol{H}_{\boldsymbol{x}}\boldsymbol{\nabla}_0 N_{\boldsymbol{x}}^A\right)\otimes\left(\boldsymbol{\Sigma}_{\bar{\boldsymbol{F}}}\boldsymbol{\nabla}_0 N_b^{\boldsymbol{x}}\right)\right]\mathrm{d}V\\
&-\int_{\mathcal{B}_0}\frac{2J_{\boldsymbol{x}}^{-5/3}}{3}\left[\left(\left(\boldsymbol{\Sigma}_{\bar{\boldsymbol{H}}}\times\boldsymbol{F}_{\boldsymbol{x}}\right)\boldsymbol{\nabla}_0 N_{\boldsymbol{x}}^A\right)\otimes\left(\boldsymbol{H}_{\boldsymbol{x}}\boldsymbol{\nabla}_0 N_{\boldsymbol{x}}^B\right)+\left(\boldsymbol{H}_{\boldsymbol{x}}\boldsymbol{\nabla}_0 N_{\boldsymbol{x}}^A\right)\otimes\left(\left(\boldsymbol{\Sigma}_{\bar{\boldsymbol{H}}}\times\boldsymbol{F}_{\boldsymbol{x}}\right)\boldsymbol{\nabla}_0 N_{\boldsymbol{x}}^B\right)\right]\mathrm{d}V\\
&+\boldsymbol{\mathcal{E}}:\int_{\mathcal{B}_0} J_{\boldsymbol{x}}^{-2/3}\left(\boldsymbol{\Sigma}_{\bar{\boldsymbol{H}}}\left(\boldsymbol{\nabla}_0 N_{\boldsymbol{x}}^A\times\boldsymbol{\nabla}_0 N_{\boldsymbol{x}}^B\right)\right)\mathrm{d}V\\
&+\boldsymbol{\mathcal{E}}:\int_{\mathcal{B}_0}\left(\Sigma_J-\frac{J_{\boldsymbol{x}}^{-4/3}}{3}\left(\boldsymbol{\Sigma}_{\bar{\boldsymbol{F}}}:\boldsymbol{F}_{\boldsymbol{x}}\right)-\frac{2J_{\boldsymbol{x}}^{-5/3}}{3}\left(\boldsymbol{\Sigma}_{\bar{\boldsymbol{H}}}:\boldsymbol{H}_{\boldsymbol{x}}\right)\right)\left(\boldsymbol{F}_{\boldsymbol{x}}\left(\boldsymbol{\nabla}_0 N_{\boldsymbol{x}}^A\times\boldsymbol{\nabla}_0 N_{\boldsymbol{x}}^B\right)\right)\mathrm{d}V\\
&+\int_{\mathcal{B}_0}\frac{4J_{\boldsymbol{x}}^{-7/3}}{9}\left(\boldsymbol{\Sigma}_{\bar{\boldsymbol{F}}}:\boldsymbol{F}_{\boldsymbol{x}}\right)\left(\boldsymbol{H}_{\boldsymbol{x}}\boldsymbol{\nabla}_0 N_{\boldsymbol{x}}^A\right)\otimes\left(\boldsymbol{H}_{\boldsymbol{x}}\boldsymbol{\nabla}_0 N_{\boldsymbol{x}}^B\right)\mathrm{d}V\\
&-\int_{\mathcal{B}_0}\frac{10J_{\boldsymbol{x}}^{-8/3}}{9}\left(\boldsymbol{\Sigma}_{\bar{\boldsymbol{H}}}:\boldsymbol{H}_{\boldsymbol{x}}\right)\left(\boldsymbol{H}_{\boldsymbol{x}}\boldsymbol{\nabla}_0 N_{\boldsymbol{x}}^A\right)\otimes\left(\boldsymbol{H}_{\boldsymbol{x}}\boldsymbol{\nabla}_0 N_{\boldsymbol{x}}^B\right)\mathrm{d}V. \qquad (115)
\end{aligned}$$

The stiffness matrix contributions $\{\boldsymbol{K}_{\boldsymbol{x}\boldsymbol{\Sigma}_{\bar{\boldsymbol{F}}}},\boldsymbol{K}_{\boldsymbol{x}\boldsymbol{\Sigma}_{\bar{\boldsymbol{H}}}},\boldsymbol{K}_{\boldsymbol{x}\Sigma_J}\}$ arising from the discretisation of the expressions in Eq. (87)

$$\begin{aligned}
\boldsymbol{K}_{\boldsymbol{x}\boldsymbol{\Sigma}_{\bar{\boldsymbol{F}}}}^{AB} &= \int_{\mathcal{B}_0}\left[J_{\boldsymbol{x}}^{-1/3}N_{\bar{\boldsymbol{F}}}^B\left(\boldsymbol{I}\otimes\boldsymbol{\nabla}_0 N_{\boldsymbol{x}}^A\right)-\frac{1}{3}J_{\boldsymbol{x}}^{-4/3}N_{\bar{\boldsymbol{F}}}^B\left(\boldsymbol{H}_{\boldsymbol{x}}\boldsymbol{\nabla}_0 N_{\boldsymbol{x}}^A\right)\otimes\boldsymbol{F}_{\boldsymbol{x}}\right]\mathrm{d}V;\\
\left[\boldsymbol{K}_{\boldsymbol{x}\boldsymbol{\Sigma}_{\bar{\boldsymbol{H}}}}^{AB}\right]_{ijI} &= \mathcal{E}_{ijk}\left[\int_{\mathcal{B}_0}J_{\boldsymbol{x}}^{-2/3}\left(\boldsymbol{F}_{\boldsymbol{x}}\times\boldsymbol{\nabla}_0 N_{\boldsymbol{x}}^A\right)N_{\bar{\boldsymbol{H}}}^B\,\mathrm{d}V\right]_{kI}-\left[\int_{\mathcal{B}_0}\frac{2}{3}J_{\boldsymbol{x}}^{-5/3}N_{\bar{\boldsymbol{H}}}^B\left(\boldsymbol{H}_{\boldsymbol{x}}\boldsymbol{\nabla}_0 N_{\boldsymbol{x}}^A\right)\otimes\boldsymbol{H}_{\boldsymbol{x}}\,\mathrm{d}V\right]_{ijI}; \qquad (116)\\
\boldsymbol{K}_{\boldsymbol{x}\Sigma_J}^{AB} &= \int_{\mathcal{B}_0}N_J^B\left(\boldsymbol{H}_{\boldsymbol{x}}\boldsymbol{\nabla}_0 N_{\boldsymbol{x}}^A\right)\mathrm{d}V.
\end{aligned}$$

Directional derivatives of $\mathrm{D}\,\bar{\Pi}_{HW}[\delta\mathfrak{s}]$. The discretisation of the expression in Eq. (88) for the Allen–Cahn density functional (42) yields the stiffness contribution $\boldsymbol{K}_{\mathfrak{s}\mathfrak{s}}$, defined as

$$\boldsymbol{K}^{AB}_{\mathfrak{s}\mathfrak{s}} = \int_{\mathcal{B}_0} N^A_{\mathfrak{s}} \left(\frac{\partial^2 \Lambda_{\bar{\boldsymbol{F}}}}{\partial \mathfrak{s}^2} \bar{w}_{\bar{\boldsymbol{F}}} + \frac{\partial^2 \Lambda_{\bar{\boldsymbol{H}}}}{\partial \mathfrak{s}^2} \bar{w}_{\bar{\boldsymbol{H}}} + \frac{\partial^2 \Lambda_J}{\partial \mathfrak{s}^2} U \right) N^B_{\mathfrak{s}} \, \mathrm{d}V + \int_{\mathcal{B}_0} \left(N^A_{\mathfrak{s}} N^B_{\mathfrak{s}} \frac{g_c}{l} + g_c l \left(\nabla_{\boldsymbol{X}} N^A_{\mathfrak{s}} \right) \cdot \left(\nabla_{\boldsymbol{X}} N^B_{\mathfrak{s}} \right) \right) \mathrm{d}V. \tag{117}$$

Analogously, for the Cahn–Hilliard crack energy density functional (43), the stiffness matrix contribution $\boldsymbol{K}_{\mathfrak{s}\mathfrak{s}}$ adopts the following expression

$$\boldsymbol{K}^{AB}_{\mathfrak{s}\mathfrak{s}} = \int_{\mathcal{B}_0} N^A_{\mathfrak{s}} \left(\frac{\partial^2 \Lambda_{\bar{\boldsymbol{F}}}}{\partial \mathfrak{s}^2} \bar{w}_{\bar{\boldsymbol{F}}} + \frac{\partial^2 \Lambda_{\bar{\boldsymbol{H}}}}{\partial \mathfrak{s}^2} \bar{w}_{\bar{\boldsymbol{H}}} + \frac{\partial^2 \Lambda_J}{\partial \mathfrak{s}^2} U \right) N^B_{\mathfrak{s}} \, \mathrm{d}V + \int_{\mathcal{B}_0} \left(N^A_{\mathfrak{s}} N^B_{\mathfrak{s}} \frac{g_c}{l} + g_c l \left(\nabla_{\boldsymbol{X}} N^A_{\mathfrak{s}} \right) \cdot \left(\nabla_{\boldsymbol{X}} N^B_{\mathfrak{s}} \right) + \frac{g_c l^3}{2} \left(\Delta_{\boldsymbol{X}} N^A_{\mathfrak{s}} \right) \left(\Delta_{\boldsymbol{X}} N^B_{\mathfrak{s}} \right) \right) \mathrm{d}V. \tag{118}$$

The incremental variation of the weak form in Eq. $(80)_b$ with respect to incremental variations $\{\Delta \boldsymbol{\Sigma}_{\bar{\boldsymbol{F}}}, \Delta \boldsymbol{\Sigma}_{\bar{\boldsymbol{H}}}, \Delta \Sigma_J\}$ is obtained as

$$\begin{aligned} \boldsymbol{K}^{AB}_{\mathfrak{s}\boldsymbol{\Sigma}_{\bar{\boldsymbol{F}}}} &= \int_{\mathcal{B}_0} N^A_{\mathfrak{s}} \frac{\partial \Lambda_{\bar{\boldsymbol{F}}}}{\partial \mathfrak{s}} \frac{\partial \bar{w}_{\bar{\boldsymbol{F}}}}{\partial \bar{\boldsymbol{F}}} N^B_{\bar{\boldsymbol{F}}} \, \mathrm{d}V; \\ \boldsymbol{K}^{AB}_{\mathfrak{s}\boldsymbol{\Sigma}_{\bar{\boldsymbol{H}}}} &= \int_{\mathcal{B}_0} N^A_{\mathfrak{s}} \frac{\partial \Lambda_{\bar{\boldsymbol{H}}}}{\partial \mathfrak{s}} \frac{\partial \bar{w}_{\bar{\boldsymbol{H}}}}{\partial \bar{\boldsymbol{H}}} N^B_{\bar{\boldsymbol{H}}} \, \mathrm{d}V; \\ \boldsymbol{K}^{AB}_{\mathfrak{s}\Sigma_J} &= \int_{\mathcal{B}_0} N^A_{\mathfrak{s}} \frac{\partial \Lambda_J}{\partial \mathfrak{s}} \frac{\partial U}{\partial J} N^B_J \, \mathrm{d}V. \end{aligned} \tag{119}$$

Directional derivatives of $\mathrm{D}\,\bar{\Pi}_{HW}[\delta\bar{\boldsymbol{F}}]$, $\mathrm{D}\,\bar{\Pi}_{HW}[\delta\bar{\boldsymbol{H}}]$ and $\mathrm{D}\,\bar{\Pi}_{HW}[\delta J]$. The stiffness matrix contributions associated to the discretisation of Eq. (90) are

$$\begin{aligned} \boldsymbol{K}^{AB}_{\bar{\boldsymbol{F}}\bar{\boldsymbol{F}}} &= \int_{\mathcal{B}_0} N^A_{\bar{\boldsymbol{F}}} N^B_{\bar{\boldsymbol{F}}} \Lambda_{\bar{\boldsymbol{F}}} \frac{\partial^2 \bar{w}_{\bar{\boldsymbol{F}}}}{\partial \bar{\boldsymbol{F}} \partial \bar{\boldsymbol{F}}} \, \mathrm{d}V; \\ \boldsymbol{K}^{AB}_{\bar{\boldsymbol{H}}\bar{\boldsymbol{H}}} &= \int_{\mathcal{B}_0} N^A_{\bar{\boldsymbol{H}}} N^B_{\bar{\boldsymbol{H}}} \Lambda_{\bar{\boldsymbol{H}}} \frac{\partial^2 \bar{w}_{\bar{\boldsymbol{H}}}}{\partial \bar{\boldsymbol{H}} \partial \bar{\boldsymbol{H}}} \, \mathrm{d}V; \\ \boldsymbol{K}^{AB}_{JJ} &= \int_{\mathcal{B}_0} N^A_J N^B_J \Lambda_J \frac{\partial^2 U}{\partial J^2} \, \mathrm{d}V. \end{aligned} \tag{120}$$

Finally, the incremental variation of the weak form in Eq. (82) with respect to incremental variations $\{\Delta \boldsymbol{\Sigma}_{\bar{\boldsymbol{F}}}, \Delta \boldsymbol{\Sigma}_{\bar{\boldsymbol{H}}}, \Delta \Sigma_J\}$ is obtained as

$$\begin{aligned} \boldsymbol{K}^{AB}_{\bar{\boldsymbol{F}}\boldsymbol{\Sigma}_{\bar{\boldsymbol{F}}}} &= -\int_{\mathcal{B}_0} N^A_{\bar{\boldsymbol{F}}} N^B_{\bar{\boldsymbol{F}}} \boldsymbol{\mathcal{I}} \, \mathrm{d}V; \\ \boldsymbol{K}^{AB}_{\bar{\boldsymbol{H}}\boldsymbol{\Sigma}_{\bar{\boldsymbol{H}}}} &= -\int_{\mathcal{B}_0} N^A_{\bar{\boldsymbol{H}}} N^B_{\bar{\boldsymbol{H}}} \boldsymbol{\mathcal{I}} \, \mathrm{d}V; \\ K^{AB}_{\Sigma_J \Sigma_J} &= -\int_{\mathcal{B}_0} N^A_J N^B_J \, \mathrm{d}V. \end{aligned} \tag{121}$$

Appendix B. Alternative static condensation for Hu–Washizu

Alternatively to the static condensation procedure as proposed in Section 5.2.1, it would have been possible to obtain the incremental value $\Delta \boldsymbol{\mathcal{D}}_e$ from the third row in Eq. (105) as

$$\Delta \boldsymbol{\mathcal{D}}_e = -\left(\boldsymbol{K}^e_{\boldsymbol{\mathcal{D}}\boldsymbol{\mathcal{D}}} \right)^{-1} \left(\boldsymbol{R}^e_{\boldsymbol{\mathcal{D}}} + \boldsymbol{K}^e_{\boldsymbol{\mathcal{D}}\mathfrak{s}} \Delta \mathfrak{s}_e + \boldsymbol{K}^e_{\boldsymbol{\mathcal{D}}\boldsymbol{\Sigma}_{\boldsymbol{\mathcal{D}}}} \Delta \boldsymbol{\Sigma}_{\boldsymbol{\mathcal{D}},e} \right). \tag{122}$$

Substitution of the above expression (122) for $\Delta \boldsymbol{\mathcal{D}}_e$ into the remaining rows renders the following system of equations (prior to static condensation in the unknown $\Delta \boldsymbol{\Sigma}_{\boldsymbol{\mathcal{D}},e}$)

$$\begin{bmatrix} \boldsymbol{K}^e_{\boldsymbol{x}\boldsymbol{x}} & \boldsymbol{0} & \boldsymbol{K}^e_{\boldsymbol{x}\boldsymbol{\Sigma}_{\mathcal{D}}} \\ \boldsymbol{0} & \tilde{\boldsymbol{K}}^e_{\mathfrak{s}\mathfrak{s}} & \tilde{\boldsymbol{K}}^e_{\mathfrak{s}\boldsymbol{\Sigma}_{\mathcal{D}}} \\ \boldsymbol{K}^e_{\boldsymbol{\Sigma}_{\mathcal{D}}\boldsymbol{x}} & \left(\tilde{\boldsymbol{K}}^e_{\mathfrak{s}\boldsymbol{\Sigma}_{\mathcal{D}}}\right)^T & \tilde{\boldsymbol{K}}^e_{\boldsymbol{\Sigma}_{\mathcal{D}}\boldsymbol{\Sigma}_{\mathcal{D}}} \end{bmatrix} \begin{bmatrix} \Delta \boldsymbol{x}_e \\ \Delta \mathfrak{s}_e \\ \Delta \boldsymbol{\Sigma}_{\mathcal{D},e} \end{bmatrix} = - \begin{bmatrix} \boldsymbol{R}^e_{\boldsymbol{x}} \\ \tilde{\boldsymbol{R}}^e_{\mathfrak{s}} \\ \tilde{\boldsymbol{R}}^e_{\boldsymbol{\Sigma}_{\mathcal{D}}} \end{bmatrix}, \tag{123}$$

where the modified stiffness matrices $\tilde{\boldsymbol{K}}^e_{\mathfrak{s}\mathfrak{s}}$, $\tilde{\boldsymbol{K}}^e_{\mathfrak{s}\boldsymbol{\Sigma}_{\mathcal{D}}}$ and $\tilde{\boldsymbol{K}}^e_{\boldsymbol{\Sigma}_{\mathcal{D}}\boldsymbol{\Sigma}_{\mathcal{D}}}$ are defined as

$$\begin{aligned} \tilde{\boldsymbol{K}}^e_{\mathfrak{s}\mathfrak{s}} &= \boldsymbol{K}^e_{\mathfrak{s}\mathfrak{s}} - \boldsymbol{K}^e_{\mathfrak{s}\mathcal{D}} \left(\boldsymbol{K}^e_{\mathcal{D}\mathcal{D}}\right)^{-1} \boldsymbol{K}^e_{\mathcal{D}\mathfrak{s}}; \\ \tilde{\boldsymbol{K}}^e_{\mathfrak{s}\boldsymbol{\Sigma}_{\mathcal{D}}} &= -\tilde{\boldsymbol{K}}^e_{\mathfrak{s}\mathcal{D}} \left(\boldsymbol{K}^e_{\mathcal{D}\mathcal{D}}\right)^{-1} \boldsymbol{K}^e_{\mathcal{D}\boldsymbol{\Sigma}_{\mathcal{D}}}; \\ \tilde{\boldsymbol{K}}^e_{\boldsymbol{\Sigma}_{\mathcal{D}}\boldsymbol{\Sigma}_{\mathcal{D}}} &= -\boldsymbol{K}^e_{\boldsymbol{\Sigma}_{\mathcal{D}}\mathcal{D}} \left(\boldsymbol{K}^e_{\mathcal{D}\mathcal{D}}\right)^{-1} \boldsymbol{K}^e_{\mathcal{D}\boldsymbol{\Sigma}_{\mathcal{D}}}. \end{aligned} \tag{124}$$

The modified residuals $\tilde{\boldsymbol{R}}^e_{\mathfrak{s}}$ and $\tilde{\boldsymbol{R}}^e_{\boldsymbol{\Sigma}_{\mathcal{D}}}$ can be expressed as

$$\begin{aligned} \tilde{\boldsymbol{R}}^e_{\mathfrak{s}} &= \boldsymbol{R}^e_{\mathfrak{s}} - \boldsymbol{K}^e_{\mathfrak{s}\mathcal{D}} \left(\boldsymbol{K}^e_{\mathcal{D}\mathcal{D}}\right)^{-1} \boldsymbol{R}^e_{\mathcal{D}}; \\ \tilde{\boldsymbol{R}}^e_{\boldsymbol{\Sigma}_{\mathcal{D}}} &= \boldsymbol{R}^e_{\boldsymbol{\Sigma}_{\mathcal{D}}} - \boldsymbol{K}^e_{\boldsymbol{\Sigma}_{\mathcal{D}}\mathcal{D}} \left(\boldsymbol{K}^e_{\mathcal{D}\mathcal{D}}\right)^{-1} \boldsymbol{R}^e_{\mathcal{D}}. \end{aligned} \tag{125}$$

Elimination of the last row in above Eq. (123) yields to local algebraic system of equations in terms of the local unknowns $\Delta \boldsymbol{x}_e$ and $\Delta \mathfrak{s}_e$ as

$$\begin{bmatrix} \boldsymbol{K}^{e\,\star}_{\boldsymbol{x}\boldsymbol{x}} & \boldsymbol{K}^{e\,\star}_{\boldsymbol{x}\mathfrak{s}} \\ \left(\boldsymbol{K}^{e\,\star}_{\boldsymbol{x}\mathfrak{s}}\right)^T & \boldsymbol{K}^{e\,\star}_{\mathfrak{s}\mathfrak{s}} \end{bmatrix} \begin{bmatrix} \Delta \boldsymbol{x}_e \\ \Delta \mathfrak{s}_e \end{bmatrix} = - \begin{bmatrix} \boldsymbol{R}^{e\star}_{\boldsymbol{x}} \\ \boldsymbol{R}^{e\star}_{\mathfrak{s}} \end{bmatrix}, \tag{126}$$

where the final stiffness matrices $\boldsymbol{K}^{e\star}_{\boldsymbol{x}\boldsymbol{x}}$, $\boldsymbol{K}^{e\star}_{\boldsymbol{x}\mathfrak{s}}$ and $\boldsymbol{K}^{e\star}_{\mathfrak{s}\mathfrak{s}}$ are defined as

$$\begin{aligned} \boldsymbol{K}^{e\,\star}_{\boldsymbol{x}\boldsymbol{x}} &= \boldsymbol{K}^e_{\boldsymbol{x}\boldsymbol{x}} - \boldsymbol{K}^e_{\boldsymbol{x}\boldsymbol{\Sigma}_{\mathcal{D}}} \left(\tilde{\boldsymbol{K}}^e_{\boldsymbol{\Sigma}_{\mathcal{D}}\boldsymbol{\Sigma}_{\mathcal{D}}}\right)^{-1} \boldsymbol{K}^e_{\boldsymbol{\Sigma}_{\mathcal{D}}\boldsymbol{x}}; \\ \boldsymbol{K}^{e\,\star}_{\mathfrak{s}\boldsymbol{\Sigma}_{\mathcal{D}}} &= \boldsymbol{K}^e_{\boldsymbol{x}\boldsymbol{\Sigma}_{\mathcal{D}}} \left(\tilde{\boldsymbol{K}}^e_{\boldsymbol{\Sigma}_{\mathcal{D}}\boldsymbol{\Sigma}_{\mathcal{D}}}\right)^{-1} \left(\tilde{\boldsymbol{K}}^e_{\mathfrak{s}\boldsymbol{\Sigma}_{\mathcal{D}}}\right)^T; \\ \boldsymbol{K}^{e\,\star}_{\mathfrak{s}\mathfrak{s}} &= \tilde{\boldsymbol{K}}^e_{\mathfrak{s}\mathfrak{s}} - \tilde{\boldsymbol{K}}^e_{\mathfrak{s}\boldsymbol{\Sigma}_{\mathcal{D}}} \left(\tilde{\boldsymbol{K}}^e_{\boldsymbol{\Sigma}_{\mathcal{D}}\boldsymbol{\Sigma}_{\mathcal{D}}}\right)^{-1} \left(\tilde{\boldsymbol{K}}^e_{\mathfrak{s}\boldsymbol{\Sigma}_{\mathcal{D}}}\right)^T. \end{aligned} \tag{127}$$

Finally, the modified residuals $\boldsymbol{R}^{e\star}_{\boldsymbol{x}}$ and $\boldsymbol{R}^{e\star}_{\mathfrak{s}}$ can be expressed as

$$\begin{aligned} \boldsymbol{R}^{e\star}_{\boldsymbol{x}} &= \boldsymbol{R}^e_{\boldsymbol{x}} - \boldsymbol{K}^e_{\boldsymbol{x}\boldsymbol{\Sigma}_{\mathcal{D}}} \left(\tilde{\boldsymbol{K}}^e_{\boldsymbol{\Sigma}_{\mathcal{D}}\boldsymbol{\Sigma}_{\mathcal{D}}}\right)^{-1} \tilde{\boldsymbol{R}}^e_{\boldsymbol{\Sigma}_{\mathcal{D}}}; \\ \boldsymbol{R}^{e\star}_{\mathfrak{s}} &= \tilde{\boldsymbol{R}}^e_{\mathfrak{s}} - \tilde{\boldsymbol{K}}^e_{\mathfrak{s}\boldsymbol{\Sigma}_{\mathcal{D}}} \left(\tilde{\boldsymbol{K}}^e_{\boldsymbol{\Sigma}_{\mathcal{D}}\boldsymbol{\Sigma}_{\bar{\mathcal{D}}}}\right)^{-1} \tilde{\boldsymbol{R}}^e_{\boldsymbol{\Sigma}_{\bar{\mathcal{D}}}}. \end{aligned} \tag{128}$$

Remark 7. In contrast to the first approach described in order to carry out the static condensation procedure, this second approach introduces further numerical difficulties. In addition to the possible scaling issue between the mechanical and phase-field problem (first and second rows of the system in (126)), an additional numerical difficulty has been introduced when arriving at the intermediate local system of equations in (123). Notice that the computation of the modified stiffness matrices in that system of equations requires the inversion of the local matrix contribution $\boldsymbol{K}^e_{\mathcal{D}\mathcal{D}}$ (refer to Eq. (120)), comprising the individual matrices $\boldsymbol{K}^e_{\bar{\boldsymbol{F}}\bar{\boldsymbol{F}}}$, $\boldsymbol{K}^e_{\bar{\boldsymbol{H}}\bar{\boldsymbol{H}}}$ and K^e_{JJ}. For tensional states, namely $II_{\bar{\boldsymbol{F}}} > 3$, $II_{\bar{\boldsymbol{H}}} > 3$ and $J > 1$, the invertibility of these matrices is compromised for the fully damaged state, i.e, $\mathfrak{s} \to 1$, as these matrices vanish $\boldsymbol{K}^e_{\mathcal{D}\mathcal{D}} \to \boldsymbol{0}$. A possible solution to overcome this drawback is the redefinition of the functions $\Lambda_{\bar{\boldsymbol{F}}}$, $\Lambda_{\bar{\boldsymbol{F}}}$ and Λ_J via the introduction of a small parameter ε as

$$\Lambda_{\bar{\boldsymbol{F}}} = \begin{cases} g(\mathfrak{s}) + \varepsilon & \text{if } II_{\bar{\boldsymbol{F}}} > 3; \\ 1 & \text{otherwise.} \end{cases} \Lambda_{\bar{\boldsymbol{H}}} = \begin{cases} g(\mathfrak{s}) + \varepsilon & \text{if } II_{\bar{\boldsymbol{H}}} > 3; \\ 1 & \text{otherwise.} \end{cases} \Lambda_J = \begin{cases} g(\mathfrak{s}) + \varepsilon & \text{if } J > 1; \\ 1 & \text{otherwise.} \end{cases} \tag{129}$$

(cf. Section 3.3.1). However, if the parameter ε is very small, numerical instabilities associated with ill-conditioning of the associated stiffness matrix might still arise. These are typically solved by the use of an appropriate pre-conditioner. A plausible solution that works as a pre-conditioner and that can efficiently solve the numerical difficulties associated to the Hu–Washizu mixed variational principle requires a slight modification of the residuals in Eq. (102). The local character of these equations (a discontinuous interpolation of each of the fields in $\{\boldsymbol{\mathcal{D}},\, \boldsymbol{\Sigma}_{\boldsymbol{\mathcal{D}}}\}$ is considered) enables to modify those equations (pre-dividing them by the appropriate function $\Lambda_\bullet$) as

$$\begin{aligned}
\boldsymbol{R}^A_{\bar{\boldsymbol{F}}} &= \int_{\mathcal{B}_0} \frac{1}{\Lambda_{\bar{\boldsymbol{F}}}} \left(\Lambda_{\bar{\boldsymbol{F}}} \frac{\partial \bar{w}_{\bar{\boldsymbol{F}}}}{\partial \bar{\boldsymbol{F}}^{\mathrm{h}}} - \boldsymbol{\Sigma}^{\mathrm{h}}_{\bar{\boldsymbol{F}}} \right) N^A_{\bar{\boldsymbol{F}}} \, \mathrm{d}V; \\
\boldsymbol{R}^A_{\bar{\boldsymbol{H}}} &= \int_{\mathcal{B}_0} \frac{1}{\Lambda_{\bar{\boldsymbol{H}}}} \left(\Lambda_{\bar{\boldsymbol{H}}} \frac{\partial \bar{w}_{\bar{\boldsymbol{H}}}}{\partial \bar{\boldsymbol{H}}^{\mathrm{h}}} - \boldsymbol{\Sigma}^{\mathrm{h}}_{\bar{\boldsymbol{H}}} \right) N^A_{\bar{\boldsymbol{H}}} \, \mathrm{d}V; \\
R^A_J &= \int_{\mathcal{B}_0} \frac{1}{\Lambda_J} \left(\Lambda_J \frac{\partial U}{\partial J^{\mathrm{h}}} - \Sigma^{\mathrm{h}}_J \right) N^A_J \, \mathrm{d}V.
\end{aligned} \tag{130}$$

It is worth pointing that this modification leads to non symmetries in (105) as $\left(\boldsymbol{K}^e_{\boldsymbol{\mathcal{D}}_{\mathfrak{s}}}\right) \neq \boldsymbol{K}^e_{\mathfrak{s}\boldsymbol{\mathcal{D}}}$ and $\left(\boldsymbol{K}^e_{\boldsymbol{\mathcal{D}}\boldsymbol{\Sigma}_{\boldsymbol{\mathcal{D}}}}\right)^T \neq \boldsymbol{K}^e_{\boldsymbol{\Sigma}_{\boldsymbol{\mathcal{D}}}\boldsymbol{\mathcal{D}}}$.

References

[1] A.A. Griffith, The phenomena of rupture and flow in solids, Philos. Trans. R. Soc. Lond. 221 (1921) 163–198.
[2] G.R. Irwin, Elasticity and plasticity: fracture, in: S. Flügge (Ed.), Encyclopedia of Physics, 1958.
[3] G.A. Francfort, J.-J. Marigo, Revisiting brittle fracture as an energy minimization problem, J. Mech. Phys. Solids 46 (1998) 1319–1342.
[4] G.T. Camacho, M. Ortiz, Computational modelling of impact damage in brittle materials, Int. J. Solids Struct. 33 (1996) 2899–2938.
[5] A. Pandolfi, M. Ortiz, An efficient adaptive procedure for three-dimensional fragmentation simulations, Eng. Comput. 18 (2002) 48–159.
[6] A. Pandolfi, K. Weinberg, A numerical approach to the analysis of failure modes in anisotropic plates, Eng. Fract. Mech. 78 (2011) 2052–2069.
[7] F.L. Stazi, E. Budyn, J. Chessa, T. Belytschko, An extended finite element method with higher-order elements for curved cracks, Comput. Mech. 31 (2003) 38–48.
[8] E. Gürses, C. Miehe, A computational framework of three–dimensional configurational–force–driven brittle crack propagation, Comput. Methods Appl. Mech. Engrg. 198 (2009) 1413–1428.
[9] C. Miehe, F. Welschinger, M. Hofacker, Thermodynamically consistent phase-field models of fracture: Variational principles and multi-field FE implementations, Internat. J. Numer. Methods Engrg. 83 (2010) 1273–1311.
[10] D. Gross, Th. Seelig, Fracture Mechanics, second ed., Springer-Verlag, Berlin, 2011.
[11] J.M. Ball, Convexity conditions and existence theorems in nonlinear elasticity, Arch. Ration. Mech. Anal. 63 (1977) 337–403.
[12] S. Hartmann, P. Neff, Polyconvexity of generalized polynomial-type hyperelastic strain energy functions for near-incompressibility, Int. J. Solids Struct. 40 (2003) 2767–2791.
[13] J. Schröder, P. Neff, Invariant formulation of hyperelastic transverse isotropy based on polyconvex free energy functions, Int. J. Solids Struct. 40 (2003) 401–445.
[14] R. Ortigosa, A.J. Gil, J. Bonet, C. Hesch, A computational framework for polyconvex large strain elasticity for geometrically exact beam theory, Comput. Mech. 57 (2016) 277–303.
[15] M. Ambati, T. Gerasimov, L. De Lorenzis, Phase-field modeling of ductile fracture, Comput. Mech. 55 (2015) 1017–1040.
[16] C. Miehe, L.M. Schänzel, H. Ulmer, Phase field modeling of fracture in multi-physics problems. Part I. Balance of crack surface and failure criteria for brittle crack propagation in thermo-elastic solids, Comput. Methods Appl. Mech. Engrg. 294 (2015) 449–485.
[17] M.J. Borden, T.J.R. Hughes, C.M. Landis, C.V. Verhoosel, A higher-order phase-field model for brittle fracture: Formulation and analysis within the isogeometric analysis framework, Comput. Methods Appl. Mech. Engrg. 273 (2014) 100–118.
[18] K. Weinberg, C. Hesch, A high-order finite-deformation phase-field approach to fracture, Contin. Mech. Thermodyn. (2015) 1–11.
[19] C. Hesch, M. Franke, M. Dittmann, İ. Temizer, Hierarchical NURBS and a higher-order phase-field approach to fracture for finite-deformation contact problems, Comput. Methods Appl. Mech. Engrg. 301 (2016) 242–258.
[20] C. Hesch, S. Schuß, M. Dittmann, M. Franke, K. Weinberg, Isogeometric analysis and hierarchical refinement for higher-order phase-field models, Comput. Methods Appl. Mech. Engrg. 303 (2016) 185–207.
[21] O.C. Zienkiewicz, R.L. Taylor, The Finite Element Method for Solid and Structural Mechanics, sixth ed., Butterworth Heinemann, 2005.
[22] J. Bonet, A. Gil, R. Ortigosa, A computational framework for polyconvex large strain elasticity, Comput. Methods Appl. Mech. Engrg. 283 (2015) 1061–1094.
[23] J. Bonet, A.J. Gil, C.H. Lee, M. Aguirre, R. Ortigosa, A first order hyperbolic framework for large strain computational solid dynamics. Part I: Total Lagrangian isothermal elasticity, Comput. Methods Appl. Mech. Engrg. 283 (2015) 689–732.
[24] J. Bonet, A.J. Gil, R. Ortigosa, On a tensor cross product based formulation of large strain solid mechanics, Int. J. Solids Struct. 84 (2016) 49–63.
[25] J. Bonet, A.J. Gil, R.D. Wood, Nonlinear Continuum Mechanics for Finite Element Analysis: Statics, Cambridge University Press, 2016.
[26] M.J. Borden, C.V. Verhoosel, M.A. Scott, T.J.R. Hughes, C.M. Landis, A phase-field description of dynamic brittle fracture, Comput. Methods Appl. Mech. Engrg. 217–220 (2012) 77–95.

[27] C. Hesch, K. Weinberg, Thermodynamically consistent algorithms for a finite-deformation phase-field approach to fracture, Internat. J. Numer. Methods Engrg. 99 (2014) 906–924.
[28] C. Truesdell, W. Noll, The Non-Linear Field Theories of Mechanics, third ed., Springer-Verlag, 2004.
[29] J.E. Marsden, T.J.R. Hughes, Mathematical Foundations of Elasticity, Prentice-Hall, INC, 1983.
[30] A.J. Gil, C.H. Lee, J. Bonet, M. Aguirre, A stabilised Petrov-Galerkin formulation for linear tetrahedral elements in compressible, nearly incompressible and truly incompressible fast dynamics, Comput. Methods Appl. Mech. Engrg. 276 (2014) 659–690.
[31] A.J. Gil, C.H. Lee, J. Bonet, R. Ortigosa, A first order hyperbolic framework for large strain computational solid dynamics. Part II: Total Lagrangian compressible, nearly incompressible and truly incompressible elasticity, Comput. Methods Appl. Mech. Engrg. 300 (2016) 146–181.
[32] A.J. Gil, R. Ortigosa, A new framework for large strain electromechanics based on convex multi-variable strain energies: variational formulation and material characterisation, Comput. Methods Appl. Mech. Engrg. 302 (2016) 293–328.
[33] R. Ortigosa, A.J. Gil, A new framework for large strain electromechanics based on convex multi-variable strain energies: Finite element discretisation and computational implementation, Comput. Methods Appl. Mech. Engrg. 302 (2016) 329–360.
[34] R. Ortigosa, A.J. Gil, A new framework for large strain electromechanics based on convex multi-variable strain energies: conservation laws and hyperbolicity and extension to electro-magnetomechanics, Comput. Methods Appl. Mech. Engrg. 310 (2016) 297–334.
[35] R. Ortigosa, A.J. Gil, C.H. Lee, A computational framework for large strain nearly and truly incompressible electromechanics based on convex multi-variable strain energies, Comput. Methods Appl. Mech. Engrg. 310 (2016) 297–334.
[36] C. Miehe, M. Hofacker, L.-M. Schänzel, F. Aldakheel, Phase field modeling of fracture in multi-physics problems. Part II. Coupled brittle-to-ductile failure criteria and crack propagation in thermo-elastic–plastic solids, Comput. Methods Appl. Mech. Engrg. 294 (2015) 486–522.
[37] M.J. Borden, Isogeometric Analysis of Phase-Field Models for Dynamic Brittle and Ductile Fracture (Ph.D. thesis), The University of Texas at Austin, 2012.
[38] B. Dacorogna, Direct Methods in the Calculus of Variations, in: Applied Mathematical Sciences, Springer-Verlag, 1989.
[39] C. Miehe, M. Hofacker, F. Welschinger, A phase field model for rate-independent crack propagation: Robust algorithmic implementation based on operator splits, Comput. Methods Appl. Mech. Engrg. 199 (2010) 2765–2778.